THE LIGAND AND MEMBRANE-BINDING BEHAVIOUR OF THE PHOSPHATIDYLINOSITOL TRANSFER PROTEINS (PITPα & PITPβ)

Matilda Baptist, MSc

Biotechnology

Submitted in partial fulfilment of the requirements
for the degree of Doctor of Philosophy

Department of Chemistry & Centre of Biotechnology
Brock University, St Catharines, Ontario

"I will lift up my eyes to the hills – from whence comes my help? My help comes from the Lord who made heaven and earth."

– Psalm 121:1-2

To my parents: James & Rosalind - for their continual love & support in every season of life & their encouragement to follow my heart.

Abstract

Human Class I phosphatidylinositol transfer proteins (PITPs) exists in two forms: PITPα and PITPβ. PITPs are believed to be lipid transfer proteins based on their capacity to transfer either phosphatidylinositol (PI) or phosphatidylcholine (PC) between membrane compartments *in vitro*. In *Drosophila*, the PITP domain is found to be part of a multi-domain protein named retinal degeneration B (RdgBα). The PITP domain of RdgBα shares 40 % sequence identity with PITPα and has been shown to possess PI and PC binding and transfer activity.

The detailed molecular mechanism of ligand transfer by the human PITPs and the *Drosophila* PITP domain remains to be fully established. Here, we investigated the membrane interactions of these proteins using dual polarization interferometry (DPI). DPI is a technique that measures protein binding affinity to a flat immobilized lipid bilayer. In addition, we also measured how quickly these proteins transfer their ligands to lipid vesicles using a fluorescence resonance energy transfer (FRET)-based assay.

DPI investigations suggest that PITPβ had a two-fold higher affinity for membranes compared to PITPα. This was reflected by a four-fold faster ligand transfer rate for PITPβ in comparison to PITPα as determined by the FRET assay. Interestingly, DPI analysis also demonstrated that PI-bound human PITPs have lower membrane affinity compared to PC-bound PITPs.

In addition, the FRET studies demonstrated the significance of membrane curvature in the ligand transfer rate of PITPs. The ligand transfer rate was higher when the accepting vesicles were highly curved. Furthermore, when the accepting vesicles contained phosphatidic acid (PA) which have smaller head groups, the transfer rate increased. In contrast, when the accepting

vesicles contained phosphoinositides which have larger head groups, the transfer rate was diminished. However, PI, the favorite ligand of PITPs, or the presence of anionic lipids did not appear to influence the ligand transfer rate of PITPs.

Both DPI and FRET examinations revealed that the PITP domain of RdgBα was able to bind to membranes. However, the RdgBα PITP domain appears to be a poor binder and transporter of PC.

ACKNOWLEDGEMENTS

Four and a half years may seem like a long time to complete a journey. But there is a Turkish proverb that says ‘no road is long with good company’ which I have found to be true. The duration of my graduate studies was eased by the presence of some amazing people who have been a blessing to me.

First and foremost, a heartfelt gratitude goes out to my supervisor and mentor, Dr. Jeffrey Atkinson. I am grateful for his willingness to learn alongside with me, his continual support and guidance, and his great sense of humor.

A special thanks goes to my lab-mates in the protein lab: Dr. Candace Panagabko, Parthajit Mukherjee and Hasam Madarati who have been my ‘lab family’. I am also thankful for Mikel Ghelfi and Andrew Hildering, my lab-mates from the chemistry lab, who helped set up experiments in the ‘intimidating’ synthetic lab.

I wish to also thank my supervisory committee: Dr. Charles Després and Dr. Paul Zelisko for their guidance and invaluable input. In addition, I am grateful to Dr. Evangelia Tsiani and Dr. Costin Antonescu for their evaluation on this work.

I am thankful for the wonderful friends that I have met within and outside the Brock community. Unfortunately, there are too many to be named here but I sincerely appreciate their friendship and encouragement and their listening ear when I just needed to ‘whine’ about work.

I wish to express my sincere appreciation for my family for their constant love and support throughout this journey of completing my graduate studies.

Last but not least, I owe my deepest gratitude to God who not only brought amazing people into my life but who also brought me this far on my journey in life.

TABLE OF CONTENTS

LIST OF TABLES

LIST OF FIGURES

LIST OF ABBREVIATIONS

ALPS	Amphipathic lipid packing sensor
ArfGAP1	ADP-ribosylation factor GTPase activating protein 1
BAR	Bin-Amphiphysin-Rvs
BSA	Bovine serum albumin
CDP	Cytidine diphosphate
CERT	Ceramide transfer protein
COPI	Coat protein complex I
COPII	Coat protein complex II
DAG	Diacylglycerol
DPI	Dual polarization interferometry
DOPC	1, 2-dioleoyl-s*n*-glycero-3-phosphocholine
DOPE	1, 2-dioleoyl-s*n*-glycero-3-phosphoethanolamine
DOPS	1, 2-dioleoyl-s*n*-glycero-3-phospho-L-serine
DSC	Differential scanning calorimetry
DTT	Dithiothreitol
EDTA	Ethylenediaminetetraacetic acid
EGF	Epidermal growth factor
ER	Endoplasmic reticulum
FRET	Fluorescence resonance spectroscopy
GLTP	Glycolipid transfer protein
KCl	Potassium chloride
LB	Luria Bertani

Liss Rhod PE	1,2-dioleoyl-sn-glycero-3-phosphoethanolamine-N-(lissamine rhodamine B sulfonyl)
LPC	Lysophosphatidylcholine
LTPs	Lipid transfer proteins
LUVs	Large unilamellar vesicles
MES	2-(N-Morpholino)ethanesulphonic acid
NaCl	Sodium chloride
NBD-PC	NBD C12-HPC (2-(12-(7-Nitrobenz-2-Oxa-1,3-Diazol-4-yl)amino)Dodecanoyl-1-Hexadecanoyl-sn-Glycero-3-Phosphocholine)
NEM	N-ethylmaleimide
NMR	Nuclear magnetic resonance
OPM	Orientation of proteins in membranes
PA	Phosphatidic acid
PBS	Phosphate buffered saline
PC	Phosphatidylcholine
PCR	Polymerase chain reaction
PE	Phosphatidylethanolamine
PI	Phosphatidylinositol
PI(3)P	Phosphatidylinositol-3-phosphate
PI(4)P	Phosphatidylinositol-4-phosphate
PI(5)P	Phosphatidylinositol-5-phosphate
$PI(3,4)P_2$	Phosphatidylinositol-3,4-phosphate
$PI(3,5)P_2$	Phosphatidylinositol-3,5-phosphate

$PI(4,5)P_2$	Phosphatidylinositol-4,5-phosphate
$PI(3,4,5)P_3$	Phosphatidylinositol-3,4,5-phosphate
PIPES	Piperazine-N,N′-bis(2-ethanesulfonic acid)
PITPs	Phosphatidylinositol transfer proteins
PH	Pleckstrin homology
PKC	Protein kinase C
PLC	Phospholipase C
PTEN	Phosphatase and tensin homolog
PS	Phosphatidylserine
RdgB	Retinal degeneration B
RMSD	Root mean square deviation
SDS-PAGE	Sodium dodecyl sulphate polyacrylamide gel electrophoresis
SRC	Subrhadomeric cisternae
START	Steroidogenic acute regulatory protein-related lipid transfer
SUVs	Small unilamellar vesicles
TE	Transverse electric
TM	Transverse magnetic
TMB	3,3′,5,5′-Tetramethylbenzidine
TNBS	Trinitrobenzene sulfonate
Tris	Tris(hydroxymethyl)aminomethane
TRITC DHPE	(N-(6-Tetramethylrhodaminethiocarbamoyl)-1,2-Dihexadecanoyl-sn-Glycero-3-Phosphoethanolamine)
VAP	VAMP-associated protein

VAMP	Vesicle-associated membrane protein

1. INTRODUCTION

1.1 Phospholipids: Essential Building Blocks of Biomembranes

Phospholipids constitute one of the main lipid structural elements of cellular membranes. Biological membranes are crucial as they function as cellular boundaries separating the ordered living cell from its surrounding chaotic environment. Glycerophospholipids are a group of lipids whose backbone is based on a three carbon glycerol molecule. Two fatty acid chains are attached at position *sn*-1 and *sn*-2 – **Figure 1** [1]. The fatty acid chain at position *sn*-1 is generally saturated and composed of 16 or 18 carbon atoms. In contrast, the fatty acid chain at position *sn*-2 is usually longer and unsaturated containing one or more *cis*-double bonds [2]. When position *sn*-3 carries a phosphate group it is called phosphatidic acid (PA). This phosphate group can be esterified to different head-groups giving rise to several types of phospholipids including phosphatidylcholine (PC), phosphatidylethanolamine (PE), phosphatidylserine (PS) and phosphatidylinositol (PI) – **Figure 1** [1]. Each phospholipid group can encompass many more species based on the length and degree of unsaturation in the fatty acid chains [3].

Phospholipids make up the bulk of membranes in eukaryotic cells (60-65 mol% of the total lipid fraction) [2, 4]. Nearly 50 % of this fraction is attributed to PC. The reason behind this phospholipid distribution in membranes is because PC has the capacity to self-assemble spontaneously into a planar bilayer due to its inherent cylindrical shape. Consequently, this characteristic of PC is essential in providing a stable bilayer membrane structure [3, 4]. Moreover, most PC molecules possess one *cis*-unsaturated acyl chain which is important for membrane fluidity. It is important to note that biological membranes are not comprised solely of phospholipids, but also contain many

more lipid species that serve different functions ranging from cell signaling to membrane trafficking [1].

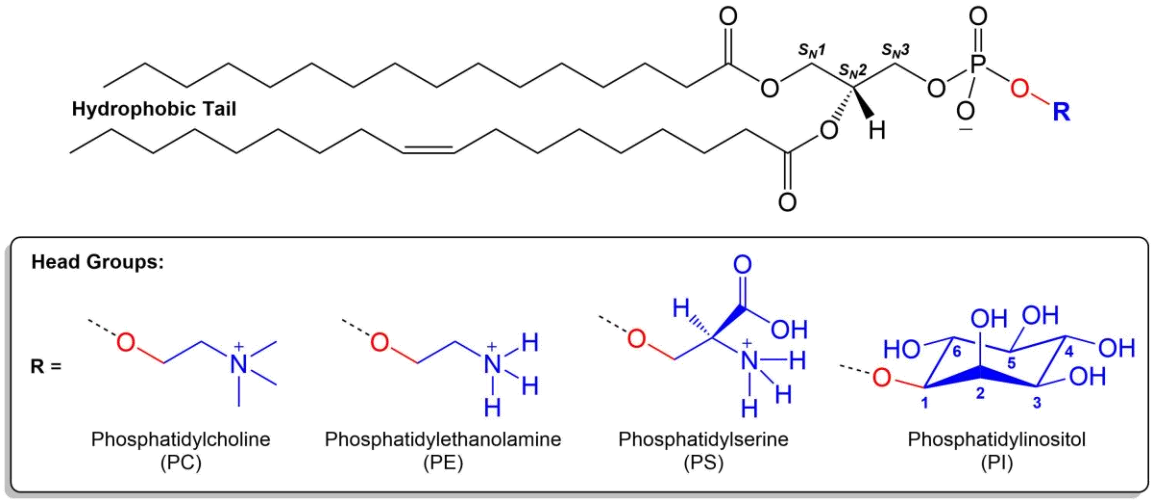

Figure 1: Phospholipid structure
The phospholipid head-groups are shown in the box. Both the glycerol backbone and inositol head-group of PI are numbered.

1.2 Phosphatidylinositol: Precursor for Phosphoinositides

PI is unique in that it acts not only as a structural lipid but also as a precursor for signaling molecules [5]. In comparison to PC, PI only accounts for approximately 10 - 20 mol% of the total lipid fraction in mammals [6]. The inositol head-group of PI can be reversibly phosphorylated by lipid kinases at positions -3, -4 and -5 giving rise to a group of signaling molecules known as phosphoinositides. To date there are seven known phosphoinositides in mammalian cells – **Table 1** [6]. Although phosphoinositides make up about 1 mol% of the total cellular lipid content they play important roles in many biological processes. These biological activities include, but are not limited to, lipid metabolism and distribution, signal transduction cascades and vesicle trafficking [6-7].

The distribution of phosphoinositides varies significantly within the cell and is dependent on the location of phosphoinositide modifying-enzymes. These enzymes include lipid kinases and phosphatases that attach and remove phosphate groups respectively. Consequently, phosphoinositides are positioned at distinct intracellular membranes and act as organelle markers – **Table 1** [8].

Table 1: Phosphoinositides – diversity and location.
A summary is shown here of the seven known phosphoinositides and their dominant membrane location in mammalian cells [7, 9].

Phosphoinositide	Abbreviation	Membrane Location
Phosphatidylinositol-3-phosphate	PI(3)P	Early endosomes
Phosphatidylinositol-4-phosphate	PI(4)P	Golgi complex
Phosphatidylinositol-5-phosphate	PI(5)P	Nucleus
Phosphatidylinositol-3,4-phosphate	PI(3,4)P_2	Early endosomes, plasma membrane
Phosphatidylinositol-3,5-phosphate	PI(3,5)P_2	Late endosomes, lysosomes
Phosphatidylinositol-4,5-phosphate	PI(4,5)P_2	Plasma membrane, nucleus
Phosphatidylinositol-3,4,5-phosphate	PI(3,4,5)P_3	Plasma membrane

Amongst the seven known phosphoinositides, both PI(4,5)P_2 and PI(3,4,5)P_3 are the most well studied phosphoinositides. Both PI(4,5)P_2 and PI(3,4,5)P_3 are located in the plasma membrane [7, 9]. PI(4,5)P_2 is synthesized in two steps: (i) the conversion of PI to PI4P by a PI 4-kinase and (ii) the conversion of PI4P to PI(4,5)P_2 by a PI(4)P 5-kinase [9]. PI(4,5)P_2 holds a key role in phosphoinositide signaling as it not only acts as a signaling molecule but also acts as a precursor for other signaling molecules. As a signaling molecule, PI(4,5)P_2 acts to recruit effector proteins that are involved in various

cellular processes which include endocytosis, exocytosis, cell migration and endosomal trafficking [10]. $PI(4,5)P_2$ can be dephosphorylated by at 5′-position by 5-phosphatases to generate PI(4)P [6].

$PI(4,5)P_2$ can be further converted to $PI(3,4,5)P_3$ by PI 3-kinase. This conversion occurs in response to extracellular stimuli such as epidermal growth factor (EGF). $PI(3,4,5)P_3$ then recruits effector proteins that regulate several cellular functions including cell growth and survival, cell cycle progression and intracellular vesicle trafficking [11]. $PI(3,4,5)P_3$ can be converted back to $PI(4,5)P_2$ through dephosphorylation at the 3′-position by PTEN (phosphatase and tensin homolog), a tumor suppressor protein [11].

In addition, $PI(4,5)P_2$ can be cleaved by phospholipases C (PLC) to generate two important lipid second messengers: diacylglycerol (DAG) and inositol 1,4,5-triphosphate. While inositol triphosphate releases Ca^{2+} stores, DAG activates protein kinase C (PKC) which in turn activates other proteins within the cell by phosphorylation [9].

1.3 Lipid Trafficking Mechanisms

The endoplasmic reticulum (ER) is the main site for the synthesis of most, if not all, lipids. Since these lipids are not confined to the ER, newly synthesized lipids are delivered to other membrane compartments where they are required [6, 12]. In the case of PI, PI transport is required for PI phosphorylation to occur at non-ER membrane compartments. Delivery of PI from the ER to other membrane locations is mainly achieved by means of vesicular transport and/or lipid carrier proteins [13].

To date several lipid trafficking mechanisms have been identified which can be broadly categorized under vesicular or non-vesicular lipid transport. Vesicular trafficking

entails the budding of a lipid vesicle from a donor membrane followed by the fusion of that vesicle with an acceptor membrane. In this manner, large amounts of lipids are transported from one organelle to another. This type of transport is observed in the endocytic and exocytic pathways [14]. Non-vesicular trafficking, on the other hand, includes several processes that can be further classified into intramembrane and intermembrane trafficking.

Intramembrane non-vesicular lipid transport can occur through the process of lateral diffusion and transbilayer flip-flop [14]. Lateral diffusion occurs when a lipid molecule moves in the lateral plane of the membrane bilayer. Typical lateral diffusion rates are in the order of 10^{-9} to 10^{-8} cm^2/sec [15]. This type of transport is usually confined within the same membrane compartment.

In contrast, transbilayer flip-flop takes place when a lipid molecule moves from one leaflet to another across the lipid bilayer. Flip-flop can occur spontaneously or with the assistance of proteins [14]. In vitro studies revealed that the rate of spontaneous flip-flop is dependent on the nature of the lipid head-groups. Lipids, such as DAG and cholesterol, which lack or possess small polar head group possess a faster flip-flop rate with half-times, $t_{1/2}$, ranging between seconds to minutes. On the contrary, lipids that carry a polar head-group such as PC possess a slower flip-flop rate with $t_{1/2}$ ranging between hours to days [1]. Taking this into consideration, spontaneous flip-flop alone is insufficient to support the lipid distribution observed in biological membranes; hence, protein-mediated flip-flop is essential here, which helps to accelerate the slow transbilayer movement of lipids [16].

Intermembrane non-vesicular transport involves monomeric lipid exchange or desorption which can occur spontaneously or by means of lipid transfer proteins (LTPs) [14]. Spontaneous lipid desorption takes place when a single lipid molecule moves from the outer leaflet of a donor membrane into the cytoplasm and inserts itself into the outer leaflet of an acceptor membrane [1]. The rate of spontaneous lipid exchange is dependent on the lipid's aqueous phase solubility. For example, lyso-phosphatidylcholine, which has a single acyl chain, undergoes spontaneous transfer more rapidly ($t_{1/2}$ of minutes) than phosphatidylcholine, which possess two acyl chains ($t_{1/2}$ of days) [1, 14]. In general, spontaneous lipid desorption is a slow process and requires a close proximity between both the donor and acceptor membranes. Despite this limitation, spontaneous lipid exchange is essential for organelles such as mitochondria that are not part of the vesicular pathway and lack the machinery to produce their own full repertoire of lipids [1]. Spontaneous lipid exchange alone is insufficient to support a significant transport of lipids, particularly of those found in the non-vesicular pathway [14]. The discovery of LTPs has led to the belief that these proteins may play a role in accelerating spontaneous lipid desorption [14]. Studies have shown that when vesicular trafficking was blocked by means of drugs such as brefeldin A, which inhibits coat protein complex I (COPI)-mediated transport vesicles, a significant amount of intermembrane lipid transport was still observed [17]. In this study, the transport of PE from its sites of synthesis to the cell surface was examined in rat hepatocytes. PE is synthesized in the endoplasmic reticulum from cytidine diphosphate (CDP)-ethanolamine and in the mitochondria by decarboxylation of PS [18]. Rat hepatocytes were first incubated with radiolabeled ethanolamine or serine, which are precursors of PE. The amount of newly synthesized

PE incorporated into the cell surface was determined by reaction with trinitrobenzene sulfonate (TNBS) to produce N-trinitrophenyl-PE. TNBS only reacts with PE when it is located on the outer surface of cells [18]. The amount of PE incorporated into the cell surface did not change in the absence or presence of brefeldin A, which disrupts protein trafficking via the Golgi [18]. This observation implies that lipid transport is not solely dependent on vesicular trafficking. Moreover, since spontaneous lipid exchange is a slow process, this type of transfer mechanism alone is insufficient to support the observed lipid transport [19]. Therefore, this observation further supports the involvement of proteins in lipid trafficking.

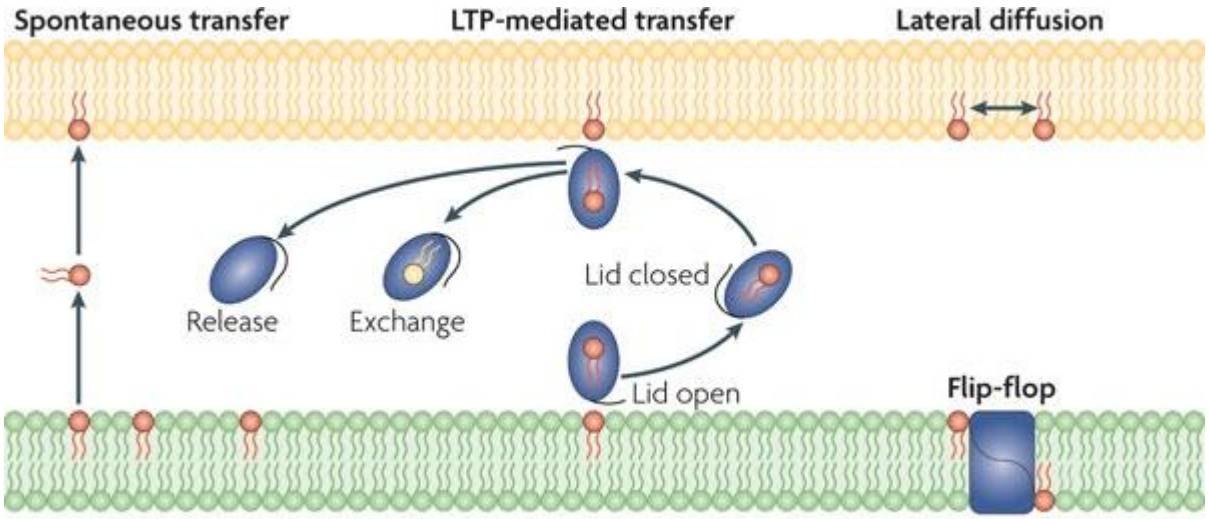

Figure 2: Types of non-vesicular lipid transfer mechanisms.
Shown here is an illustration of the intermembrane and intramembrane non-vesicular lipid transport mechanisms. Intermembrane transport includes spontaneous and LTP-mediated transfer while intramembrane transport comprises both flip-flop and lateral diffusion. (Reproduced with permission from reference 14)

LTPs were first discovered as soluble factors that accelerate lipid exchange between membranes *in vitro* [14]. Since then, many LTPs have been identified and they can be grouped according to the type of lipid they transfer: phospholipid transfer proteins,

fatty acid transfer proteins, sterol transfer proteins and sphingolipid transfer proteins. Generally, LTPs transfers a single lipid molecule at a time and are specific for one type of lipid molecule. However, some LTPs can bind more than one lipid molecule [14]. A summary of the non-vesicular transport mechanisms is shown in **Figure 2**.

1.4 The Phosphatidylinositol Transfer Protein Family

1.4.1 Introduction

It is understood that PI transport is essential for supplying PI to other non-ER membrane compartments for the generation of phosphoinositides and for structural purposes. As mentioned previously, PI transfer is accomplished by means of vesicular transport and/or carrier proteins. Carrier proteins that have the capacity to bind and transfer PI *in vitro* in an energy-independent manner have been identified. This group of transfer proteins is collectively known as the phosphatidylinositol transfer proteins (PITPs). The unique feature of these proteins is their capacity to not only bind PI but PC also. However, PITPs have a 16-fold higher affinity for PI compared to PC and accommodate only one lipid molecule at a time [20].

PITPα, the first mammalian PITP discovered, was purified in 1974 from brain cytosol [21]. The purified protein was found to exist as two species that differ only by charge. This charge variance was attributed to the type of ligand that was bound to PITPα. The more negatively charged species was found to contain PI while the less negatively charged form bound PC [22]. Since the discovery of PITPα, the number of PITP proteins has expanded. Currently, there are at least five PITP proteins in humans that can be grouped as Class I and II PITPs [22].

Class I PITPs consists of PITPα and PITPβ, which share 77 % sequence identity and 94% sequence similarity [23]. Both PITPα (270 amino acids) and PITPβ (270 amino acids for sp1 and 271 amino acids for sp2) are soluble proteins with a molecular weight of ~32 kDa containing a single lipid-binding domain (the PITP domain). The gene locations for both proteins are on chromosome 17q13 and 22q12 respectively [24]. PITPβ can be alternatively spliced to produce two splice forms, sp1 and sp2, which differ by 17 amino acids at the C-terminus [24]. In addition, studies revealed that PITPβ is capable of transferring sphingomyelin in addition to both PC and PI [25]. While PITPα is mainly localized in the nucleus and cytoplasm, PITPβ is associated with the endoplasmic reticulum and Golgi apparatus [25]. PITPα is highly expressed in the brain while PITPβ is found mainly in liver cells [23]. Their different localization and expression imply that both proteins perform different functions.

PITPα is believed to play a role in neuronal, liver, and intestinal function [26]. When PITPα expression is reduced, as seen in the mouse *vibrator* phenotype, neurodegeneration in the brain and spinal cord is observed. Moreover, *vibrator* mice die thirty days after birth [27]. The *vibrator* phenotype is a result of a mutation that involves a retroposon insertion in an intron of the PITPα gene, *PITPNA*. Consequently, both mRNA levels and protein expression are reduced [27]. However, mice that completely lack PITPα not only exhibit spinocerebellar disease but also possess lower body fat and abnormal accumulation of lipids in both enterocytes and hepatocytes. In addition, these mice are hypoglycemic and are prone to neonatal death. Both the intestinal disorder and hypoglycemia can be rectified by re-expression of PITPα but not the neonatal lethality [26].

PITPβ, on the other hand, was observed to be required for the Golgi-endoplasmic reticulum retrograde traffic and the maintenance of PI(4)P levels in Golgi membranes [27]. PITPβ was deemed to play an essential role in mammals compared to PITPα. Deletion of the PITPβ gene in murine cells was shown to be embryonically lethal [28]. In PITPβ knockdown cells, defects in the retrograde transport between the Golgi complex and ER were observed. The retrograde transport can be restored by the expression of wild type PITPβ [23]. The PITPβ knockdown cells also displayed a decrease in PI(4)P levels suggesting that PITPβ may play a role in maintaining the levels of this lipid in the Golgi. The details of this mechanism are still not fully established. In fact, the cellular functions of both PITPα and PITPβ remain unclear. The close association of PITPs with signaling molecules, particularly the phosphoinositides, poses a challenge in deciphering their actual cellular function. This closely linked relationship between the PITPs and phosphoinositides makes it difficult to differentiate whether an outcome is the result of a PITP malfunction or a defect in phosphoinositide signaling.

The Class II PITPs encompasses both single domain (RdgBβ) and multi-domain (RdgBαI and RdgBαII) proteins. The PITP domain of these proteins share approximately 40 % sequence identity with PITPα. Similarly to PITPβ, RdgBβ undergoes alternative splicing to generate two variants, sp1 and sp2, that vary at the C-terminus [27]. The RdgBα proteins are large proteins containing the PITP domain at the N-terminus. These proteins also possess a FFAT motif (diphenylalanine, **FF**, in an **A**cidic **T**ract), a DDHD heavy-metal binding domain and a LNS2 domain (Lipin/Ned1/Smp2) [24]. The FFAT motif acts as a targeting signal to the endoplasmic reticulum via interaction with VAP proteins (VAP stands for VAMP-associated-protein; VAMP stands for vesicle-associated

membrane protein) [29]. The DDHD domain contains four non-contiguous conserved amino acid residues: three aspartates and a histidine that form a metal binding site. However, the function of the LNS2 domain remains to be defined [24]. Given that the multi-domain RdgBα proteins possess the capacity to target membranes with the aid of targeting signals, the following question arises for the single domain PITPs: how do these proteins identify their target membranes for transferring PI or PC? The focus of this thesis will be addressing this question for the Class I PITPs.

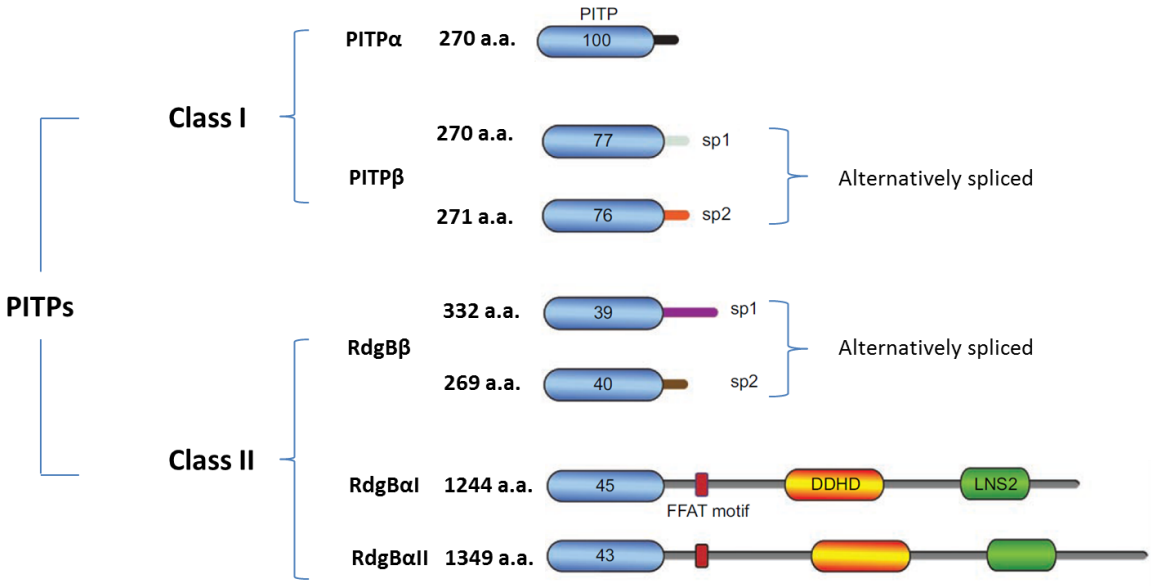

Figure 3: The human PITP family and their domain structure.
The human PITP family consists of five members grouped into two classes – Class I and II. Each member possesses the PITP domain (blue) at the N-terminus. Class I PITPs consists of PITPα and PITPβ which are single domain proteins. Class II PITPs are made up of both single (RdgBβ) and multi-domain proteins (RdgBαI and RdgBαII). Both PITPβ and RdgBβ undergo alternative splicing to produce two variants that differ at the C-terminus. The other domains present are colour coded: red (FFAT), orange (DDHD) and green (LNS2). The number of amino acids and percent sequence identity of the PITP domain for each member is shown as well. (Adapted with permission from reference 27)

1.4.2 The PITP Domain Structure

The crystal structures of PITPα in the ligand-bound (either with PC or PI) and the apo form have been solved by x-ray diffraction [30-32]. Rat PITPα was used to generate the PC-loaded structure (PDB code: 1T27) while human PITPα was used to produce the PI-loaded form (PDB code: 1UW5). Human PITPα shares an almost identical sequence to rat PITPα with the exception of a single deletion at position 52 and conservative changes I140V and K219R [30]. For convenience and consistency purposes, the rat numbering system for PITPα will be used throughout this thesis. Comparison between human PITPα-PI and rat PITPα-PC reveal no significant difference in the overall protein conformation with a root mean square deviation (rmsd) of 0.914 $Å^2$ – **Figure 4** [33]. The crystal structure of rat PITPβ bound to PC has also been resolved. When compared to human PITPα-PC, no substantial change was observed to the overall protein fold; the rmsd calculated was 0.934 $Å^2$ - **Figure 4** [25, 33].

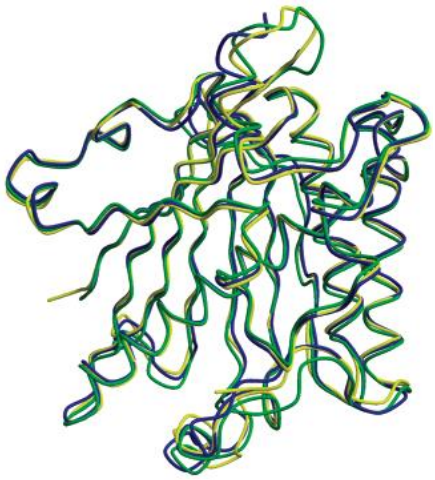

Figure 4: Superposition of rat and human PITPs
The green trace represents rat PITPα, the golden trace is human PITPα and the blue trace signifies rat PITPβ. (Reproduced with permission from reference 33)

The ligand-bound conformations of both PITPα and PITPβ, regardless of species origin, reveal the presence of a single phospholipid binding site. This lipid binding cavity is a characteristic feature of LTPs and accommodates a single lipid molecule. In PITPs, this binding site is made up of eight β-strands flanked by two long α-helices, helices A (residues 14-33) and F (residues 206-236) [34]. The binding site is closed by a "lid" that is made up of a C-terminal α-helix (G helix, residues 240-261) and an 11 amino acid extension. The "lid" also contains another small helix (helix B, residues 70-75) which is referred to as the "lipid exchange loop" [32]. In addition to the hydrophobic pocket, there are three α-helices that make up the regulatory loop – **Figure 5**. This loop region contains a serine residue, S166, which is conserved in almost all PITPs. S166 is located in a consensus sequence for phosphorylation by protein kinase C [34]. The specific role of PITP's regulatory loop remains to be established.

Comparison between the ligand-bound and apo state of PITP reveal that the G-helix adopts a different conformation in the apo form – **Figure 5**. In the ligand-free state, the G-helix is dislodged by 20 ° exposing hydrophobic residues that reside in the lipid-binding pocket. In addition, the lipid exchange loop is swung out by 90 ° contributing to the opening of the hydrophobic cavity [32]. It is unlikely that PITP will adopt this conformation in solution as exposing so much of the hydrophobic surface would be thermodynamically unfavorable. Studies revealed that the C-terminus of PITPα is subject to trypsin digestion only in the presence of lipid vesicles. This observation implies that PITPα adopts a tightly closed conformation in an aqueous environment (while transporting lipids) but adopts an open conformation upon interaction with vesicles [35]. Therefore, it is proposed that the open conformation is likely to occur only when PITP is

bound to membranes. The opening of the cavity either allows the protein-bound phospholipid to access entry into the membrane's interface or phospholipids from the membrane to access the hydrophobic cavity for transport purposes [27]. The open conformation thus provides a structural basis for the extraction of PC or PI by PITPs [32].

Observations of the ligand-bound structure reveal that the phospholipid molecule is buried within the protein. The lipid-binding site is composed of a polar binding pocket and two hydrophobic channels [27]. The polar binding pocket, located at the opposite end of the cavity's opening, recognizes the phospholipid head-groups. The fatty acid chains are located in the two hydrophobic channels which projects toward the opening of the cavity [27]. This closed conformation of PITP provides a means by which PITPs transfers its ligands through aqueous environments.

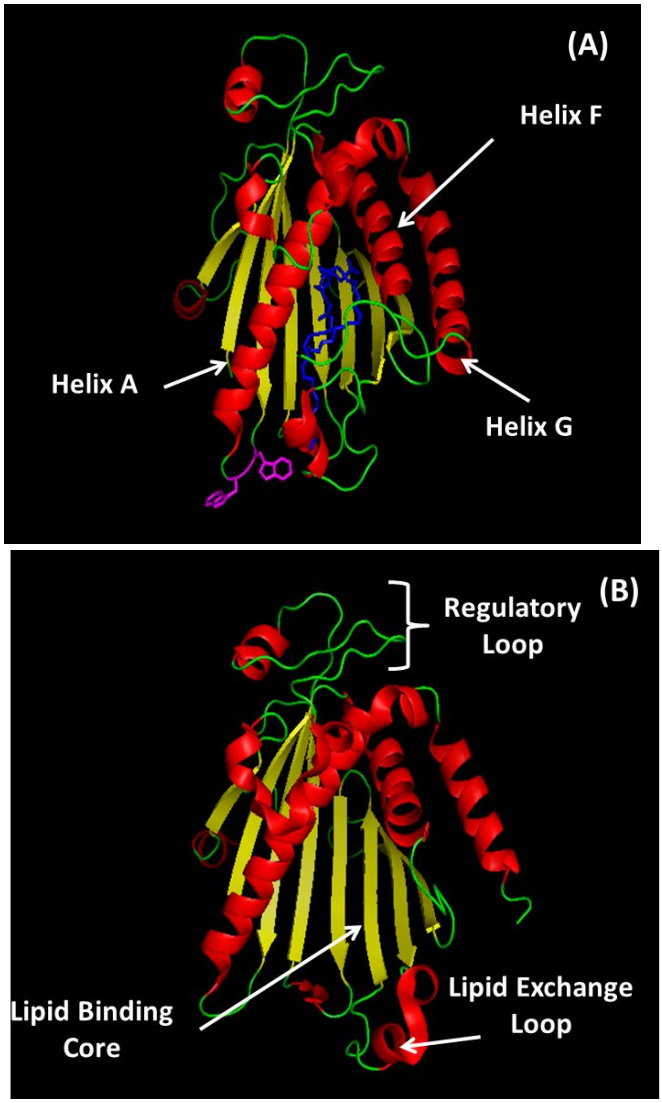

Figure 5: Closed (A) and open (B) conformation of PITPα.
For both structures the beta sheets are in yellow, alpha helices are in red and loops are in green. The lipid binding core is made up of the eight β-strands and α-helices A and F. The 'lid' region is made up of helix G and an 11 amino acid extension. The lipid exchange loop also make up part of the 'lid'. Three helices form the regulatory loop. PC is shown in blue and two tryptophan residues (W203/W204) involved in membrane binding are highlighted in purple. Structures were generated by PYMOL software using Protein Data Bank (PDB) files 1T27 and 1KCM.

1.4.3 PITP Membrane Docking

In order for PITP to bind to membranes and facilitate lipid exchange, a mechanism is required to explain the conformational change involved in this process. Two tryptophan residues at positions 203 and 204 have been identified to play a role in the membrane docking process of PITP – violet residues in **Figure 5A**. Both tryptophan residues are exposed on the loop between β-strand 8 (residues 191-201) and α-helix F (residues 206-236) instead of being buried in the protein core [30]. Mutation of both W203 and W204 to alanine results in a loss of membrane docking and lipid transfer [30, 36]. This evidence was observed in two different *in vitro* assays. The first assay utilized permeabilized HL60 cells as the donor membrane, while the second assay used rat liver microsomes. The acceptor membranes in both assays were synthetic liposomes consisting of 98 mol% PC and 2 mol% PI [36-37]. In both assays, the donor membranes were labeled with either [^{3}H]PI or [^{3}H]PC and the amount of radioactivity transferred to the acceptor liposomes was quantified to determine transfer activity. In the presence of the W203A/W204A mutant both PI and PC transfer was diminished [30, 36-37]. However, the W203A/W204A mutant was still able to bind to either PI or PC but significantly lower compared to wild type PITPα [30].

The Orientation of Proteins in Membranes (OPM) database is a web resource providing a collection of transmembrane, peripheral and monotopic integral proteins whose position in the lipid bilayer has been determined theoretically. The purpose of the OPM is to determine the optimal membrane positions of membrane-associated proteins which are important for biological function [38]. The method used here for membrane positioning is based on the minimization of the transfer energy of the protein from water

to a planar hydrophobic slab, which is a crude approximation of the membrane bilayer. The original method employed decadiene as a representation of the planar slab. However, in an updated method, the decadiene was replaced with 1,2-dioleoyl-sn-glycero-3-phosphocholine (DOPC) [38].

The structures in **Figure 6** were obtained from the OPM database which depicts PITPα in both the ligand-bound and ligand-free conformations with respect to a membrane bilayer. By visual observations, both W203 and W204 appear to be buried deeper into the membrane bilayer when PITPα is in the open conformation as opposed to the closed conformation. Theoretical calculations revealed that the protein depth with respect to the membrane is 2.3 ± 1.9 Å in the closed conformation compared to 5.3 ± 1.4 Å in the open conformation [39]. This information provides a plausible explanation for PITPs to have a higher binding affinity to membranes in the open conformation where it can either extract or deposit the phospholipid ligand. In contrast, in the closed conformation, PITPs would penetrate the membrane bilayer to a lesser extent, which implies a lower binding affinity for the membrane bilayer. This in turn promotes the ligand-bound PITP to dissociate and target the next binding site.

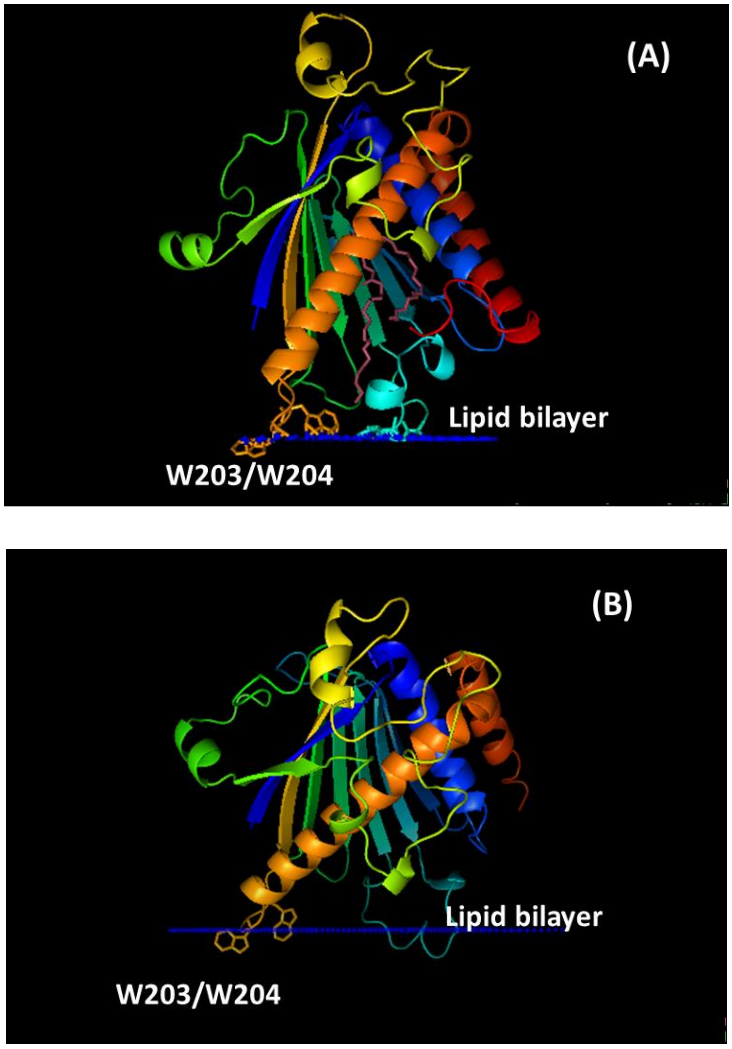

Figure 6: Orientation of PITPα in membranes – closed (A) versus open (B) conformation.
The blue dots are a representation of the calculated membrane bilayer. Both W203 and W204 are shown in stick form. Calculated protein depth for (A) was 2.3 ± 1.9 Å and for (B) was 5.3 ± 1.4 Å. Structures were generated using the PYMOL software obtained from the OPM website.

In addition to the double tryptophan residues, the lipid-exchange loop also appears to penetrate the membrane bilayer. Tilley *et al.* performed a mutational analysis on F72 located within this loop, which has the most likelihood to have membrane interaction properties. The F72A mutant was completely functional in the lipid binding and transfer assay [30]. This implied that the lipid-exchange loop is not critical for PITP

membrane docking compared to W203 and W204. Tryptophan residues are commonly associated with membrane interactions due to their physicochemical properties [40]. It is therefore proposed that insertion of both W203 and W204 into the membrane bilayer may cause an indirect perturbation of the 'lid' region eliciting a conformational change from the closed to the open state. In fact, it has been observed that one or two tryptophan residues at these positions are conserved in most of the PITP members [27].

1.4.4 PITP Ligand Binding: PC versus PI Binding

Observations of the closed conformation of PITPα loaded either with PC or PI revealed that both phospholipid molecules occupy the same shape within the lipid-binding pocket. The main difference between the two structures, PC-PITPα and PI-PITPα, is that PI makes more hydrogen bond contacts with specific amino acids within the polar lipid-binding pocket via its inositol head-group [27, 30]. This evidence accounts for the higher affinity of PITPs for PI compared to PC, nearly 16-fold greater as determined through relative affinities [20, 41]. To date, no actual K_d values have been reported for PITP binding to its ligands. In mammalian cells, PC makes up about 50 mol% of cellular phospholipids while PI makes up approximately 15 mol% [5]. Therefore, it is plausible that PITP's higher affinity for PI compensates for the lipid distribution of PI in mammalian cells.

The amino acid residues that contact the phospholipid head-group can be divided into three main groups: (i) residues that contact both PC and PI; (ii) residues that are important for PI binding; and (iii) residues that are important for PC binding – **Figure 7**. The residues that recognize both PC and PI do so by making contacts with the phosphate moiety. Specifically, Q22 and T114 form hydrogen bonds to the phosphate moiety via a

water molecule while T97 and K195 directly hydrogen bond to the phosphate moiety [27, 30, 34].

The residues that have been identified that are unique for the binding of PI include T59, K61, E86 and N90. These four residues are located on two separate β-strands and are conserved in all PITP proteins [34]. Besides interacting with the head-group of PI, both T59 and E86 also interact with the head-group of PC but in distinct ways. Therefore mutation of either T59 or E86 affects both PI and PC binding. However, the effect of the mutation is dependent on the type of amino acid substitution. In contrast, mutation of either K61 or N90 results in a decrease of PI binding and transfer with K61 providing the most significant loss. PC binding and transfer remained unaffected upon mutation of either K61 or N90. Hence, it can be inferred that both K61 and N90 are suitable residues for examining PI and PC binding and transfer by PITPs since these residues are able to differentiate between PI and PC binding [23, 27, 30].

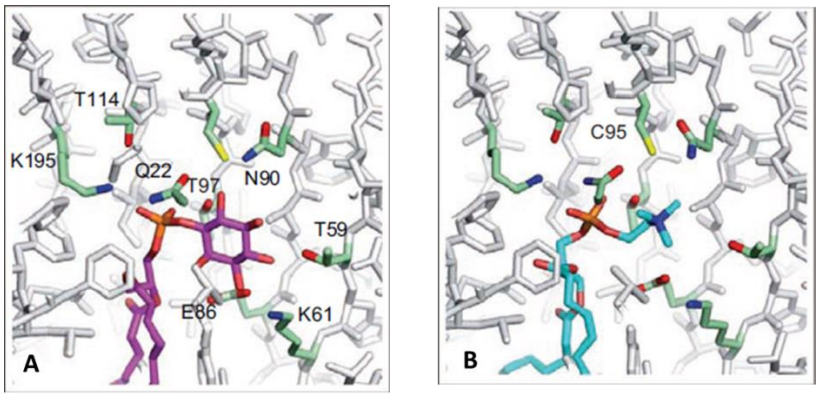

Figure 7: The lipid binding site of PITPα with PI (A) and PC (B).
The four residues that contact the phosphate moiety of the phospholipid ligand include Q22, T97, T114 and K195. The residues important for PI binding include T59, K61, E86 and N90. C95 that is important for PC binding is also shown. (Reproduced with permission from reference 27)

C95 is a residue that is important for PC binding. C95 resides in the lipid-binding cavity and hydrogen bonds to the PC head-group indirectly via a water molecule. Mutation of this residue to threonine and/or alanine reduced PC but not PI transfer. C95 is conserved only in the Class I PITPs. In Class II PITPs C95 is replaced by threonine suggesting that PC binding and transfer may not be essential for the Class II PITPs [34]. Another residue that has been identified to play a role in PC binding is F225. When phenylalanine was replaced with leucine, a small aliphatic residue, as found in rodent PITPβ, PC transfer activity was lowered by nearly half compared to PITPα [33]. Similar to C95, F225 is conserved in Class I but not Class II PITPs. In Class II PITPs, residue 225 is variable in different PITPs [34]. For example, human RdgBα possess an alanine at this position while human RdgBβ contains a glycine; both residues contribute to a lower PC transfer activity in human RdgB proteins [27]. This suggests that the human RdgB proteins may play a lesser role in PC transfer compared to the Class I PITPs.

1.4.5 PITP Lipid Exchange Model

Studies show that PITPs is linked to the production of phosphoinositides. One such study revealed that both PITPα and PITPβ enhanced the phosphorylation of PI to PI(3)P using an *in vitro* lipid kinase assay [34]. In addition, the yeast PITP, Sec14p, was also able to enhance the production of PI(3)P using the same assay. Sec14p possess a similar biochemical activity as PITPs but does not share any sequence or structural homology [34]. It was also observed that phosphoinositide production was only enhanced in the presence of wild type PITPs and not PITP mutants that lack PI binding and transfer activity. Therefore, the PI binding and transfer activity is crucial for the generation of phosphoinositides [34].

The molecular mechanism for PITPs remains to be fully established. So far, two models have been proposed to explain the molecular mechanism of PITPs: the PI delivery model and the PI presentation model – **Figure 8** [34]. The PI delivery model suggests that the main role of PITPs is to simply transfer PI from the ER to other non-ER membrane compartments. In this manner, membranes that lack and require PI are ensured a constant supply of PI. On the other hand, in the PI presentation model, instead of delivering PI to the membrane, a PITP presents its PI ligand to lipid kinases for phosphorylation to occur [34, 42-43]. As of yet, there is no concrete evidence to prove one model over the other.

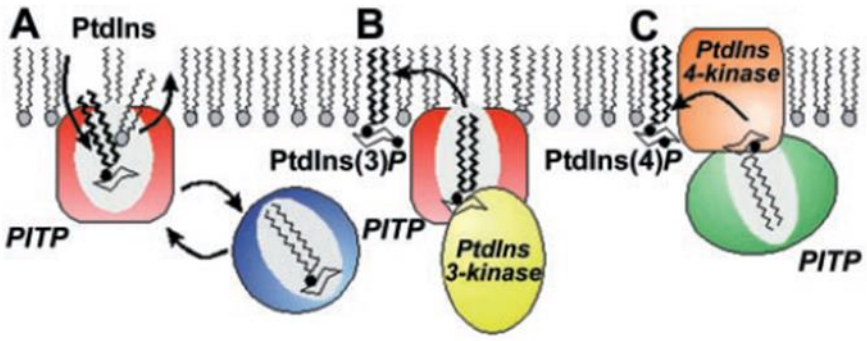

Figure 8: Proposed molecular mechanisms of PITPs.
A – The lipid delivery model; PITP delivers its phospholipid ligand directly to membranes. B and C – The lipid presentation model; PITP presents PI cytosolic PI 3-kinase and membrane-bound PI 4-kinase for phosphorylation to occur. (Reproduced with permission from 31)

Structural analyses and *in vitro* studies both indicated that PITPs are designed to bind and transfer lipids. However, a lipid exchange activity has not been previously shown in intact cells. On the basis of this query, Shadan *et al*. carried out investigations that showed membrane interactions by PITPα and PITPβ in intact cells. Their study involved using *N*-ethylmaleimide (NEM) as a tool to determine PITPs' membrane

association in intact cells [36]. C95 located in the lipid-binding pocket of PITP can be covalently modified by NEM. Since C95 is buried deep in the lipid-binding cavity, NEM can only access C95 when PITP is in the open conformation. In other words, C95 is only accessible to NEM when PITP is undergoing lipid exchange at the membrane [36]. The outcome of this study showed that PITPs are continuously associating with membranes as determined by the amount of protein retained in the membrane versus cytosolic fractions [36]. Interestingly, PITPβ appeared to have a higher propensity for membrane interactions compared to PITPα. Within a 10 minute time frame, nearly 90 % of PITPβ interacted with membranes whereas only 50 % of PITPα was found to be membrane associated [36]. Moreover, when the mutant form of PITP was used (W203/W204A), no membrane interaction was observed. This piece of evidence further verifies the significance of W203 and W204 in the membrane docking process of PITP [36]. The data provided by Shadan *et al.* provides a basis that PITPs are likely to function as LTPs – in other words PITPs delivers PI from one membrane site to another.

Thus the current lipid exchange model of PITPs can be described as follows – **Figure 9**. PITPs transfers PI/PC in the closed conformation shielding the phospholipid ligand from the surrounding aqueous environment. Upon docking to a membrane via the two tryptophan residues, PITPs take on the open conformation allowing the exchange of PI for PC or vice versa. PITPs then revert back to the closed conformation and diffuse away from the membrane [36].

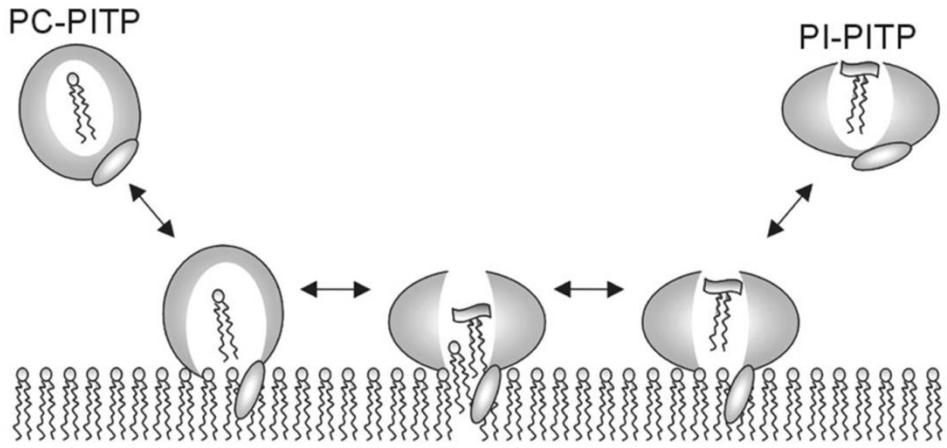

Figure 9: Proposed lipid exchange model by PITPs.
PITPs transfer either PI/PC in the closed conformation. PITPs docking unto membranes are aided by W203 and W204 residues and consequently PITP adopts an open conformation allowing lipid exchange to occur. PITPs then take on the closed conformation with its new ligand and diffuse away. (Reproduced with permission from reference 32)

1.5 Drosophila RdgBα

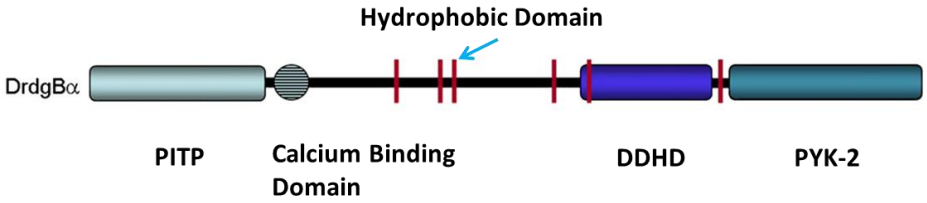

Figure 10: The domain structure of Drosophila RdgBα.
RdgBα comprises an N-terminal PITP domain, a calcium binding domain and six hydrophobic regions for membrane association. In addition, RdgBα also holds a metal binding site (DDHD) and a PYK-2 domain for interaction with protein tyrosine kinases. (Reproduced with permission from reference 44)

*R*etinal *deg*eneration *B* (RdgB) is a name derived from a *Drosophila* protein mutant whose phenotype exhibits degeneration of photoreceptors. The gene encodes a 160 kDa protein referred to as *Drosophila melanogaster* RdgBα [45-46]. RdgBα is a

multi-domain protein with an N-terminal PITP domain (281 residues) which shares about 40 % sequence identity with PITPα – **Figure 10** [47]. The PITP domain has been shown to possess PC/PI binding and transfer activity [46-47]. In addition to the PITP domain, RdgBα contains a short acidic region of 15 amino acid residues and six small hydrophobic domains. The acidic region, enriched in glutamic and aspartic acid residues, is proposed to be involved in calcium binding while the hydrophobic domain is thought to interact with membranes [44]. RdgBα also holds a DDHD domain that may be involved in metal binding and a PYK-2 binding domain. The PYK-2 binding domain is believed to aid in association with protein tyrosine kinases [44]. The isolation of RdgBα consequently led to the discovery and nomenclature of the human Class II PITPs.

Drosophila photoreceptor cells are polarized cells that contain an apical domain known as the rhabdomere – **Figure 11**. The rhabdomere is composed of microvilli and is the site for $PI(4,5)P_2$ hydrolysis. RdgBα is located on a region known as the subrhadomeric cisternae (SRC) [27, 44]. The SRC is located in close proximity to the rhabdomere and is continuous with the ER of the photoreceptor cell, where PI synthesis occurs. Hydrolysis of $PI(4,5)P_2$ by phospholipase Cβ, with the assistance of the G-protein, G_q, is part of the phototransduction pathway in *Drosophila* and is initiated by rhodopsin [27, 44]. The phototransduction pathway consumes $PI(4,5)P_2$ generating both inositol 1,4,5 triphosphate (PI3) and DAG. Therefore the levels of $PI(4,5)P_2$ must be replenished during cell signaling. DAG can be recycled to form PI by the following enzymes: DAG kinase (RdgA), CDP-DAG synthase (cds) and PI synthase (PIS). These enzymes are located in the SRC and mutations in these enzymes lead to retinal degeneration – **Figure 11** [27]. As of yet, it is still not understood how DAG is

transported to the SRC. Since RdgBα is located at the SRC it is proposed that RdgBα functions to deliver PI to the rhabdomere to maintain PI(4,5)P_2 levels [27, 44]. The PITP domain of RdgBα alone has shown the ability to prevent photoreceptor degeneration in mutant flies, *rdgB*^{2}, which are characterized by retinal degeneration [47]. This piece of evidence suggests that the main function of RdgBα is PI transfer.

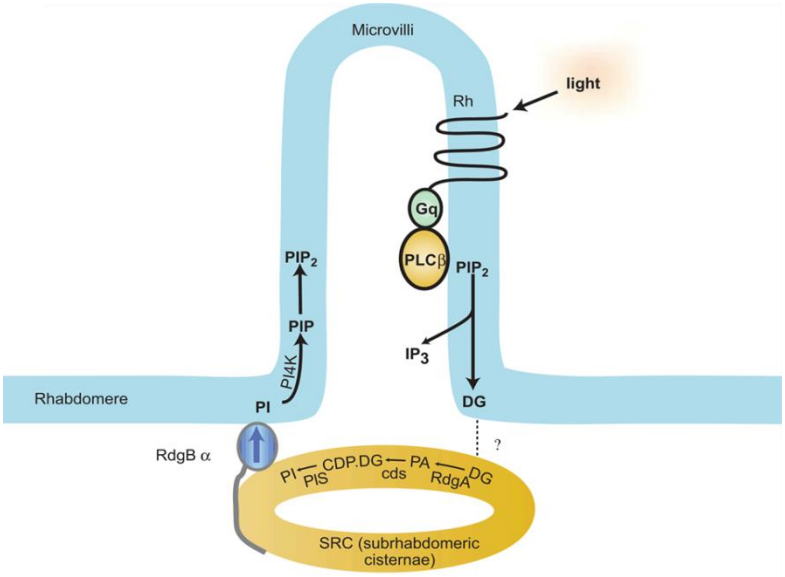

Figure 11: Proposed function of RdgBα in *Drosophila* phototransduction.
Photoreceptor cells of Drosophila contain an apical domain (rhabdomere) which is composed of microvilli. Phototransduction, initiated by rhodopsin (Rh), takes place at the microvilli and involves PI(4,5)P_2 hydrolysis by PLCβ via G-protein, G_q. Depletion of PI(4,5)P_2 requires replenishing of PI in the rhabdomere. RgdBα is located in the SRC and is proposed to supply PI to the rhabdomere via its PITP domain. At the rhabdomere, it is believed that PI is first converted to PI(4)P and subsequently PI(4,5)P_2. (Reproduced with permission from reference 27)

1.6 Protein-Membrane Interactions

Recruitment of soluble proteins to membranes is an integral part of many biological processes including cell signaling and membrane trafficking [48]. Peripheral proteins can interact reversibly with lipid membranes through one of these methods: (i)

recognition of lipid species, predominantly phosphoinositides, by lipid-binding domains; (ii) insertion of an amphipathic helix or a hydrophobic loop; and (iii) recognition of physicochemical parameters of the membrane including electrostatics, curvature or lipid packing [49-51].

1.6.1 Recognition of Lipid Species by Lipid Binding Domains

To date, at least 10 different globular lipid-binding domains have been identified and are being investigated. While most of these domains target phosphoinositides, a handful of these domains target other lipid species that include phosphatidylserine (PS) and phosphatidic acid (PA) [52]. The interaction between these lipid-binding domains and membranes can be highly specific or non-specific. The highly specific association usually involves recognition of a specific lipid species within the membrane while the non-specific interaction involves attraction to a physical property of the membrane such as charge and/or curvature [52]. The first phosphoinositide-binding domain reported was the 'pleckstrin homology' or PH domain [52]. The designation of the PH domain stems from the identification of an amino acid sequence that occurs twice in pleckstrin, the major protein kinase C (PKC) substrate in platelets [52]. The PH domain is conserved among a large number of proteins. For example, the PLCδ1 PH domain binds $PI(4,5)P_2$ and its head-group IP_3 while that of Akt/PKB (protein kinase B) binds both $PI(3,4,5)P_3$ and $PI(3,4)P_2$ [49]. An example of a non-phosphoinositide lipid-binding domain is the C2 domain found in PKCα. This C2 domain is a phosphatidylserine-binding domain [52].

1.6.2 Insertion of Amphipathic Helix or Hydrophobic Loop

In addition to lipid recognition by protein domains, the direct protein insertion into membranes is another type of protein-membrane interaction. Proteins that employ this method of interaction generally utilize an amphipathic helix or a hydrophobic loop for membrane insertion [51]. When the amphipathic helix is used, the helix is inserted into the membrane with the hydrophilic surface facing the cytosol while the hydrophobic surface is buried in the membrane hemilayer [51]. An example of a protein that exploits this type of protein-membrane interaction is ArfGAP1 (ADP-ribosylation factor GTPase-activating protein 1) which is involved in COPI coat disassembly. ArfGAP1 have been found to contain an amphipathic lipid packing sensor (ALPS) motif, which appears unstructured in solution. However, upon binding to membranes, this motif forms an amphipathic helix that has a propensity for membrane curvature and loosely packed lipids [51].

1.6.3 Recognition of Physicochemical Parameters of the Membrane by Proteins

A third mechanism employed by peripheral proteins in membrane interactions involves the recognition of the membrane's physicochemical properties, which includes charge, lipid packing, and curvature. Biological membranes contain varying amounts of anionic lipids largely PS, PI, and phosphoinositides. Protein-membrane association is thus facilitated via electrostatic interactions between anionic lipids and cationic patches located on peripheral proteins. However, electrostatic interactions alone are inadequate in anchoring peripheral proteins to membrane surfaces [50]. Instead it has been suggested that electrostatic interactions may direct initial protein docking unto membranes. Consequently, hydrophobic insertion is required to form a stable membrane

interaction [50]. The glycolipid transfer protein (GLTP) is an example of a LTP whose initial binding to membranes is influenced by electrostatic interactions. GLTP is a 24 kDa protein that transfers glycolipids between membrane compartments *in vitro* and is positively charged at neutral pH (pI=9.0) [53]. Studies revealed that the presence of negatively charged lipids increases the affinity of GLTP for lipid membranes [54]. In addition to electrostatic interactions, it has been shown that a tryptophan residue, W142, is also important for GLTP's membrane interaction [55].

Lipid-packing defects in membranes are imperfections in the geometrical arrangement of lipid molecules [49]. Lipid-packing defects are brought about by the inherent shape of non-cylindrical lipids. For example, phosphatidylethanolamine (PE) adopts a conical shape due to its smaller head-group in comparison to its fatty-acid tail [49]. Lysophosphatidylcholine (LPC) on the other hand, possesses an inverted cone shape due to its larger head-group relative to the single acyl chain [56]. Lipid packing defects in membranes are also influenced by the fatty acyl chains. Fatty acyl chains that contain a 'kink' due to the presence of double bonds such as the oleyl chain (C18:1) are thought to occupy a larger conformational space due to mobile bond rotation next to the double bonds compared to fatty acyl chains that lack a 'kink'. Therefore, lipid packing in membranes is dependent on two factors: 1) the ratio between small and large lipid head-groups; and 2) the ratio between saturated and unsaturated fatty acyl chains [52]. Examples of proteins whose membrane interactions are influenced by lipid-packing include GLTP and ceramide transfer protein (CERT). GLTP has shown to preferentially bind to tightly-packed membranes. However, GLTP-mediated transfer activity is greater from more fluid membranes [57]. CERT, a 68 kDa protein, consists of three domains:

steroidogenic acute regulatory protein-related lipid transfer (START) domain, PH domain and FFAT motif. The START domain located at the C-terminal end is responsible for ceramide transfer. The PH domain located at the N-terminal end is involved in protein binding to the Golgi while the FFAT motif targets the protein to the ER [58]. Studies reveal that the intermembrane ceramide transport by CERT is preferred when ceramide is present in a fluid environment [58].

Biological membranes are understood to be dynamic in nature. At any given time, numerous processes are taking place from membrane remodeling to membrane-protein interactions. The majority of these activities influence local membrane curvature. There are several means by which changes to membrane curvature can arise including lipid metabolism, protein scaffolding and protein interaction [51].

The inherent shape of each lipid molecule is different and is chiefly influenced by the compatibility between the size of the polar head-group and its fatty acyl chain [59]. A lipid molecule adopts a cylindrical shape when both the head-group and hydrophobic tail are compatible in cross-sectional size. A lipid molecule is conical when the tail is wider or inverted conical when the head-group is larger [59]. Enrichment of the membrane with any of these lipids in turn influences the local membrane curvature. While cylindrical-shaped lipids give rise to a planar bilayer, both conical and inverted conical lipids form negatively curved and positively curved monolayers respectively [59]. Enrichment of the membrane with any one of these lipids is brought about by an increase in lipid metabolism. Lipid metabolism in turn is achieved by means of lipid synthesis and/or lipid transport [51].

Membrane curvature can also be brought about by protein scaffolding. The most well-studied proteins that act as protein scaffolds include coat proteins such as clathrin, COPI and COPII (coat protein complex II) [60]. Clathrin plays a role in endocytosis, a process that involves the formation of vesicles from the plasma membrane to form endosomes. COPI/II proteins on the other hand mediate vesicle transport between the ER and Golgi apparatus [51]. These coat proteins deform the membrane by polymerizing into curved structures without direct membrane interactions. Instead, they interact with membranes via adaptor or cargo proteins [51, 60].

Finally, the third mechanism that induces membrane curvature involves direct protein interaction. Two well-known proteins that perform this function include the BAR proteins and the ArfGAP1 protein [51]. BAR proteins contain Bin-Amphiphysin-Rvs (BAR) domains, which are banana-shaped lipid binding domains. These lipid-binding domains associate with membranes via their concave surface [60]. BAR proteins mainly bind to membranes through electrostatic interactions. In contrast, the ArfGAP1 protein utilizes an amphipathic helix to induce membrane curvature by direct protein insertion into the membrane as described previously [51].

1.7 Research Outline

As mentioned previously, there are two theories regarding the molecular function of PITPs: the PI delivery model and the PI presentation model. The focus of this thesis is on investigating the ligand transfer mechanism by PITPs in order to gain a better understanding of the molecular function of PITPs. As yet, the details of the ligand transfer mechanism by PITPs remain to be fully established. Since PITPs lack membrane targeting signals, unlike other multi-domain LTPs, the question that needs to be

addressed is – how do PITPs recognize one membrane compartment from another during ligand transfer? One way of approaching this question is to examine the types of membrane environment that favor PITP binding to membranes. Specifically the role of lipid composition and the physicochemical parameters of membranes are investigated here to determine their effects on PITP binding to membranes.

At present there are several methods that can be used to study protein-lipid interactions including nuclear magnetic resonance (NMR) spectroscopy and differential scanning calorimetry (DSC) [61]. However, in this thesis, two main techniques are used: dual polarization interferometry (DPI) and fluorescence spectroscopy.

1.7.1 Dual Polarization Interferometry (DPI)

DPI is an optical technique that employs a sensor chip made of silicon oxynitride. The sensor chip consists of two optical waveguides stacked on top of each other; the top layer being the sensing waveguide while the bottom layer serves as the reference waveguide [62]. The surface of the sensing waveguide contains two etched sample wells where the analyte of interest may bind.

The principle of DPI can be explained as follows. Polarized laser light enters one end of the sensor chip, which then produces an interference pattern in the far-field. The interference pattern formed is dependent upon the phase relationship of the light that travels through and emerges from the two waveguides. When no analyte is bound to the surface of the sensor chip, light passing through both waveguides is in phase [62]. However, when an analyte is bound to the surface of the sensor chip, light passing through both waveguides is no longer in phase due to the change in refractive index at the sensing waveguide surface. Consequently, the interference pattern that is formed also

changes. In DPI two parameters of the polarized light are used instead of one – transverse electric (TE) and transverse magnetic (TM) – which provides two independent measurements. The resulting measurements can then be resolved into thickness, refractive index and mass values [62-63].

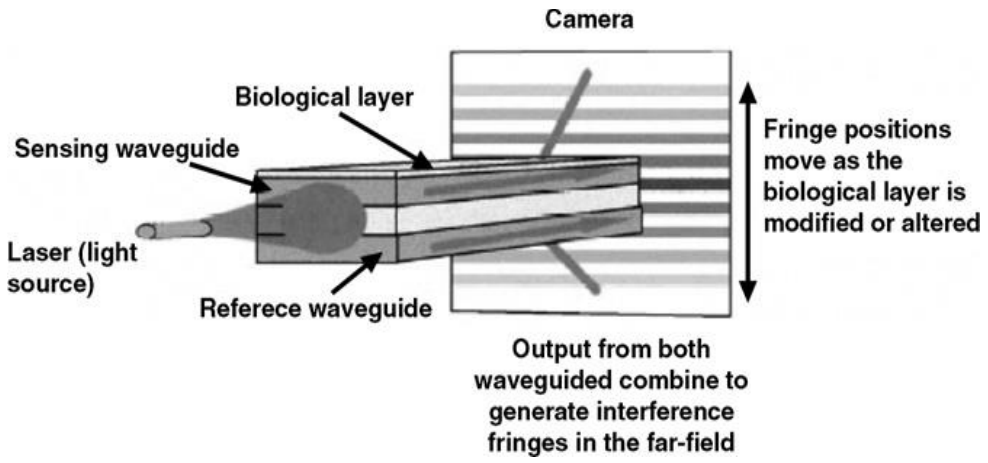

Figure 12: DPI principle.
Polarized light from a laser source passes through the sensor chip producing an interference pattern in the far-field. The interference pattern changes as analyte is bound to the sensor chip surface. (Reproduced with permission from reference 64)

In this thesis, the binding affinity of PITPs to immobilized planar lipid layers will be examined. Here, lipid vesicles will first be adsorbed and unrolled unto the sensor chip surface to produce a planar lipid layer. Consequently the interaction between PITPs and the lipid layer will be monitored by measuring the mass of PITPs bound to the chip surface.

1.7.2 Fluorescence Resonance Energy Transfer (FRET) Assay

In addition to measuring the binding affinity of PITPs to membranes, the ligand transfer rate of PITPs to membranes will also be examined. In order to achieve this, a fluorescence resonance energy transfer (FRET) based transfer assay will be employed.

FRET is the transfer of energy from an excited donor molecule to an acceptor molecule [65]. Energy transfer is manifested by the decrease in fluorescence (quenching) of the donor molecule or an increase in fluorescence of the acceptor molecule. However, the acceptor molecule does not necessarily have to be fluorescent. In order for FRET to occur, the fluorescence emission spectrum of the donor molecule must overlap the absorption or excitation wavelength of the acceptor molecule. Furthermore, both the donor and acceptor molecules must be in close proximity, typically between 1 – 10 nm [65].

In the FRET-based transfer assay, the rate at which PITPs can deliver its ligand to lipid vesicles of different compositions and size will be determined. In contrast, a FRET-based pick up assay will also be utilized to measure the rate at which PITP can extract its ligand from lipid vesicles. By employing both techniques, the aim of this thesis is to gain a better understanding of the interactions between PITPs and membranes in the hope of further understanding the ligand transfer mechanism of PITPs.

The proteins that will be examined in this thesis include the human PITPα and PITPβ. Three PITPα mutants will also be investigated which are W203A/W204A, K61A and C95A. While the W203A/W204A mutant lacks the capability to bind to membranes, K61A and C95A are unable to bind PI and PC respectively. Lastly, the *Drosophila* RgdBα and its mutant form Y210A/W211A, which is thought to mimic the human PITPα W203A/W204A mutant, will also be tested here. It should be noted that only the PITP domain of the RdgBα proteins will be examined here.

2. MATERIALS AND METHODS

2.1 Chemicals and Reagents

2.1.1 DNA Transformation, Bacterial Cell Culture and Protein Expression

Ampicillin (BioShop, Burlington, ON, Canada); 100 mg/mL in MilliQ (ultrapure water – 18.2 MΩ.cm) water

Chloramphenicol (BioShop, Burlington, ON, Canada); 25 mg/mL in MilliQ water

Sodium Chloride [NaCl] (Bioshop, Burlington, ON, Canada)

Yeast Extract (BioShop, Burlington, ON, Canada)

Tryptone (BioShop, Burlington, ON, Canada)

Agar (BioShop, Burlington, ON, Canada)

Isopropyl-D-thiogalactoside [IPTG] (BioShop, Burlington, ON, Canada); 1M in MilliQ water

2.1.2 DNA Isolation, DNA Digestion and DNA Gel Electrophoresis

NdeI Restriction Enzyme (New England BioLabs, Ipswich, MA, USA)

HindIII Restriction Enzyme (New England BioLabs, Ipswich, MA, USA)

DpnI Restriction Enzyme (New England BioLabs, Ipswich, MA, USA)

Boric Acid (Sigma-Aldrich, Oakville, ON, Canada)

Ethylenediaminetetraacetic acid [EDTA] (BioShop, Burlington, ON,Canada)

Agarose (BioShop, Burlington, ON, Canada)

HighRanger 1kb DNA Ladder (Norgen, Thorold, ON, Canada)

2.1.3 Polymerase Chain Reaction

PfuTurbo DNA Polymerase (Agilent Technologies, Santa Clara, CA, USA)

PCR Nucleotide Mix (Boehringer Mannheim, Laval, QC, Canada)

2.1.4 Protein Purification and Quantitation

TALON Metal Affinity Resin (Clontech, Moutain View, CA, USA)

Sodium Phosphate Monobasic (BioShop, Burlington, ON,Canada)

Imidazole (BioShop, Burlington, ON, Canada)

Glycerol (BioShop, Burlington, ON, Canada)

Triton X-100 (Sigma-Aldrich, Oakville, ON, Canada)

Deoxyribonuclease I (Invitrogen, Burlington, ON, Canada)

ProteoGuard EDTA-Free Protease Inhibitor Tablets (Clontech, Mountain View, CA, USA)

2-(N-Morpholino)ethanesulphonic acid [MES] (BioShop, Burlington, ON, Canada)

Piperazine-N,N-bis(ethanesulphonic acid) [PIPES] (BioShop, Burlington, ON, Canada)

Potassium Chloride [KCl] (Caledon Laboratories, Georgetown, ON, Canada)

Sodium Azide (BioShop, Burlington, ON, Canada)

Bradford Reagent (Sigma-Aldrich, Oakville, ON, Canada)

2.1.5 Sodium Dodecyl Sulfate Polyacrylamide Gel Electrophoresis (SDS-PAGE)

Tris(hydroxymethyl)aminomethane [Tris] (BioShop, Burlington, ON, Canada)

Glycine (BioShop, Burlington, ON, Canada)

Sodium Dodecyl Sulfate [SDS] (Sigma-Aldrich, Oakville, ON, Canada)

Dithiothreitol [DTT] (Sigma-Aldrich, Oakville, ON, Canada)

Bromophenol Blue (Sigma-Aldrich, Oakville, ON, Canada)

Ammonium Persulfate (BioShop, Burlington, ON, Canada)

Acrylamide/Bis-acrylamide 30 % (w/v) (BioShop, Burlington, ON, Canada)

Tetramethylethylenediamine [TEMED] (Bio-Rad, Hercules, CA, USA)

Methanol (Fisher Scientific, Fair Lawn, NJ, USA)

Acetic Acid (Caledon Laboratories, Georgetown, ON, Canada)

ProtoBlue Safe (Colloidal Coomassie G-250 Stain) (National Diagnostics, Atlanta, GA, USA)

Pre-stained Protein Marker Broad Range (New England BioLabs, Ipswich, MA, USA)

2.1.6 Western Blot

Fluka Skim Milk Powder (Sigma-Aldrich, Oakville, ON, Canada)

Tween-20 (Sigma-Aldrich, Oakville, ON, Canada)

Anti-His (Mouse) antibody [recognizes $(histidine)_6$-tagged proteins] (GE Healthcare Life Sciences, Baie d'Urfe, QC, Canada)

Anti-mouse IgG HRP conjugate (Promega, Madison, WI, USA)

3,3′,5,5′-Tetramethylbenzidine (TMB) liquid substrate system for membranes (Sigma-Aldrich, Oakville, ON, Canada)

2.1.7 Fluorescence-based Binding Assay

NBD C_{12}-HPC (2-(12-(7-Nitrobenz-2-Oxa-1,3-Diazol-4-yl)amino)Dodecanoyl-1-Hexadecanoyl-*sn*-Glycero-3-Phosphocholine) [NBD-PC] (Life Technologies, Burlington, ON, Canada)

Sucrose (BioShop, Burlington, ON, Canada)

2.1.8 Reduction of NBD-PC by Sodium Hydrosulfite

Sodium Hydrosulfite (Sigma-Aldrich, Oakville, ON,Canada)

2.1.9 Fluorescence Resonance Energy Transfer (FRET) Assays

L-α-phosphatidylcholine (Liver, Bovine) [Liver PC] (Avanti Polar Lipids Inc., Alabaster, AL, USA)

L-α-phosphatidylinositol (Liver, Bovine) [Liver PI] (Avanti Polar Lipids Inc., Alabaster, AL, USA)

L-α-phosphatidylserine (Brain, Porcine) [Brain PS] (Avanti Polar Lipids Inc., Alabaster, AL, USA)

1,2-dioleoyl-*sn*-glycero-3-phosphate [18:1 PA] (Avanti Polar Lipids Inc., Alabaster, AL, USA)

1,2-dioleoyl-*sn*-glycero-3-phosphoethanolamine-N-(lissamine rhodamine B sulfonyl) [18:1 Liss Rhod PE] (Avanti Polar Lipids Inc., Alabaster, AL, USA)

L-α-phosphatidylinositol-4-phosphate (Brain, Porcine) [Brain PI(4)P] (Avanti Polar Lipids Inc., Alabaster, AL, USA)

L-α-phosphatidylinositol-4,5-bisphosphate (Brain, Porcine) [Brain $PI(4,5)P_2$] (Avanti Polar Lipids Inc., Alabaster, AL, USA)

Phosphatidylinositol 3,4,5-trisphosphate diC16 [$PI(3,4,5)P_3$ diC16] (Echelon Biosciences Inc., Salt Lake City, UT, USA)

(N-(6-Tetramethylrhodaminethiocarbamoyl)-1,2-Dihexadecanoyl-*sn*-Glycero-3-Phosphoethanolamine) [TRITC DHPE] (Life Technologies, Burlington, ON, Canada)

2.1.10 Dual Polarization Interferometry

1, 2-dioleoyl-*sn*-glycero-3-phosphocholine [DOPC] (Avanti Polar Lipids Inc., Alabaster, AL, USA)

1, 2-dioleoyl-*sn*-glycero-3-phospho-L-serine [DOPS] (Avanti Polar Lipids Inc., Alabaster, AL, USA)

1, 2-dioleoyl-*sn*-glycero-3-phosphoethanolamine [DOPE] (Avanti Polar Lipids Inc., Alabaster, AL, USA)

2.2 Buffers and Solutions

2.2.1 DNA Transformation

LB-Amp agar plates: 5 g/L NaCl, 5 g/L yeast extract, 10 g/L tryptone, 15 g/L agar supplemented with 100 μg/mL ampicillin

LB-Amp/Chlor agar plates: 5 g/L NaCl, 5 g/L yeast extract, 10 g/L tryptone, 15 g/L agar supplemented with 100 μg/mL ampicillin and 25 μg/mL chloramphenicol

2.2.2 DNA Agarose Gel Electrophoresis

10X TBE: 108 g/L Tris, 55 g/L boric acid, 40 mL of 0.5 M EDTA, pH 8

2.2.3 Bacterial Cell Culture and Protein Expression

Luria Bertani (LB) Broth: 5 g/L NaCl, 5 g/L yeast extract, 10 g/L tryptone

LB-Amp/Chlor medium: LB medium supplemented with 100 μg/mL ampicillin and 25 μg/mL chloramphenicol

2.2.4 Protein Purification

Resuspension Buffer: 50 mM potassium phosphate monobasic, 300 mM NaCl, 10 % glycerol, pH 7.5

Wash Buffer: 50 mM potassium phosphate monobasic, 300 mM NaCl, 20 mM imidazole, 10 % glycerol, pH 7.5

Elution Buffer: 50 mM potassium phosphate monobasic, 300 mM NaCl, 150 mM imidazole, 10 % glycerol, pH 7.5

Resin Regeneration Buffer: 20 mM MES, 100 mM NaCl, pH 5

Storage Buffer: 20 % ethanol

PIPES Buffer: 20 mM PIPES, 137 mM NaCl, 2.7 mM KCl, pH 6.8

10X Phosphate Buffered Saline (PBS): 137 mM NaCl, 2.7 mM KCl, 10 mM potassium phosphate dibasic, 1.8 mM potassium phosphate monobasic, pH 7.4

Storage Buffer: 1X PBS supplemented with 0.02 % sodium azide

2.2.5 SDS-PAGE

Stacking Buffer: 0.5 M Tris, pH 6.8

Separating Buffer: 1.5 M Tris, pH 8.8

5X Running Buffer: 125 mM Tris, 960 mM glycine, 0.5 % SDS, pH 8.3

5X Loading Dye: 50 mM Tris, 16 % glycerol, 16% SDS (10 %), 0.02 % DTT, 0.08 % bromophenol blue (1 %)

Gel Drying Solution: 40 % methanol, 10 % glycerol, 7.5 % acetic acid

2.2.6 Western Blot

Native PAGE Running Buffer: 0.025 M Tris, 0.192 M Glycine, pH 8.3

Blotting Buffer: 80 % Native PAGE running buffer, 20 % methanol

Blocking Buffer: 10 % skim milk powder, 10 mM Tris, 150 mM NaCl, 0.05 % Tween-20, pH 8

TBST Buffer: 10 mM Tris, 150 mM NaCl, 0.05 % Tween-20, pH 8

2.2.7 Fluorescence-based Binding Assay

SET Buffer: 250 mM sucrose, 100 mM KCl, 50 mM Tris, 1 mM EDTA, pH 7.4

TKE Buffer: 50 mM Tris, 100 mM KCl, 1 mM EDTA, pH 7.4

2.2.8 FRET Assays

SET Buffer: 250 mM sucrose, 100 mM KCl, 50 mM Tris, 1 mM EDTA, pH 7.4

TKE Buffer: 50 mM Tris, 100 mM KCl, 1 mM EDTA, pH 7.4

2.2.9 Dual Polarization Interferometry

DPI Buffer: 10 mM potassium phosphate dibasic, 137 mM NaCl, pH 7.4

Calibration Solutions: 80 % ethanol, MilliQ water

Wash Solutions: 2 % SDS, 80 % ethanol, MilliQ water

2.3 Materials and Equipment

QIAprep Spin Miniprep Kit (Qiagen, Germantown, MD, USA)

PD-10 Desalting Columns (GE Healthcare Life Sciences, Baie d'Urfe, QC, Canada)

New Brunswick Incubator shaker I-26 (Eppendorf, Mississauga, ON, Canada)

VWR Gravity Convection Incubators (VWR, Mississauga, ON, Canada)

MLS-3751L-PE Laboratory Autoclave (Panasonic Biomedical, Loughborough, Leicestershire, UK)

PURELAB Flex (ELGA Labwater, Mississauga, ON, Canada)

Sub-Cell GT Electrophoresis Cell (Bio-Rad, Mississauga, ON, Canada)

Hoefer Scientific PS 500 XT DC Power Supply (Hoefer Inc., Holliston, MA, USA)

Mastercycler Nexus (Eppendorf, Mississauga, ON, Canada)

Eppendorf PCR tubes 0.2 mL (Eppendorf, Mississauga, ON,Canada)

GENESYS 10S UV-Vis Spectrophotometer (Thermo Scientific, Waltham, MA, USA)

Mini-PROTEAN III Cell (Bio-Rad, Mississauga, ON, Canada)

Allegra X-30 Benchtop Centrifuge (Beckman Coulter, Mississauga, ON, Canada)

IEC Micromax Microcentrifuge (Thermo Electron Corporation, Gormley, ON, Canada)

Orion Dual Star Meter (Thermo Scientific, Waltham, MA, USA)

Liposofast-Basic (Avestin, Ottawa, ON, Canada)

Polycarbonate Filters (Avestin, Ottawa, ON, Canada)

Nitrocellulose Membranes (Sigma-Aldrich, Oakville, ON, Canada)

Gel Drying Film (Promega Corporation, Madison, WI, USA)

Cryogenic Vials (Corning Inc., Corning, NY, USA)

Quartz Cuvettes (Hellma, Concord, ON, Canada)

NESLAB EX-111 Heating Circulator Temperature Bath (Thermo Electron Corporation, Gormley, ON,Canada)

Gel Doc EZ System (Bio-Rad, Mississauga, ON, Canada)

Rocker II Platform Rocker (Boekel Scientific, Feasterville, PA, USA)

Roto-Torque Rotator (Cole-Parmer, Montreal, QC, Canada)

Reax Control Vortex (Heidolph, Elk Grove Village, IL, USA)

QuantaMaster-QM-2001-4 Spectrofluorometer (Horiba Scientific, London, ON, Canada)

SFA-20 Stopped-flow (TgK Scientific Limited, Bradford-on-Avon, UK)

Analight Bio200 (Biolin Scientific, Linthicum Heights, MD, USA)

Q500 Sonicator (QSonica, Newtown, CT, USA)

Protein Solutions DynaPro-99-E (Wyatt Technologies, Santa Barbara, CA, USA)

2.4 Software

GraphPad Prism for Windows, Version 5.0 (GraphPad Software Inc., La Jolla, CA, USA)

Image Lab Software, Version 4.1 (Bio-Rad, Mississauga, ON, Canada)

Felix32 Spectroscopy Software, Version 1.2 (Horiba Scientific, London, ON, Canada)

AnaLight Bio200, Version 2.1.0 (Biolin Scientific, Linthicum, MD, USA)

AnaLight Explorer, Version 1.6.0.27583 (Biolin Scientific, Linthicum, MD, USA)

2.5 Bacterial Strains

BL21(DE3)pLysS-T1 Competent Cells (Sigma-Aldrich, Oakville, ON, Canada); stored at -80° C

NovaBlue Singles Competent Cells (EMD Millipore, Billerica, MA, USA); stored at -80° C

2.6 Bacterial Expression Vectors

Recombinant human PITPα and PITPβ were expressed from the pRSET-C plasmid vector. Similarly, recombinant *Drosophila melanogaster* RdgBα and the Y210A/W211A mutant were also expressed from the pRSETC plasmid vector. These plasmids were a gift from our collaborator, Dr. Shamshad Cockcroft, University College London (UK). PITP mutants were created by site-directed mutagenesis of recombinant

PITPα. pRSET vectors contain an N-terminal His-tag which is used for protein purification purposes.

2.7 Methods

2.7.1 Site-Directed Mutagenesis (Production of PITPα Mutants)

PITPα mutants were developed according to the QuikChange protocol (Agilent Technologies, formerly Stratagene). The human PITPα gene cloned into the pRSET-C plasmid vector was used for site-directed mutagenesis. All primers (**Table 2**) were designed using either PrimerX or OligoPerfect Designer (Life Technologies) and were manufactured by Sigma-Aldrich. *PfuTurbo* DNA polymerase was employed to generate the following mutants: C95A, K61A and W203A/W204A. The cycling parameters utilized in generating the PITPα mutants are listed in **Table 3**. The PCR reaction mixture was set up as follows: 5 μL 10X *Pfu* reaction buffer, 1 μL dNTP mix (10 mM), 5 μL forward primer (125 ng), 5 μL reverse primer (125 ng), 0.5 μL DNA template (50 ng), 32.5 μL MilliQ water, 1 μL *PfuTurbo* DNA polymerase.

The PCR products were subject to DpnI endonuclease digestion for 1 h at 37 °C and the presence of the PCR products were verified by gel electrophoresis. The purpose of the DpnI digestion is to remove template, non-mutated DNA. Since the template DNA is methylated, it is selectively digested by DpnI. Consequently, the PCR products were transformed into NovaBlue competent cells for propagation. Plasmid DNA containing the mutant gene of interest was then isolated from NovaBlue cells using the QIAprep Spin Miniprep kit and the sequence of the mutant gene was confirmed through DNA sequencing. Upon confirmation, the plasmid containing the mutant gene of interest was then transformed into BL21(DE3)pLysS competent cells for protein expression.

Table 2: Oligonucleotide primers utilized for creating the PITPα mutants (sequence in red represents nucleotide substitutions)

Primer	Sequence (5′ - 3′)	Tm
C95A-FW	AATGCTTACCCCTAC**GC**CAGAACCGTTATTACAAATG	76.7 °C
C95A-RV	CATTTGTAATAACGGTTCTG**GC**GTAGGGGTAAGCATT	76.7 °C
K61A-FW	GCCAGTACACAC**GC**GATCTACCACCTGC	79.1 °C
K61A-RV	GCAGGTGGTAGATC**GC**GTGTGTGTACTGGC	79.1 °C
W203A/ W204A-FW	ACCGTCAAGTTCAAG**GCGGCG**GGCCTGCAGAACAA	88.1 °C
W203A/ W204A- RV	TTGTTCTGCAGGCC**CGCCGC**CTTGAACTTGACGGT	88.1 °C

Table 3: Cycling parameters employed for creating the PITPα mutants

Program	Cycles	Temperature	Time	Activity
1	1	95 °C	30 s	Initial denaturation
2	18	95 °C	30 s	Denaturation
		55 °C	1 min	Annealing
		68 °C	8 min	Extension
3	1	4 °C	24 hrs	End

2.7.2 DNA Transformation

Plasmid DNA transformation of *E. coli* was performed using the heat shock method [66]. Competent cells were obtained commercially. NovaBlue competent cells were used for the purpose of DNA propagation. This is due to NovaBlue's high transformation efficiency (> 1.5 x 10^8 cfu/μg) [67]. It also lacks the endonuclease (*endA*) and (*recA*) genes that enable the host strain to produce high quality plasmid DNA. For recombinant protein production, BL21(DE3)pLysS competent cells were employed. This strain lacks the *Ion* and *ompT* proteases that promote the production of stable recombinant proteins. In addition, the BL21(DE3)pLysS cells contain an inducible T7 RNA polymerase which is under the control of the *lac*UV5 promoter. Therefore, protein expression is easily induced by the addition of IPTG. The presence of the T7 lysozyme in BL21(DE3)pLysS cells naturally inhibits T7 polymerase which aids in a tighter transcriptional control and aids cell lysis.

Competent cells were thawed on ice for 10 min. Plasmid DNA (50 ng) was then added to each aliquot of cells (50 μL) and incubated on ice for 30 min. Next, the cell mixture was heat shocked at 37 °C for 45 s (for BL21(DE3)pLysS cells) or at 42 °C for 30 s (for NovaBlue cells). The cells were then placed on ice for 2 min. LB media (450 μL) was added to the cell mixture and incubated at 37 °C on a shaker to allow cell growth. Cells (100 – 200 μL) were then plated unto LB agar plates with the appropriate antibiotic for selection of colonies. Ampicillin was used when selecting for NovaBlue cells while ampicillin and chloramphenicol were used for BL21(DE3)pLysS cells as chloramphenicol selects for the pLysS plasmid. The plated cells were allowed to grow overnight at 37 °C.

2.7.3 DNA Isolation

Plasmid DNA isolation from NovaBlue cells was performed using the QIAprep Spin Miniprep Kit according to the manufacturer's protocol. Pre-cultures were grown overnight in LB media containing 100 μg/mL ampicillin. Aliquots (3 mL) of culture were centrifuged in a microcentrifuge tube at 5000 rpm for 3 min. The supernatant was removed and the cell pellet was resuspended in 250 μL of Buffer P1 containing RNase A. Following that, 250 μL of Buffer P2 was added and mixed by gently inverting the tube 4 to 6 times. 350 μL of Buffer N3 was then added followed by inverting the tube 4 to 6 times. Next, the mixture was centrifuged at 12000 rpm for 10 min. The supernatant was then applied to the QIAprep spin columns and centrifuged for 1 min at 12000 rpm. The supernatant was discarded and 500 μL of Buffer PB was added to the column. The column was centrifuged for 1 min at 12000 rpm. The flow-through was discarded and the column was washed with 750 μL of Buffer PE. Again, the column was centrifuged for 1 min at 12000 rpm. The flow-through was discarded and the column was centrifuged for a further 1 min to remove residual wash buffer. The column was then transferred to a 1.5 mL microcentrifuge tube and 50 μL of MilliQ water was added to the column to elute the plasmid DNA. The column was allowed to stand for 1 min prior to centrifugation for 1 min at 12000 rpm.

2.7.4 DNA Quantification

Plasmid DNA concentration was determined by means of spectrophotometric analysis. DNA samples were diluted in MilliQ water in a quartz cuvette and the absorbance was measured at a wavelength of 260 nm. Since the optical density of 1

corresponds to 50 μg/mL of double-stranded DNA, plasmid DNA concentration can be calculated as follows:

$[DNA] = Abs_{260} * 50\ \mu g/mL * Dilution\ Factor$ (1)

2.7.5 Restriction Enzyme Digestion of DNA

Restriction enzyme digestion of plasmid DNA was performed to confirm the presence of the gene of interest (wild-type or mutant gene) within the plasmid prior to DNA sequencing. A typical restriction enzyme digest performed contained the following components: 1 μL of DNA, 1 μL of each restriction enzyme, 2 μL of 10X restriction enzyme buffer, 0.5 μL BSA (if recommended) and 15.5 μL of MilliQ water to bring the final volume of the reaction mixture to 20 μL. For all plasmids used in this project, a double restriction enzyme digest was conducted using both NdeI and HindIII. The prepared sample mixture was then mixed and pulsed briefly in a microcentrifuge to ensure all the solution remained at the bottom of the microcentrifuge tube. The reaction mixture was then incubated in a water bath at 37° C for 1 h.

2.7.6 DNA Agarose Gel Electrophoresis

Typically, 1 % agarose gels were used for analyzing plasmid DNA fragments from restriction digests and also for examining PCR products. Agarose gels were prepared by dissolving 0.5 g of agarose in 50 mL 1X TBE. The mixture was microwaved for approximately 45 s or until the agarose was dissolved. Once the mixture cooled to about 50° C, 25-30 μL of 500 μg/mL of ethidium bromide was added (final concentration of 0.2 – 0.3 μg/mL) to allow visualization of DNA. Once the gel set, approximately 2 μL of gel loading buffer dye was added to 10 μL of DNA samples prior to loading onto the DNA gel. DNA molecular weight markers were also loaded alongside the DNA samples.

The gel was run at 80 – 100 V until the gel loading buffer dye reached 5 – 10 mm from the bottom of the gel.

2.7.7 DNA Sequencing

Sequencing of all plasmid DNA samples was performed at Robarts Research Institute (London, ON).

2.7.8 Bacterial Glycerol Stocks

Once the sequence of the gene containing the protein of interest was confirmed, bacterial glycerol stocks were prepared for long-term storage of plasmids. Colonies from the transformed NovaBlue or BL21(DE3)pLysS cells were picked and grown overnight in 10 mL of autoclaved LB broth at 37 °C. Once bacterial growth is achieved, 750 µL of overnight culture was mixed with 750 µL of 30 % glycerol in a 2 mL cryogenic vial. The glycerol stock was then frozen at -80 °C and kept for long-term storage.

2.7.9 Protein Expression

Pre-cultures were prepared in test tubes containing 10 mL of autoclaved LB broth supplemented with 100 µg/mL ampicillin and 25 µg/mL chloramphenicol. Each test tube was inoculated with a frozen culture of BL21(DE3)pLysS *E. coli* cells containing the desired pRSET vector. The cultures were then grown overnight at 37°C in a test tube roller. An aliquot of the overnight pre-culture (5 mL) was used to inoculate 500 mL of LB broth to produce a 1:100 dilution factor. The cultures were allowed to grow in 1L baffled flasks at 37°C on a shaker at 180 rpm until an OD_{600} of 0.4 – 0.6 was achieved. Following that, protein expression was induced by the addition of 0.4 mM IPTG. The cultures were then allowed to grow overnight on a shaker at 28 °C except for C95A which was induced at 20 °C to improve protein yield. Finally, the cells were harvested

by centrifugation at 4400 rpm for 15 min. The supernatant was decanted and the cell pellet was stored at -80°C until further use.

2.7.10 Protein Purification

The frozen cell pellet was thawed and frozen at -80°C twice to promote cell lysis. The cell pellet was then suspended in 10 mL of Resuspension Buffer. In addition, 50 µL of Triton X-100 (final concentration of 0.5 %) was added to the suspension along with 10 µL of DNAse (20 Units) and one tablet of Protease Inhibitor Cocktail. The cell suspension was incubated for 15 min on ice. Following that, the lysate was passed through an 18 ½ gauge needle attached to a 10 mL syringe approximately 10 times. The cells were centrifuged at 11400 rpm for 45 min at 4°C. If required, the supernatant obtained was centrifuged for a further 30 min at 11400 rpm.

A column containing 1 mL of Talon Metal Affinity Resin was prepared by equilibrating with 10 mL Wash Buffer. All solutions were allowed to pass through the column by gravity flow. The supernatant was then added to the column and allowed to incubate overnight on a shaker at 4°C. Subsequently, the column was washed with 10 mL of Wash Buffer. Protein fractions (5 mL) were then eluted, 1 mL at a time, using Elution Buffer. The column was then regenerated with 8 mL of Regeneration Buffer followed by 8 mL of MilliQ water. Subsequently the resin was stored in 1 mL of 20 % ethanol solution.

A PD-10 desalting column was also prepared by equilibrating with 10 mL of PIPES Buffer. Normally, the first three protein fractions obtained were added to the desalting column. The protein was then eluted with 4 mL of PIPES Buffer and stored at 4°C until further use. The use of the desalting column is chiefly for buffer exchange

purposes. Finally the column was regenerated with 10 – 20 mL of 1X PBS containing 0.02 % sodium azide. The column was then stored in the same solution at room temperature.

2.7.11 Protein Quantitation: Bradford Assay

The Bradford assay was employed to determine the protein concentration from a given purification. A standard curve was prepared using bovine serum albumin (BSA) with concentrations ranging between 0-1 mg/mL. Typically, each standard was prepared by adding 50 μL of BSA solution to 1 mL of Bradford reagent. The standards were prepared in plastic cuvettes and allowed to incubate for 5 min at room temperature. The absorbance was then measured at 595 nm. The concentration of the unknown protein samples were determined from the standard curve and the conditions used were similar to those of the BSA samples.

2.7.12 Protein Characterization: SDS-PAGE Analysis

The purity of the proteins purified was determined by means of SDS-PAGE. To achieve this analysis, a 15 % acrylamide resolving gel with a 5.5 % acrylamide stacking gel was used. For protein samples of known concentrations, loading dye was added to 5 μg samples of protein. For protein samples of unknown concentrations, typically 6 μL of loading dye was added to 24 μL of protein sample. The protein samples were then heated at 95 °C for 5 min to fully denature the proteins. Subsequently, the samples were loaded onto the gel along with a protein molecular weight marker and allowed to run for approximately 2 h at 110 V. The gels were then stained with ProtoBlue Safe Colloidal Coomassie G-250 Stain overnight and destained with distilled water. The stain was prepared by combining one part of ethanol to nine parts of staining solution.

The gels were then preserved by soaking in gel drying solution for 5-10 min along with gel drying film. The gel was then assembled on top of a clean glass plate sandwiched between two gel drying films and allowed to air dry.

2.7.13 Western Blotting of Purified Proteins

The identity of the purified protein was confirmed using Western Blot analysis. An SDS-PAGE was first run containing the protein of interest. Subsequently, the protein was transferred from the SDS-PAGE gel to a nitrocellulose membrane as shown in **Figure 13**.

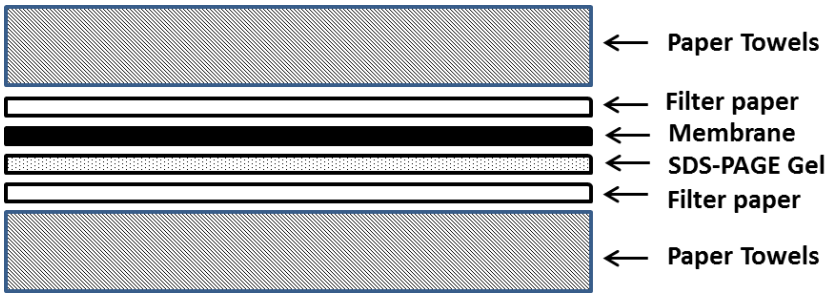

Figure 13: Western Blot set-up for transferring protein from the SDS-PAGE gel to nitrocellulose membranes.

The above set-up was prepared in a plastic dish using blotting buffer and left overnight to dry. The membrane was then removed from the blotting sandwich and blocked with 30 mL of blocking buffer for 15 min at room temperature on a rocker. The blocked membrane was washed twice with 20 mL of TBST buffer (5 min per rinse). Following that, the membrane was incubated with mouse anti-His antibody (1:3000 dilution in 20 mL TBST buffer) for 30 min at room temperature on a rocker. The membrane was then washed 3 times with 25 mL of TBST buffer (10 min per rinse). Consequently, the membrane was incubated with anti-mouse IgG HRP (horseradish peroxidase) conjugate (1:2500 dilution in 20 mL TBST buffer) for 30 min at room temperature on a rocker. The

membrane was washed again with 3 washes of 25 mL of TBST buffer (10 min per rinse) prior to incubation with TMB for signal development. Typically the membrane was incubated with TMB for 5-10 min. Once bands are visible, the membrane was washed with MilliQ water to remove the TMB reagent.

2.7.14 Fluorescence-based Binding Assay

Each protein used in this project, regardless of wild-type or the mutant form, was tested for its capability to bind to NBD-PC, the fluorescent analog of PC. Protein (0.2 μM) in either SET or TKE buffer was titrated in a 3 mL quartz cuvette with serial additions of either 0.5 or 1 μL aliquots of concentrated stocks of NBD-PC prepared in ethanol. The final volume of ethanol was kept below 1 % (v/v) of the total volume. After each addition of NBD-PC, the mixture was allowed to equilibrate for 10 min on a rotator. The fluorescence emission was measured between 515 and 550 nm. The excitation wavelength was set at 469 nm. The maximum fluorescence obtained at 527 nm for each NBD-PC concentration was then used to plot a one site binding (hyperbola) curve using GraphPad Prism. The equation is as follows:

$$Y = B_{max}.X / K_d + X \qquad (2)$$

With reference to (2), Y = specific binding, B_{max} = maximum number of binding sites, expressed in the same units as the Y-axis, X = concentration of the ligand and K_d = equilibrium dissociation constant, expressed in the same units as the X-axis. The K_d values were used to reflect the binding affinity of each protein for NBD-PC.

2.7.15 Reduction of NBD-PC by Sodium Hydrosulfite

The reduction assay was performed by preparing 2 μM of protein in TKE buffer in a 500 μL quartz cuvette. Following that, the protein solution was incubated with 0.2

μM of NBD-PC for 15 min at room temperature on a rotator. The protein-ligand mixture was then titrated with sodium hydrosulfite and the fluorescence was monitored at 532 nm over time. The excitation wavelength was set at 469 nm.

2.7.16 Concentration Measurement of NBD-PC, Liss Rhod PE and TRITC DHPE

Concentrated stocks of NBD-PC were prepared in ethanol. Each stock concentration was determined by measuring the absorbance at 469 nm using a UV spectrophotometer. Using the Beer-Lambert law the concentration of NBD-PC stock solutions can be established. The extinction coefficient for NBD-PC in ethanol is 21000 $cm^{-1}M^{-1}$ as provided by the manufacturer. Similarly, the concentrations of Liss Rhod PE and TRITC DHPE were determined using the same method. The extinction coefficient of Liss Rhod PE and TRITC DHPE are 88000 $cm^{-1}M^{-1}$ and 91000 $cm^{-1}M^{-1}$ respectively as provided by the manufacturer.

2.7.17 Lipid Vesicle Preparation for FRET Assays

Lipid vesicles used for the FRET assay were prepared at a final concentration of 200 μM. Generally the vesicles used in the FRET-based transfer assay contained 3 mol% FRET acceptor molecules unless stated otherwise. The FRET quencher used here includes either TRITC DHPE or Liss Rhod PE. The remaining mole fraction consisted of PC unless stated otherwise. Commercial lipid stocks were purchased dissolved in chloroform. Lipid vesicles were prepared in glass vials and dried under nitrogen gas to remove chloroform. Residual chloroform was then further removed by evaporation under vacuum for at least 1 h. The dried lipid mixture was rehydrated with SET or TKE buffer and left to sit overnight at 4 °C. For LUV preparation, rehydrated lipids were subject to extrusion using Liposofast-Basic. Prior to lipid extrusion, lipid mixtures were vortexed

thoroughly. Each lipid mixture was passed through a 100 nm polycarbonate filter at least 15 times to produce uniform vesicles. Rehydrated vesicles were stored overnight at 4 °C prior to being used and were usually consumed within 3 to 5 days. SUVs on the other hand were prepared by probe sonication. Rehydrated lipid mixtures were probe sonicated on ice for 15 min and stored at 4 °C. SUVs were consumed within 3 days.

2.7.18 Lipid Vesicle Preparation for DPI Analysis

LUVs (100 nm) for DPI analysis were prepared as described in **Section 2.7.17**. The only exception was that the LUVs were made up of only DOPC, unless stated otherwise and the final lipid concentration was 1 mM in DPI buffer.

2.7.19 Dynamic Light Scattering Analysis of SUV and LUV Sizes

Vesicle sizes were determined by dynamic light scattering using Protein Solutions DynaPro-99-E. Measurements were performed at either 25 or 37 °C with a laser power of 40-50 %. The average diameter of LUVs prepared by extrusion using a 100 nm polycarbonate filter was ~150 nm with a polydispersity index of 0.15. The mean diameter of SUVs prepared by probe sonication was ~ 29 nm with a polydispersity index of 0.12.

2.7.20 FRET-based Transfer Assay

The QuantaMaster-QM-2001-4 fluorometer equipped with a stopped-flow device was used to examine the transfer rate of NBD-PC from NBD-PC bound to protein to acceptor vesicles. The excitation wavelength was set at 469 nm while the emission wavelength was set at 532 nm. The FRET assay was performed by incubating 4 μM of protein with 0.4 μM of NBD-PC for 15 min at room temperature on a rotator. The protein:ligand ratio was kept at 9:1 to ensure all ligand was bound by the protein. Using

the stopped-flow device the pre-incubated protein-ligand mixture was mixed with 200 μM acceptor vesicles. The actual protein, ligand and lipid concentration during fluorescence measurement was 2 μM, 0.2 μM and 100 μM respectively. The acceptor vesicles were kept at a 50-fold molar excess, unless stated otherwise, to ensure sufficient delivery of the ligand. The fluorescence decay was monitored over a time frame of 200 to 360 s. Typically, 3 replicates were obtained for each assay condition. The fluorescence values were then normalized to the starting fluorescence intensity, which corresponds to NBD-PC bound to protein. The rate of NBD-PC transfer was fit to a two-phase exponential decay curve using GraphPad Prism. The fast rate obtained corresponds to the ligand transfer rate by PITP. The equation is as follows:

$$Y=\text{Span1}.e^{-k_1.X} + \text{Span2}.e^{-k_2.X} + \text{Plateau} \qquad (3)$$

With reference to (3), Y = normalized fluorescence intensity, X = time and k_1 and k_2 = rate constants. Only the fast rate is considered here.

2.7.21 FRET-based Pick-up Assay

The FRET-based pick-up assay is simply the reverse of the transfer assay. Here, NBD-PC is incorporated into the donor vesicles and the ability of PITP to extract NBD-PC from the donor vesicles is monitored over time. Donor vesicles contained 2.5 mol% NBD-PC and 2 mol% Liss Rhod PE and the remaining mole fraction consisted of PC. The concentration of the donor vesicles was 200 μM while protein concentration was 4 μM. However, after mixing protein and lipids together, the final protein and lipid concentration was 2 μM and 100 μM respectively. The increase in NBD-PC fluorescence was monitored for 400 s and the assay was performed in duplicates. Similar to the FRET transfer assay, the excitation wavelength was set at 469 nm while the emission

wavelength was set at 532 nm. The rate at which PITP picked up NBD-PC from lipid vesicles was fit to a two-phase exponential association equation using GraphPad Prism. The fast rate corresponds to the ligand pick-up rate. The equation is as follows:

$$Y=Ymax_1.(1-e^{-k_1.X}) + Ymax_2.(1-e^{-k_2.X}) \qquad (4)$$

where Y = fluorescence intensity, X = time, $Ymax_1$ and $Ymax_2$ = maximum fluorescence when the maximum amount of PITP is bound to NBD-PC for the fast and slow rate, k_1 and k_2 = rate constants. Only the fast rate is considered here.

2.7.22 Tryptophan Fluorescence Quenching Assay

The binding affinity of both wild-type PITPα and PITPβ to membranes was examined by measuring the quenching of the protein's tryptophan fluorescence. 0.5 μM of protein in TKE buffer was prepared in a 500 μL quartz cuvette. The protein mixture was titrated with serial additions of 100 nm PC LUVs in TKE buffer. After each addition of acceptor vesicles, the reaction mixture was allowed to incubate for 10 min at room temperature on a rotator. The fluorescence emission was measured between 315 and 375 nm while the excitation wavelength was set at 295 nm. Alternatively, the tryptophan fluorescence quenching assay was performed by titrating 100 nm PC LUVs into a 2 μM protein solution with a final volume of 3 mL. Acceptor vesicles contained 3 mol% of pyrene-labeled PE. The fluorescence emission was measured between 300 and 500 nm while the excitation wavelength was set at 295 nm.

2.7.23 Dual Polarization Interferometry

Prior to performing any analysis, the Analight Bio200 was allowed to warm up by passing DPI running buffer through the instrument for 1 h. Following that, the instrument was loaded with an unmodified silicon oxynitride sensor chip. Calibration of

the instrument was then performed with 80 % ethanol and milliQ water. Once a stable baseline was attained, 800 μL samples containing the desired 100 nm LUVs were passed over the sensor chip at a flow rate of 25 μL per minute for 8 min. The lipid layer was allowed to adsorb on to the sensor chip until a stable bilayer was formed. After each lipid injection, DPI running buffer was passed over the lipid layer at a flow rate of 50 μL per minute for 4 min. This step was to remove any excess lipid that was deposited on top of the lipid layer. Subsequently, 800 μL of protein sample at the desired concentration was passed over the lipid layer at a flow rate of 25 μL per minute for 8 min. The sensor chip was then regenerated with the following washes: 2 % SDS, 80 % ethanol followed by milliQ water.

The association of protein with the lipid layer on the Analight Bio200 was determined by the maximum mass of protein deposited on to the lipid layer. Typically, the mass data from the first 480 s of protein injection was fit to a one-phase exponential association model to obtain the maximum mass of protein bound. The equation is as follows:

$$Y = Y_{max} (1 - e^{-kt}) \qquad (5)$$

With reference to (5), Y = mass of protein bound, Y_{max} = maximum mass of protein bound, t = time, k = rate constant. To obtain a K_d value of a protein for a given lipid composition, the Y_{max} values for each protein concentration were used to plot a saturation binding curve using equation (2).

3. RESULTS

3.1 Protein Expression, Purification and Characterization

3.1.1 Wild type PITPα and PITPβ

PITPα and PITPβ were previously cloned into the pRSETC vector [34] and were gifts from our collaborator, Dr. Shamshad Cockcroft, University College London. The pRSETC vector contains an N-terminal His-tag and was expressed in the *E. coli* strain BL21(DE3)pLysS. His-tagged PITPα was initially purified by means of a nickel affinity chromatography using Ni-NTA agarose. However, the pure protein fractions appeared to contain a contaminant of about 20 kDa – see **Figure 14**.

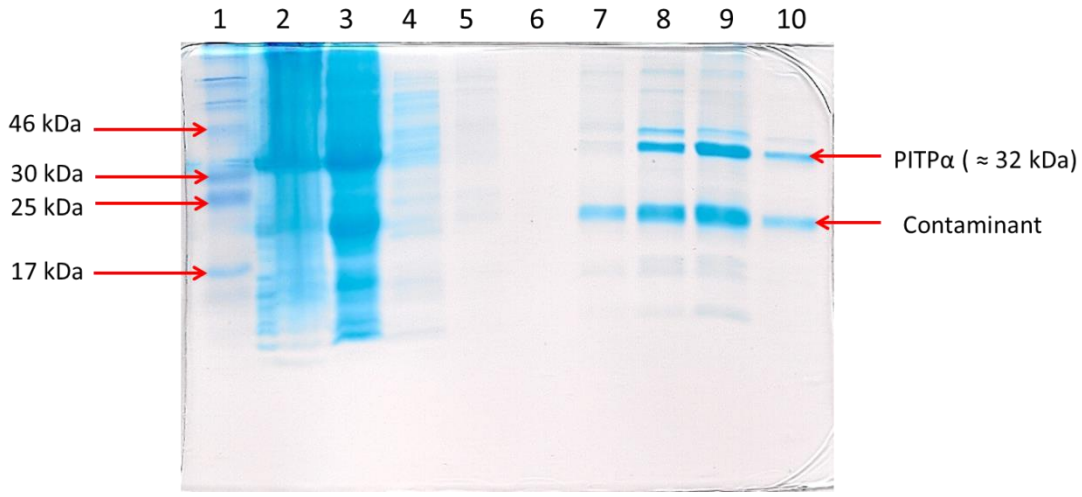

Figure 14: SDS-PAGE analysis of PITPα purification using Ni-NTA column
Molecular weight marker (1), cell lysate (2), supernatant (3), supernatant flow-through (4), wash flow-through (5-7) eluted 3 mL PITPα fraction (8), eluted 2 mL PITPα fraction (9) and PITPα in PIPES buffer (10).

When Co^{2+}-loaded Talon resin was used instead of Ni-NTA agarose, the contaminant was successfully removed – **Figure 15**. Consequently, Co^{2+}-loaded Talon resin was used to purify all the proteins used in this thesis. The bulk of pure PITPα and PITPβ eluted in the first three 1 mL fractions of 150 mM imidazole washes. The first 3 fractions were then pooled and subjected to buffer exchange with PIPES buffer using a desalting column. Protein purity was determined by SDS-PAGE and the identity of the proteins was confirmed by Western Blot using anti-His antibodies. See **Figures 16** and **17**.

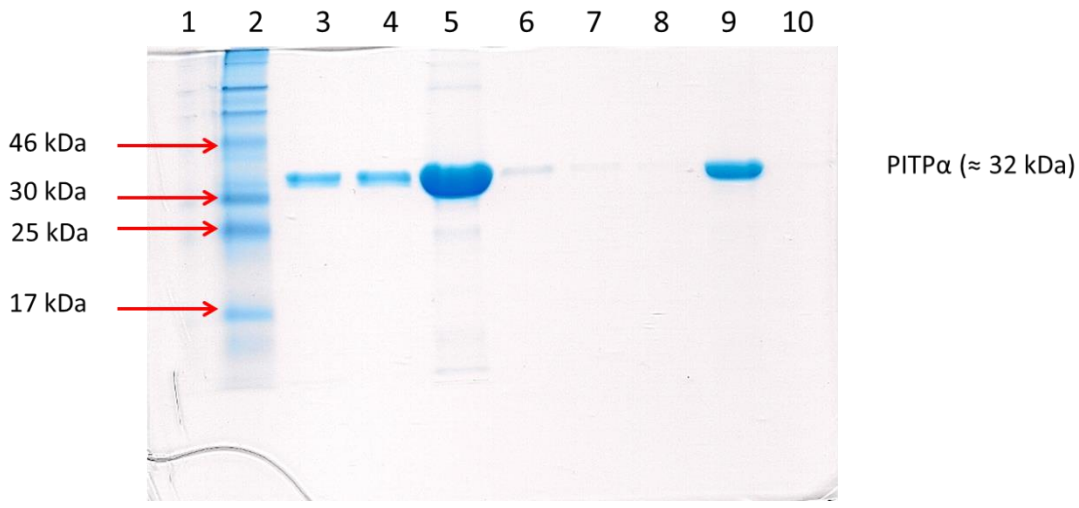

Figure 15: SDS-PAGE analysis of PITPα purification using cobalt affinity column
Molecular weight marker (2), wash flow-through (3) eluted PITPα fraction one to five (4-8) and PITPα in PIPES buffer (9).

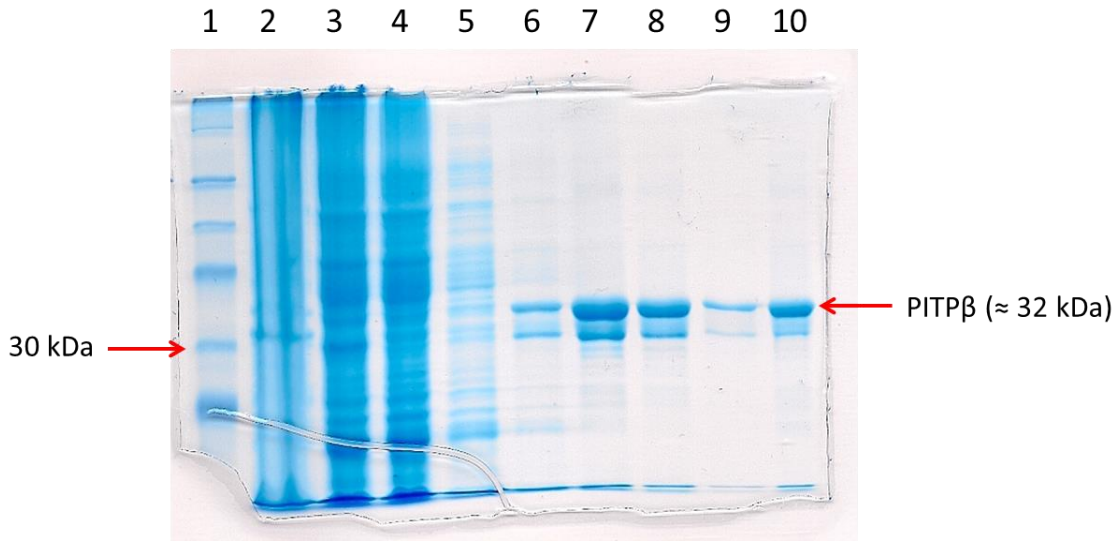

Figure 16: SDS-PAGE analysis of PITPβ purification using cobalt affinity column
Molecular weight marker (1), cell lysate (2), supernatant (3), supernatant flow-through (4), wash flow-through (5), eluted PITPβ fraction one to four (6-9), PITPβ in PIPES buffer.

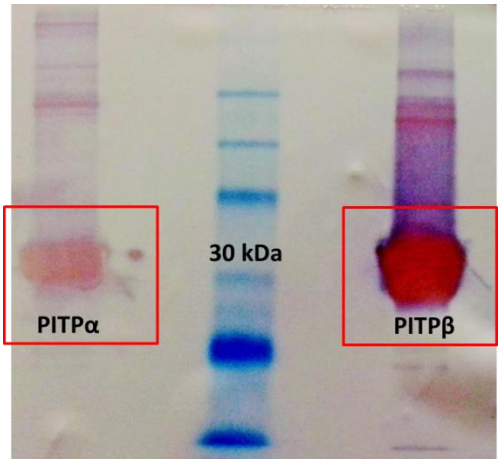

Figure 17: Western blot analysis of PITPα and PITPβ
PITPα and PITPβ examined by Western blotting using anti-His antibodies.

3.1.2 PITPα Mutants: W203A/W204A, K61A and C95A

The PITPα mutants created here were previously described in Tilley *et al.* and Shadan *et al.* [28, 34]. The W203A/W204A mutant no longer has the capacity to bind to membranes. As mentioned previously in **Section 1.4.3**, both W203 and W204 were identified in PITPs to play a role in membrane docking. Mutation of both tryptophan residues to alanine resulted in loss of membrane binding [28].

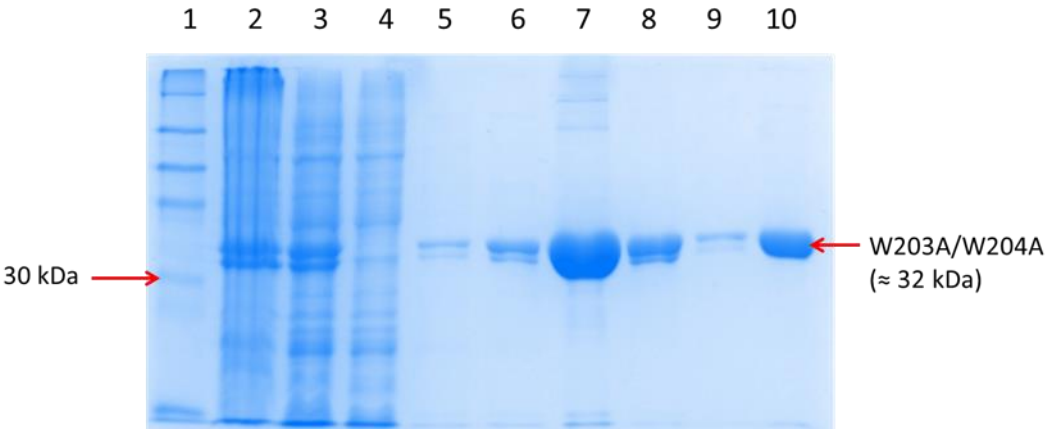

Figure 18: SDS-PAGE analysis of W203A/W204A purification by cobalt affinity column
Molecular weight marker (1), cell lysate (2), supernatant (3) supernatant flow-through (4), wash flow-through (5), eluted W203A/W204A fraction one to four (6-9), W203A/W204A in PIPES buffer (10).

K61A is a mutant that is able to bind to PC but whose PI binding is compromised. K61A is one of four important residues in the ligand binding pocket that is required for PI binding [28]. In contrast, C95A is a mutant that is unable to transfer PC – however, there is no data in the literature that shows C95A is not able to bind PC [25, 34]. Since C95A is unable to transfer PC, it is assumed that it lacks the capability to bind PC and therefore C95 is thought to be important for PC binding. However, the ability of C95A to bind and transfer PI is not compromised.

All mutants were successfully created from PITPα plasmid by means of site-directed mutagenesis as described in **Section 2.7.1** using the QuikChange protocol. The sequences of the mutants were confirmed through DNA sequencing (Appendix I). Similar to wild type PITPα, all mutant proteins were expressed in *E. coli* strain BL21(DE3)pLysS and purified using Co^{2+}-charged Talon resin. The mutant proteins were then characterized by means of SDS-PAGE and Western blot – **Figures 18-21**.

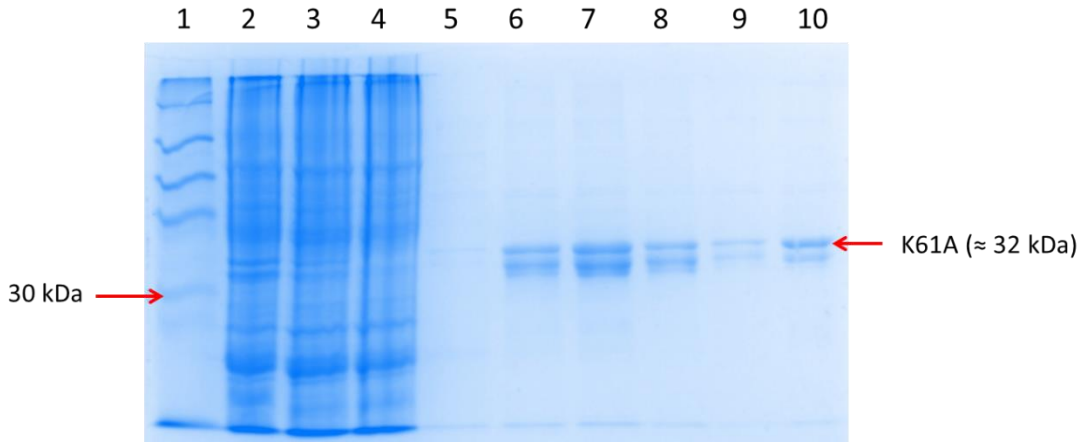

Figure 19: SDS-PAGE analysis of K61A purification by cobalt affinity column. Molecular weight marker (1), cell lysate (2), supernatant (3), supernatant flow-through (4), wash flow-through (5), eluted K61A fraction one to four (6-9) and K61A in PIPES buffer (10).

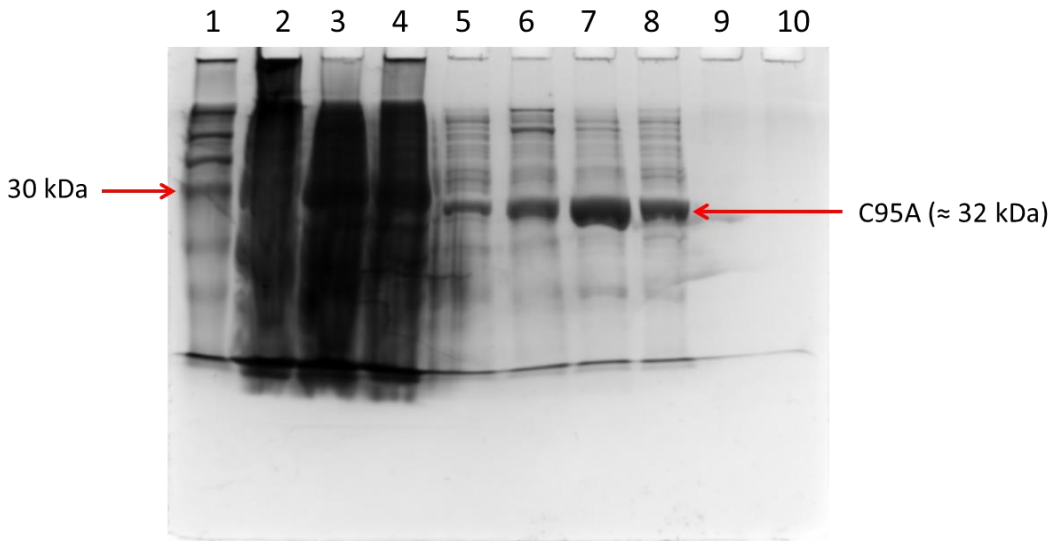

Figure 20: SDS-PAGE analysis of C95A purification by cobalt affinity column.
Molecular weight marker (1), supernatant (2), supernatant flow-through (3), wash flow-through (4), eluted C95A fraction one to three (6-9) and C95A in PIPES buffer (10).

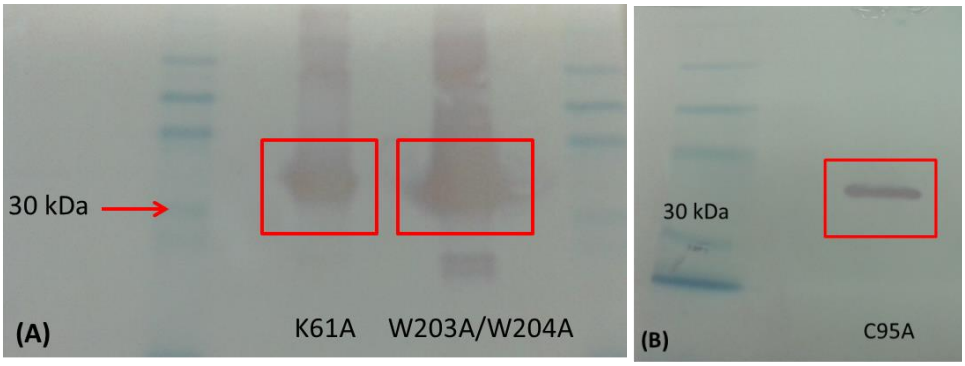

Figure 21: Western Blot analysis of PITPα mutants
PITPα mutants – K61A, W203A/W204A (A) and C95A (B) – examined by Western blotting using anti-His antibodies.

3.1.3 RdgBα and Y210A/W211A Mutant.

RdgBα and its mutant form, Y210A/W211A, were expressed from the pRSETC vector, which was also provided by our collaborator. The Y210A/W211A is a mutant that mimics the W203A/W204A mutant in wild type PITP. Therefore, it is believed that the Y210A/W211A mutant lacks the capacity to bind to lipid membranes. Similar to the other proteins, RdgBα and Y210A/W211A were expressed in *E. coli* strain BL21(DE3)pLysS and purified using Co^{2+}-charged Talon resin. The purity and identity of RdgBα and Y210A/W211A were determined by means of SDS-PAGE and Western blot respectively – **Figures 22-24**.

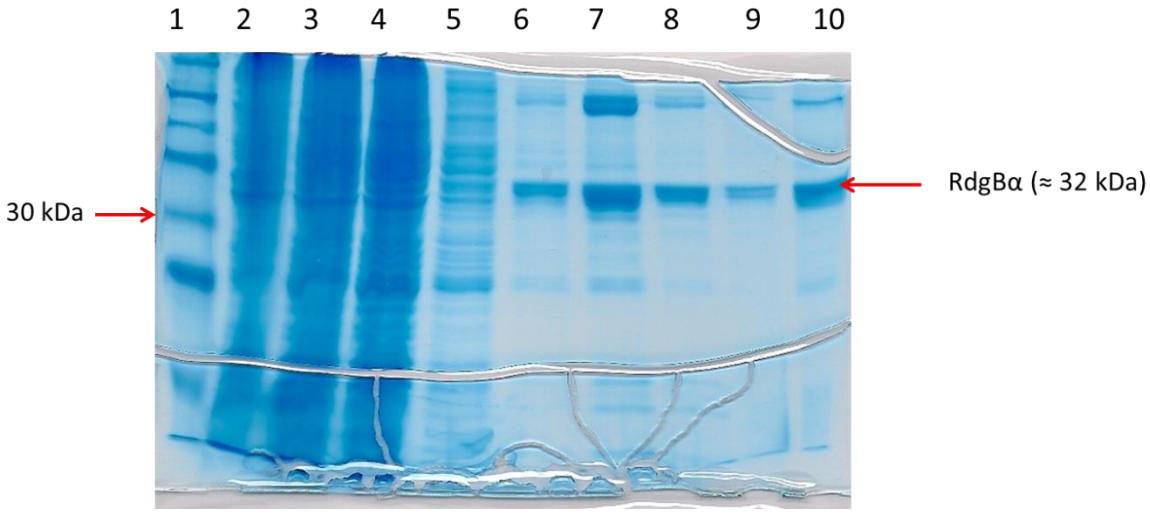

Figure 22: SDS-PAGE analysis of RdgBα purification using cobalt affinity column
Molecular weight marker (1), cell lysate (2), supernatant (3), supernatant flow-through (4), wash flow-through (5), eluted RdgBα fraction one to four (6-9) and RdgBα in PIPES buffer.

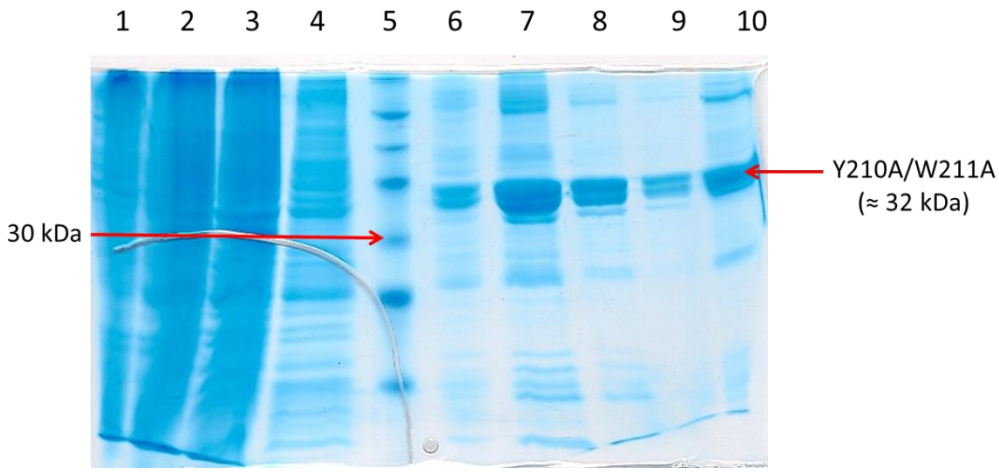

Figure 23: SDS-PAGE analysis of Y210A/W211A purification using cobalt affinity column

Cell lysate (1), supernatant (2), supernatant flow-through (3), wash flow-through (4), molecular weight marker (5) eluted Y210A/W211A fraction one to four (6-9) and Y210A/W211A in PIPES buffer.

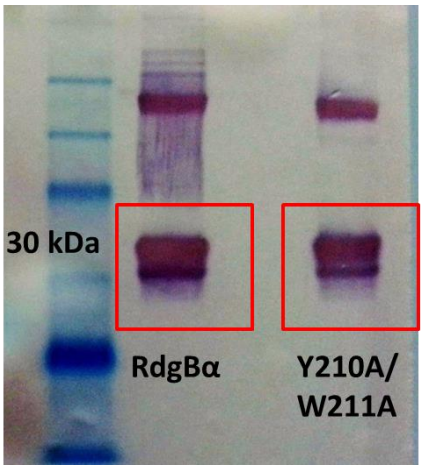

Figure 24: Western blot analysis of RdgBα and Y210A/W211A

RdgBα and Y210A/W211A examined by Western blotting using anti–His antibodies.

3.2 Determination of Protein Binding Affinity to NBD-PC

In **Section 1.7** it was stated that one of the main aims of this thesis is to determine the ligand transfer rates of PITPs. In order to do so, a FRET-based transfer assay was employed. It should be noted that all the transfer assays performed in this thesis was conducted with only NBD-PC since it is the only commercially available fluorescent ligand of PITP. Prior to performing the FRET assay, it was crucial to determine the binding capacity of PITPs to NBD-PC, the fluorescent analogue of PC. The binding affinity to NBD-PC was determined using a fluorescence binding assay. NBD-PC was obtained commercially from Life Technologies and the structure is shown in **Figure 25**. NBD-labeled lipids are useful tools for studying a variety of processes, which include membrane fusion, intracellular lipid transfer and localization of lipids and proteins in membranes [68]. The NBD group is sensitive to its environment in that it has only marginal fluorescence in a polar environment but fluoresces significantly in a hydrophobic environment [68].

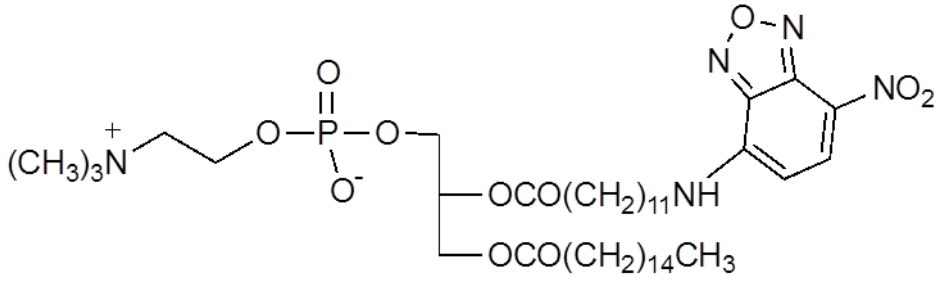

Figure 25: Structure of NBD-PC

The results from the fluorescence binding assay revealed that the proteins tested possessed the capacity to bind NBD-PC – see **Table 4**. The K_d values obtained were at nanomolar concentrations, which are typical of most biological systems. A typical binding curve is shown in **Figure 26** compared with a control assay where no protein was

present – **Figure 27**. In **Table 4** the maximum fluorescence for each protein analyzed is also included. As mentioned above, the NBD group is sensitive to its environment; the variation in maximum fluorescence from protein to protein is indicative of the way the NBD-PC is bound by each protein. A lower fluorescence implies that the bound-NBD group is more solvent exposed. This was observed particularly with the following proteins: C95A (PITPα), RdgBα, Y210A/W211A and BSA. BSA was included in the analysis as a control protein. BSA was chosen as a control protein since it is capable of binding hydrophobic molecules but lacks the PITP phospholipid binding pocket [69-70].

Table 4: Affinity of wild type and mutant PITPs, RdgBα, Y210A/W211A and BSA to NBD-PC

The equilibrium dissociation constants of wild type and mutant PITPs, RdgBα, Y210A/W211A and BSA to NBD-PC. Data represents the average of two measurements.

Protein	K_d **(nM)**	**Maximum Fluorescence (a.u)**
PITPα	104 ± 13	347054
PITPβ	43 ± 8	89117
W203A/W204A	67 ± 12	159088
K61A	19 ± 4	130999
C95A	17 ± 2	13804
RdgBα	27 ± 3	8495
Y210A/W211A	13 ± 17	36815
BSA	138 ± 19	39029

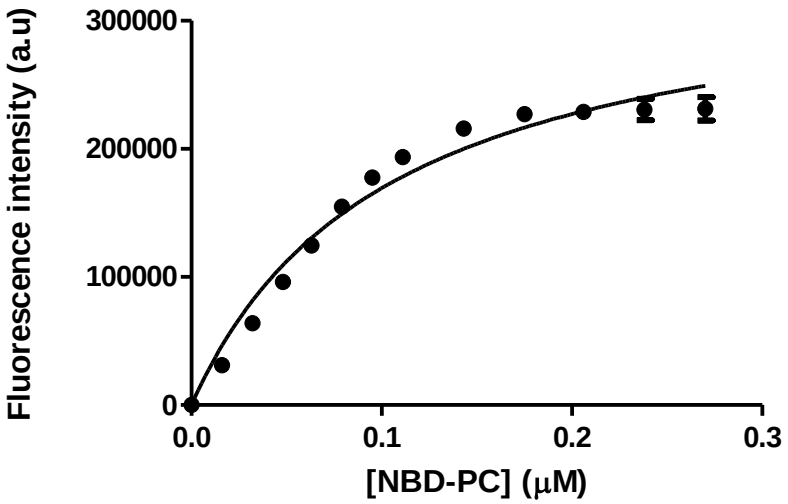

Figure 26: Binding curve of PITPα to NBD-PC

Binding of PITPα (0.2 μM) to NBD-PC measured by the increase in NBD-PC fluorescence. Data represents the average of two measurements with standard error of measurement.

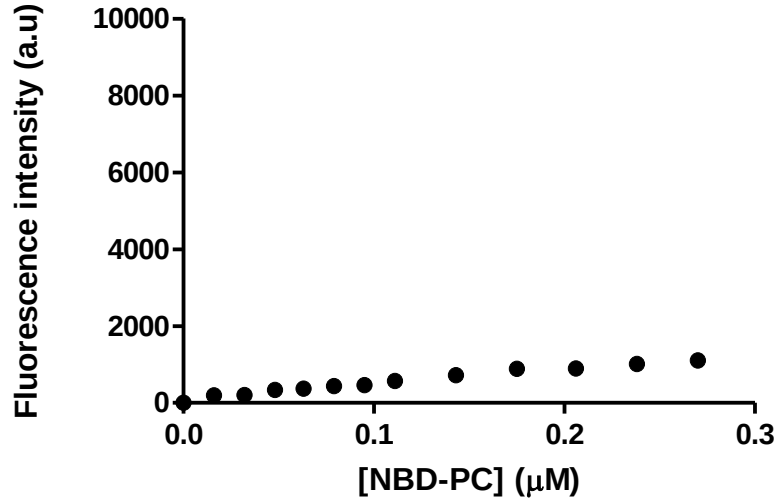

Figure 27: No protein control for the fluorescence binding assay

The fluorescence increase measurement when NBD-PC was added to buffer without the presence of proteins. Data represents the average of two measurements with standard error of measurement.

3.3 Reduction of NBD-PC by Sodium Dithionite ($Na_2S_2O_4$)

Sodium dithionite has been used as a reducing agent toward NBD. Specifically, dithionite reduces the nitro group in NBD to an amine and as a result NBD fluorescence is quenched [71]. In the previous section, it was mentioned that each protein tested in this thesis may bind NBD-PC differently. This was deduced by the variation in maximum fluorescence observed for each protein. To further verify this conclusion a dithionite reduction assay was performed. In this assay, the protein of interest was incubated with NBD-PC for 15 min. NBD fluorescence was then measured up to 500 s or until a stabilized fluorescence reading was achieved. Following that, dithionite was added to the pre-incubated protein mixture and fluorescence quenching was followed. It was determined that a minimum dithionite concentration of 4 mM was sufficient to generate the quenching of bound NBD-PC – **Figure 28**. As a control measure, the same volume of buffer was added to the pre-incubated mixture instead of dithionite – **Figure 29**. No change in fluorescence was observed. This step implies that a small change in volume does not affect the fluorescence measurement and therefore the fluorescence quenching observed is solely from the reducing ability of dithionite.

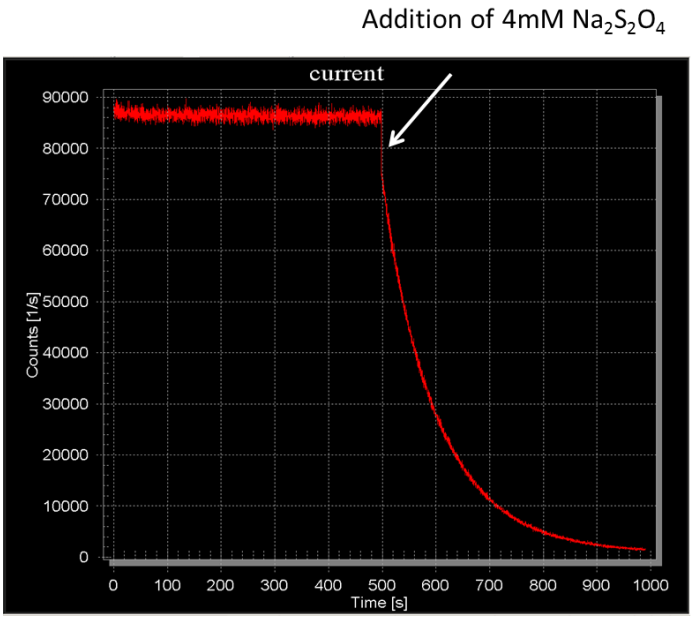

Figure 28: Reduction of NBD-PC by sodium dithionite
2 µM of PITPα was pre-incubated with 0.2 µM of NBD-PC in a total volume of 500 µL for 15 min. NBD-PC fluorescence was measured before and after the addition of 4 mM $Na_2S_2O_4$.

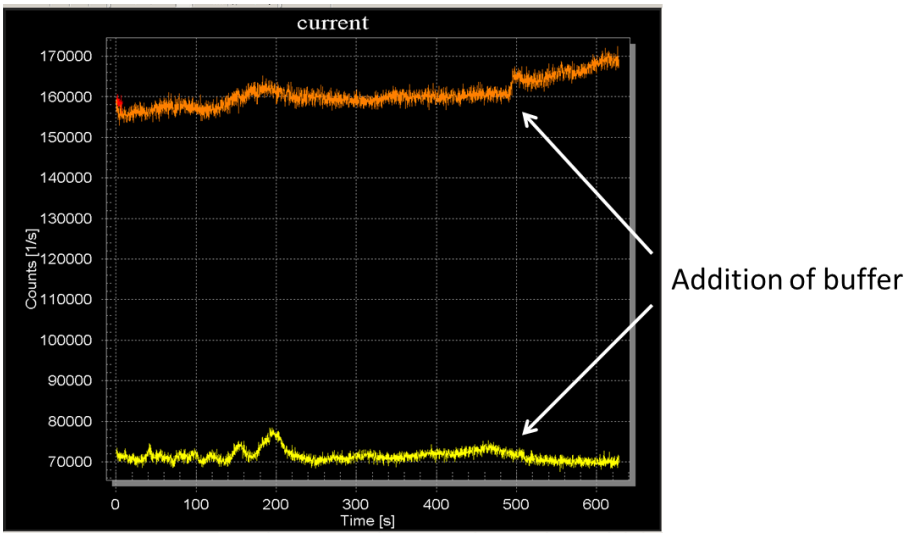

Figure 29: Reduction of NBD-PC by sodium dithionite – control experiment
2 µM of PITPα (orange trace) and PITPβ (yellow trace) was pre-incubated with 0.2 µM NBD-PC in a total volume of 500 µL for 15 min. NBD-PC fluorescence was measured before and after the addition of TKE buffer.

The reduction assay was performed with the following proteins: PITPα, PITPβ, C95A (PITPα) and RdgBα. The reduction rates were determined from the fluorescence decay curves. It appears that both PITPα and PITPβ, which had a higher maximum fluorescence from the binding assay, had slower reduction rates compared to C95A and RdgBα – **Table 5**. Since both C95A and RdgBα had the lowest maximum fluorescence (**Table 4**), it is anticipated that both proteins would have a faster reduction rate, which is shown here – **Table 5**. This means that NBD-PC is bound by both C95A and RdgBα in a manner whereby the NBD portion is more solvent accessible compared to PITPα. Consequently, in the presence of dithionite the more solvent exposed NBD will be reduced faster.

Table 5: Rate constants from NBD-PC reduction by sodium dithionite
NBD-PC reduction rates by sodium dithionite. Data represents the average of two measurements.

Protein	**Rate Constant (s^{-1})**
PITPα	0.0099 ± 0.000009
PITPβ	0.0073 ± 0.00002
C95A	0.040 ± 0.0003
RdgBα	0.036 ± 0.0003

3.4 FRET Transfer Studies

3.4.1 Characterization of FRET Transfer Assay

The FRET transfer assay used in this thesis has been previously described by Zhang *et al.* [72]. The conditions used by Zhang *et al*. included SET buffer and TRITC DHPE as the FRET acceptor molecule. Here TKE buffer was used instead of SET buffer while Liss Rhod PE was used instead of TRITC DHPE. Prior to data collection, the

assay was optimized under these new conditions. The optimization of the FRET transfer assay was performed using PITPβ and lipid vesicles prepared by bath sonication. Under the new conditions, the overall trend observed was similar – **Figures 30** and **31**. This means that changing the buffer system or the FRET acceptor molecule did not affect the outcome of the assay.

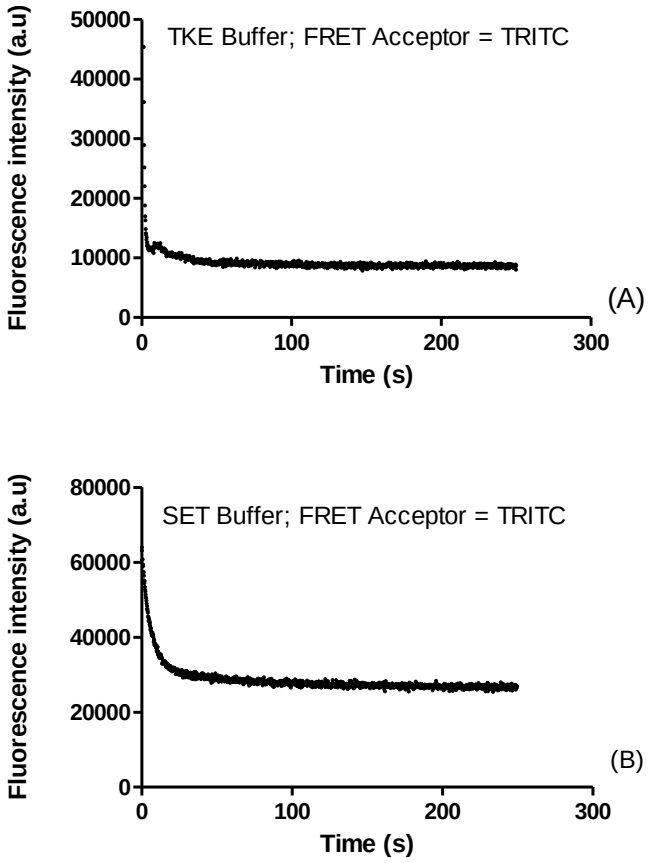

Figure 30: Comparison between SET and TKE buffer conditions for the FRET transfer assay

Fluorescence loss during ligand transfer by PITPβ (2 μM) in TKE (A) and SET (B) buffer; FRET acceptor used was TRITC and lipid vesicles were PC SUVs (100 μM). A single representative data trace is shown.

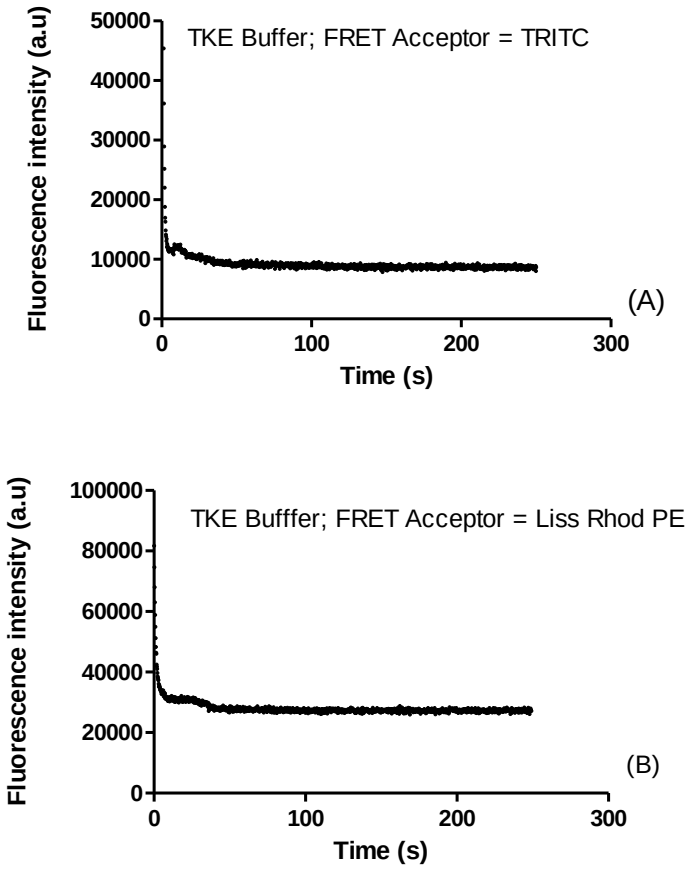

Figure 31: Comparison between TRITC and Liss Rhod PE as FRET acceptor molecules in the FRET transfer assay
Raw fluorescence trace of PITPβ (2 μM) in TKE buffer in the presence of PC SUVs (100 μM) containing either 3 mol% TRITC (A) or Liss Rhod PE (B). A single representative data trace is shown.

3.4.2 FRET Transfer Studies: Control Experiments

Prior to performing the FRET transfer studies a series of control experiments were carried out to ensure the validity of the data obtained from the FRET transfer assays. One of the control experiments conducted was to observe what takes place when NBD-PC was present in the absence of both protein and lipid vesicles. It appeared that negligible background fluorescence was observed which did not change over time – especially

within the time frame of the measurement (**Figure 32**). This is consistent with the property of NBD, which fluoresces marginally in polar environments [68].

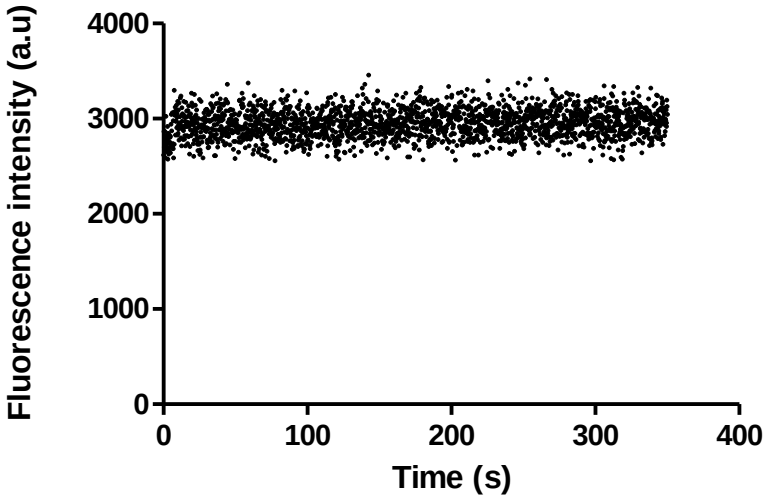

Figure 32: Fluorescence measurement of NBD-PC in TKE buffer
The fluorescence trace of NBD-PC (0.2 μM) in TKE buffer in the absence of protein and lipid vesicles. A single representative data trace is shown.

In order to determine the rate of spontaneous transfer of NBD-PC to lipid vesicles, PC SUVs were mixed with NBD-PC and the fluorescence of NBD was monitored. The PC SUVs prepared did not contain any FRET acceptor molecules. It was observed that an insignificant increase in NBD fluorescence was seen over time – **Figure 33**. This means that the rate of spontaneous transfer of NBD-PC was negligible in the absence of protein. In contrast a test was conducted to determine the maximum fluorescence when the amount of NBD-PC used in the transfer studies were completely transferred to lipid vesicles. This analysis involved preparing PC SUVs containing the amount of NBD-PC used in the transfer assays and the NBD fluorescence was measured. The results showed that a fluorescence count of approximately 260000 a.u. was observed – **Figure 34**. In comparison with data from **Figure 33** – this observation further verifies

that the rate of spontaneous transfer of NBD-PC to lipid vesicles is insignificant especially within the time frame of the assay.

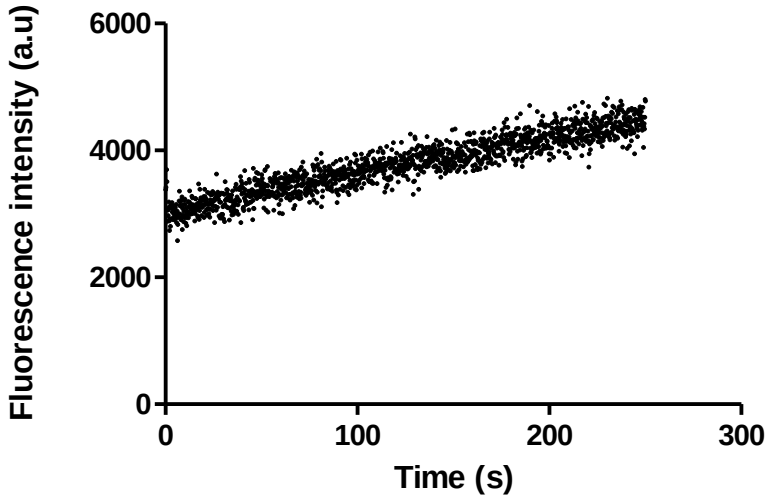

Figure 33: Fluorescence measurement of NBD-PC in the presence of PC SUVs
The fluorescence trace of NBD-PC (0.2 μM) in the presence of PC SUVs (100 μM) without FRET acceptor molecules and protein. A single representative data trace is shown.

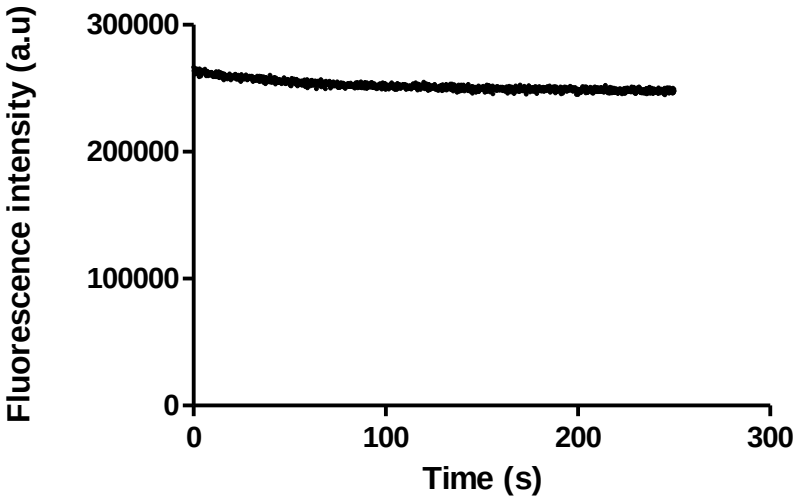

Figure 34: Fluorescence measurement of NBD-PC incorporated into PC SUVs
The fluorescence trace of NBD-PC (0.2 μM) incorporated into PC SUVs (100 μM) without FRET acceptor molecules. A single representative data trace is shown.

The final control experiment involved measuring the fluorescence of NBD-PC in the presence of protein but in the absence of lipid vesicles. NBD-PC was incubated with the protein of interest for 15 min and the fluorescence of NBD-PC-bound protein was determined. It was noted that a fluorescence count of about 90000 a.u. was obtained. Moreover, the fluorescence signal did not vary within the time frame of measurement – **Figure 35**. This observation also revealed that photobleaching of NBD-PC was not a significant problem here.

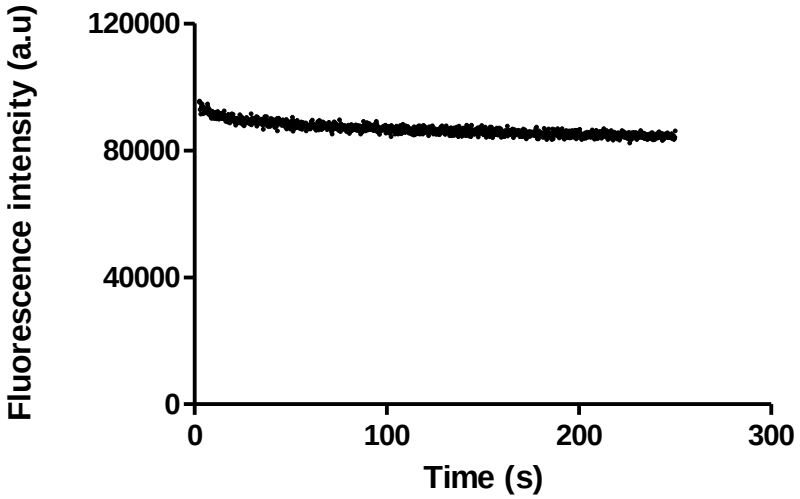

Figure 35: Fluorescence measurement of NBD-PC bound to PITPα without the presence of lipid vesicles
Raw fluorescence trace of NBD-PC (0.2 μM) bound to PITPα (2 μM) in the absence of lipid vesicles. A single representative data trace is shown.

Figure 36 shows a successful transfer assay where pre-incubated NBD-PC bound to protein was mixed with lipid vesicles. The initial fluorescence count is a result of NBD-PC bound to protein. If the transfer of NBD-PC to lipid vesicles is successful, quenching of the NBD fluorescence is observed as seen in **Figure 36**. The quenching of the NBD fluorescence is a result of the presence of a FRET quencher present in the lipid vesicles.

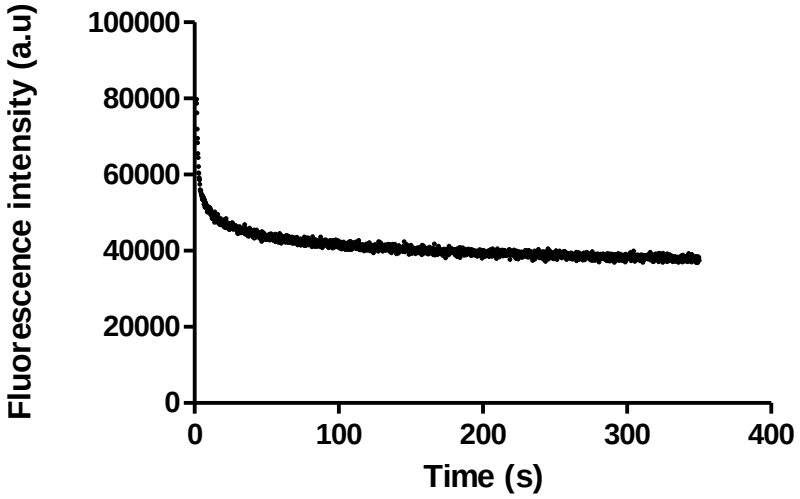

Figure 36: Fluorescence measurement of NBD-PC bound to PITPα in the presence of PC SUVs

The fluorescence loss of NBD-PC (0.2 μM) bound to PITPα (2μM) in the presence of PC SUVs (100 μM). A single representative data trace is shown.

3.4.3 FRET Transfer Studies with PITPα and PITPβ

3.4.3.1 The Effect of Membrane Curvature on PITP's Ligand Transfer Rate

The rate of ligand transfer by both PITPα and PITPβ were first measured to PC SUVs containing 3 mol% Liss Rhod PE. Interestingly both PITPα and PITPβ transferred NBD-PC to lipid vesicles at significantly different rates. The results revealed that PITPβ deliver NBD-PC to lipid vesicles twice as fast as PITPα – **Figure 37.** It should be noted that the lipid vesicle concentration used for both PITPα and PITPβ measurements differ; 100 μM for PITPα and 50 μM for PITPβ. This is because the ligand transfer rate for PITPβ was too fast for complete data-capture using our stopped-flow device. Therefore, with regards to the FRET transfer assays, all PITPβ measurements were performed with 50 μM lipid concentration instead of 100 μM. Taking this into consideration, the ligand transfer rate of PITPβ is nearly four times faster compared to PITPα. It is known that although both PITPα and PITPβ are structurally similar, their localization within cells and

expression in tissues differ. Thus, it is assumed that both proteins may possess different cellular functions. The variation in the ligand transfer rate observed here between PITPα and PITPβ may point towards this direction.

When PC SUVs were substituted with PC LUVs, the ligand transfer rate for both PITPα and PITPβ decreased significantly – **Figure 37**. The ligand transfer rate for PITPβ to PC-LUVs dropped by nearly ten-fold when compared to PC SUVs. However for PITPα, no rate constant could be extracted as the ligand transfer rate slowed down drastically when PC LUVs replaced PC SUVs. This observation for both proteins implies the preference for highly curved or curvature stressed membrane surfaces during ligand transfer.

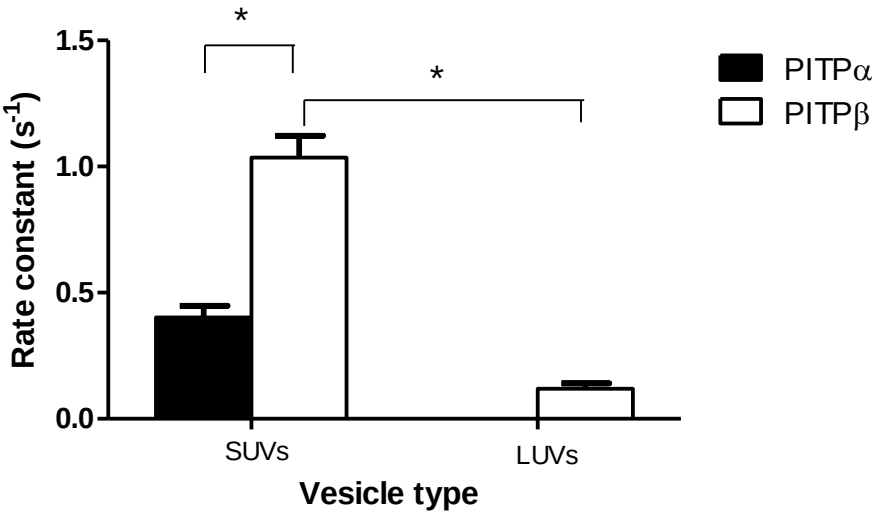

Figure 37: Comparison of ligand transfer rates between PITPα and PITPβ to PC vesicles

Ligand transfer rates for PITPα (2 μM) and PITPβ (2 μM) to PC vesicles. 100 μM lipid vesicles were used for PITPα and 50 μM for PITPβ. Data are of the average of six measurements with standard error of measurement. (* denotes unpaired t-test, $p < 0.0001$).

3.4.3.2 The Effect of PI on PITP's Ligand Transfer Rate

It is known that both PITPα and PITPβ possess a higher affinity for PI compared to PC [20]. Based on this observation, it is thought that the presence of PI in lipid membranes may increase the ligand transfer rate of PITP. However when PI was present in lipid vesicles, the ligand transfer rate for PITPβ did not change significantly compared to when no PI was present – **Figure 38**. In the case of PITPα, there was a slight increase in the transfer rate when 4 mol% PI was present in lipid vesicles. However, when the PI content in lipid vesicles were increased from 4 to 16 mol%, the increase in transfer rate actually diminished by ~30 % – **Figure 38**.

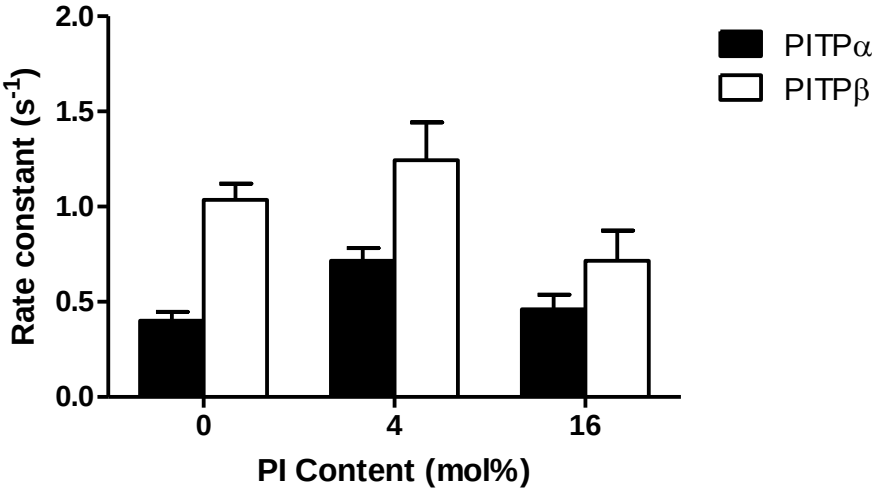

Figure 38: The effect of PI on the ligand transfer rates of PITPs
Ligand transfer rates for PITPα (2 μM) and PITPβ (2 μM) to PC SUVs containing PI. 100 μM lipid vesicles were used for PITPα and 50 μM for PITPβ. Data are the average of six measurements with standard error of measurement. Data for PITPα were significantly different between 0 and 4 % PI (unpaired t-test, p = 0.0031) and between 4 and 16 % PI (unpaired t-test, p = 0.0314). Data for PITPβ were not significantly different.

3.4.3.3 The Effect of PS on PITP's Ligand Transfer Rate

An alternative anionic lipid was tested to determine if charge played a role in the ligand transfer rate of PITP. In this case, PS was used instead of PI. The results showed that the transfer rate increased for PITPβ when 4 mol% PS was present in lipid vesicles but no further increase in transfer rate was observed when the PS content was increased to 16 mol% - **Figure 39**. In contrast, PITPα showed gradual increase in transfer rate as the PS concentration increased from 0 to 16 mol% in lipid vesicles – **Figure 39**.

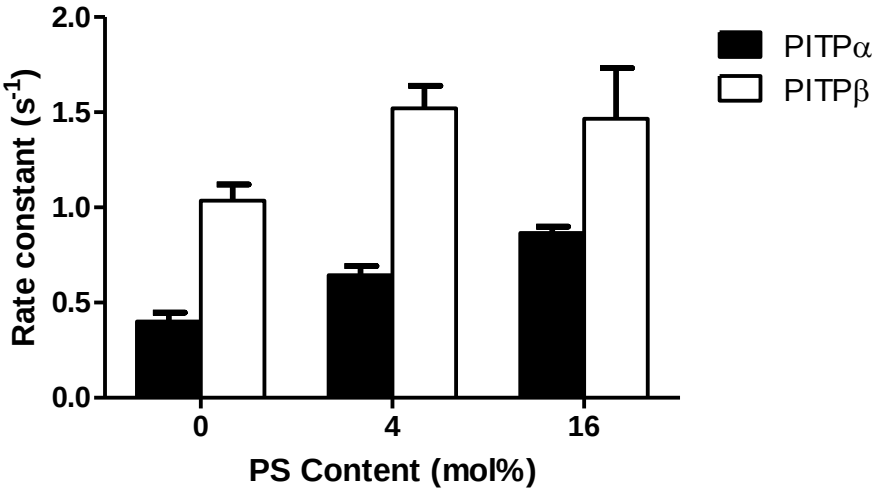

Figure 39: The effect of PS on the ligand transfer rates of PITPs
Ligand transfer rates for PITPα (2 μM) and PITPβ (2 μM) to PC SUVs containing PS. 100 μM lipid vesicles were used for PITPα and 50 μM for PITPβ. Data are averages of three to six measurements with standard error of measurement. Data for PITPα were significantly different (unpaired, t-test, $p < 0.05$). Only data for PITPβ between 0 and 4 % PS were significantly different (unpaired t-test, $p = 0.014$).

3.4.3.4 The Effect of PA on PITP's Ligand Transfer Rate

The presence of PA in lipid vesicles was also tested to establish whether PA played a role on the ligand transfer rate of PITPs. Besides being an anionic lipid, PA has recently been shown to play a plausible role in recruiting Nir2 to membranes [73]. Nir2 or RdgB α1 is a human Class II PITP – see **Section 1.4.1**. PA is an indirect product of $PI(4,5)P_2$ hydrolysis at the plasma membrane. The two main products of $PI(4,5)P_2$ hydrolysis are inositol 1,4,5-triphosphate and DAG, both which are signaling molecules [74]. DAG in turn can be phosphorylated to produce PA. In order to maintain the signaling cascade at the plasma membrane, PI(4,5)P2 needs to be replenished by supplying PI to the plasma membrane. At the same time, the accumulated PA at the plasma membrane needs to be transferred to the ER for conversion to PI [74]. In the study conducted by Kim *et al.* it was shown that Nir2 could bind PA at the plasma membrane and in turn deliver PI from the Golgi apparatus. Based on the PA-binding capacity and PI-transfer ability of Nir2, it was proposed that Nir2 may play a role in coupling PA to phosphoinositide signaling [73-74].

Despite $PI(4,5)P_2$ existing predominantly in the plasma membrane, $PI(4,5)P_2$ may be present in the Golgi apparatus transiently [75]. Therefore, the effect of PA was tested on the ligand transfer rate of both PITPα and PITPβ. The results showed that the presence of PA in lipid vesicles significantly increased the ligand transfer rate of PITPα and PITPβ – **Figure 40**.

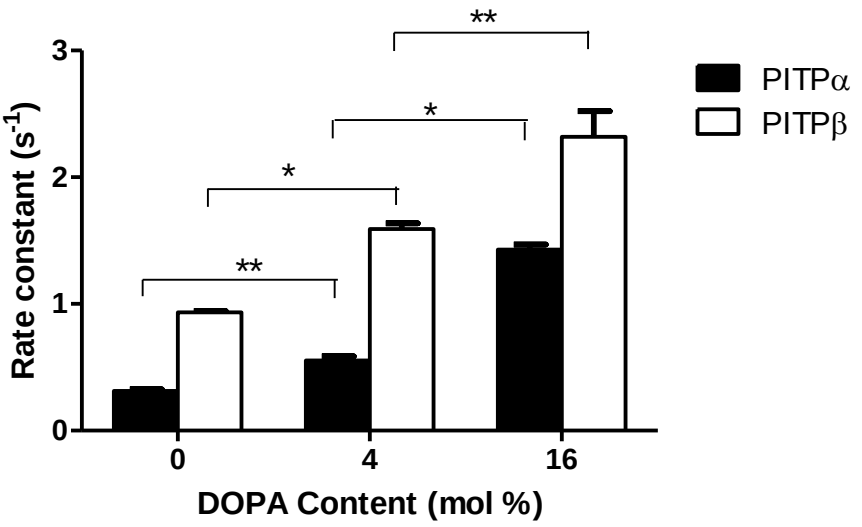

Figure 40: The effect of PA on the ligand transfer rates of PITPs to lipid vesicles
Ligand transfer rates for PITPα (2 μM) and PITPβ (2 μM) to PC SUVs containing PA. 100 μM lipid vesicles were used for PITPα and 25 μM for PITPβ. Data are averages of three measurements with standard error of measurement. (* denotes unpaired t-test, $p < 0.0001$; ** denotes $p < 0.05$)

3.4.3.5 The Effect of Phosphoinositides on PITP's Ligand Transfer Rate

PI delivery to membranes by PITPs has been shown to be associated with the production of phosphoinositides. Therefore, whether the presence of phosphoinositides in membranes played a role in PITP ligand transfer was examined. PITPα is localized mainly in the nucleus and cytoplasm [25]. $PI(4,5)P_2$ is the dominant phosphoinositide present in the nucleus. However, $PI(3,4,5)P_3$ is also thought to be present in the nucleus but in smaller quantities [7, 9]. For this reason the presence of both $PI(4,5)P_2$ and $PI(3,4,5)P_3$ in membranes was investigated to determine if these phosphoinositides have an effect on the ligand transfer rate of PITPα. The results obtained reveal that the transfer rate decreased by nearly half when 2 mol% $PI(4,5)P_2$ was present in lipid vesicles as opposed to when no $PI(4,5)P_2$ was present – **Figure 41**. Further increasing the concentration of $PI(4,5)P_2$ in lipid vesicles to 4 mol% did not decrease the ligand transfer

rate of PITPα. A similar trend was observed when $PI(3,4,5)P_3$ was present instead – **Figure 41**.

In contrast to PITPα, PITPβ is mainly localized in the ER and Golgi apparatus [25]. The main phosphoinositide present in Golgi apparatus is PI4P [7]. Therefore the effect of the presence of PI4P in lipid vesicles on PITPβ's ligand transfer rate was also investigated. It appears that the presence of 2 mol% PI4P in lipid vesicles reduces the ligand transfer rate of PITPβ – **Figure 42**. Further increasing the concentration of PI4P to 4 mol% did not decrease the ligand transfer rate.

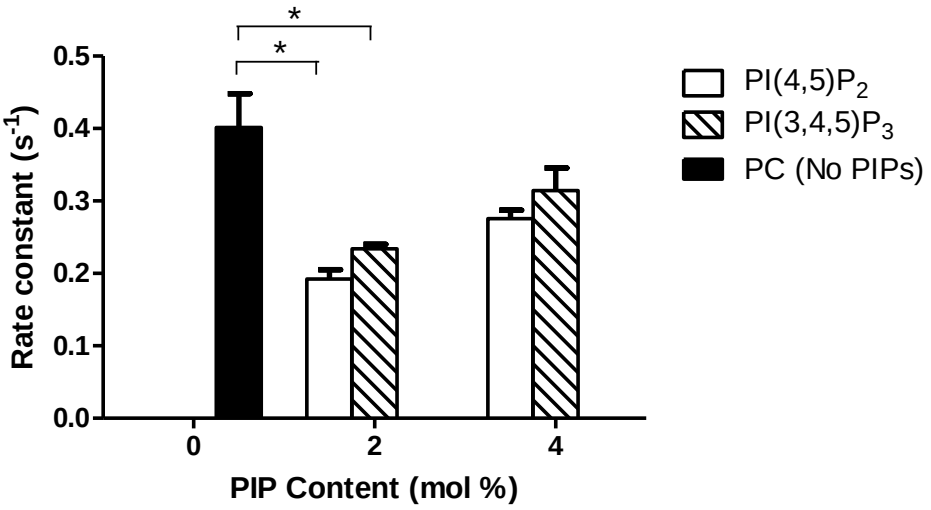

Figure 41: The effect of $PI(4,5)P_2$ and $PI(3,4,5)P_3$ on the ligand transfer rate of PITPα to lipid vesicles

Ligand transfer rates of PITPα (2 μM) to lipid vesicles (100 μM) containing either $PI(4,5)P_2$ or $PI(3,4,5)P_3$. Data are averages of three to six measurements with standard error measurement. (* denotes unpaired t-test, $p < 0.05$)

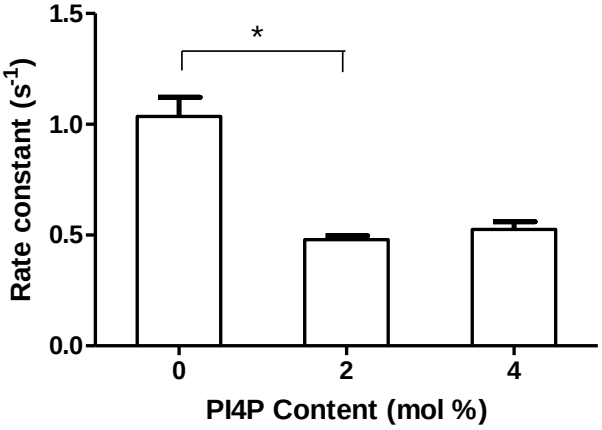

Figure 42: The effect of PI4P on the ligand transfer rate of PITPβ to lipid vesicles
Ligand transfer rates of PITPβ (2 μM) to lipid vesicles (50 μM) containing PI4P. Data are averages of three to six measurements with standard error measurement. (* denotes unpaired t-test, $p < 0.001$)

3.4.4 FRET Transfer Studies with W203A/W204A, K61A and C95A

The ligand transfer rate for the PITPα mutants namely W203A/W204A, K61A and C95A were also determined. For all three proteins, the transfer rate was measured with only PC SUVs. It is clear that both W203A/W204A and C95A were unable to transfer NBD-PC to lipid vesicles – **Figure 43**. No rate constant could be extracted; therefore, the raw data for both W203A/W204A and C95A are shown instead. The results observed for W203A/W204A were anticipated since the capacity of this mutant to bind to membranes had been compromised. Likewise the results for C95A were also expected since it was previously shown that C95A lacks the capability to transfer PC [23, 36]. Since K61A is still able to transfer PC but not PI it is no surprise that the ligand transfer rate of K61A with NBD-PC were closely related to those seen with wild type PITPα (**Figure 44)**.

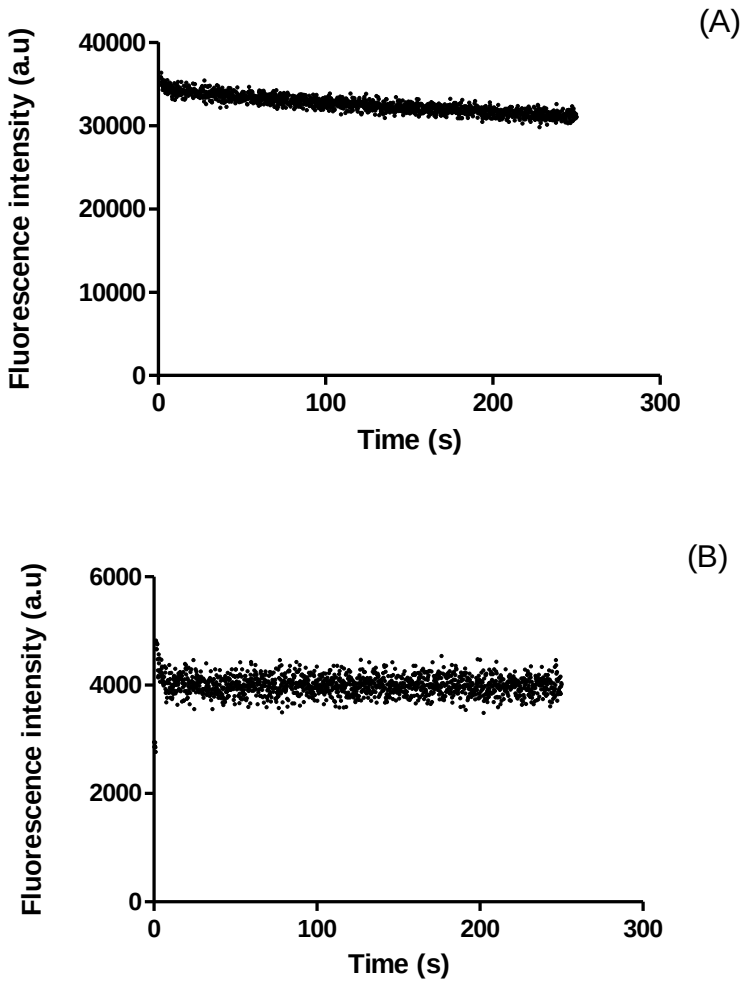

Figure 43: Ligand transfer for W203A/W204A and C95A to PC SUVs
The fluorescence loss during ligand transfer by W203A/W204A (2 μM) [A] and C95A (2 μM) [B] to PC SUVs (100 μM). A single representative data trace is shown.

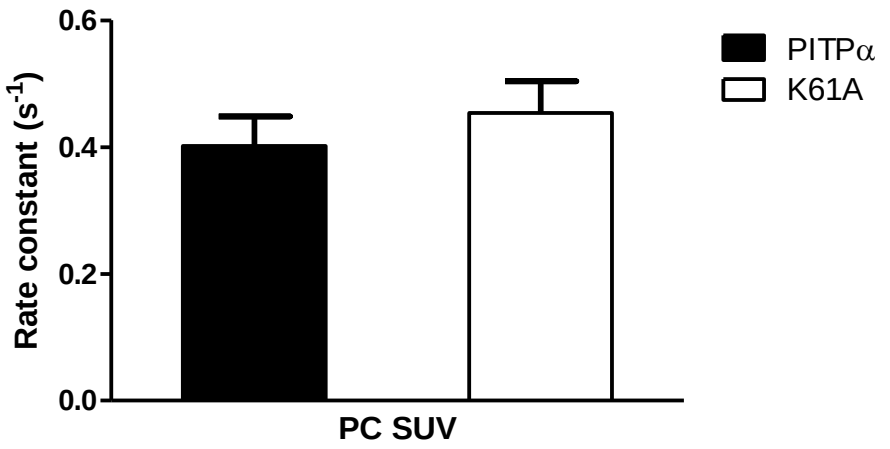

Figure 44: Comparison of ligand transfer rates between PITPα and K61A to PC SUVs

Ligand transfer rates of PITPα (2 μM) and K61A (2 μM) to PC SUVs (100 μM). Data are averages of three to six measurements with standard error measurement.

3.4.5 FRET Transfer Studies with RdgBα and Y210A/W211A

FRET transfer studies with RdgBα revealed that the protein was unable to transfer NBD-PC to PC lipid vesicles – **Figure 45**. It should be noted that for all previous transfer assays, the protein concentration was set at 2 μM. However, due to the poor expression of RdgBα a protein concentration of 1 μM was used instead. The transfer data for RdgBα is not surprising since despite having a high affinity for NBD-PC, K_d of 27 ± 3 nM, the maximum fluorescence obtained was low (8495 a.u.) compared to wild type PITPα (347054 a.u.). A similar trend was observed for the PITPα mutant, C95A, which showed a high affinity for NBD-PC (K_d = 17 ± 2 nM) but a low maximum fluorescence (13804 a.u.) and the inability to transfer NBD-PC to lipid vesicles. It can, therefore, be deduced that both RdgBα and C95A bind NBD-PC differently than wild type PITPα and in a manner where the NBD group is more solvent exposed, which explains the lower maximum fluorescence. Moreover, the NBD reduction assay by sodium dithionite

revealed that NBD-PC bound to either RdgBα or C95A had a faster reduction rate, by nearly four times compared to wild type PITPα. This assay verifies the binding variation of NBD-PC by RdgBα and C95A compared to wild-type PITPα. Taking into consideration the data at hand, it can be inferred that both RdgBα and C95A binds NBD-PC differently from wild type PITPα and in a manner that makes both proteins poor transporters of NBD-PC to lipid vesicles. The RdgBα data obtained here are in agreement with a recent study conducted by Yadav *et al.* [76]. The authors demonstrated that the PITP domain of RdgBα was a poor binder and transporter of PC [76].

In contrast, the mutant form of RdgBα, Y210A/W211A, which is supposed to lack membrane binding capabilities, was able to transfer NBD-PC to PC lipid vesicles but at a low rate, $k = 0.04 \pm 0.01\ s^{-1}$, as determined from two measurements. The Y210A/W211A mutant was designed to mimic the PITPα mutant, W203A/W204A, which also lacks the capacity to bind to membranes. While W203A/W204A showed the inability to transfer NBD-PC to lipid vesicles, Y210A/W211A did. However, the transfer rate was slower by 12 times compared to wild type PITPα, which had an average transfer rate of $0.48 \pm 0.05\ s^{-1}$. The RdgBα protein is a multi-domain protein unlike wild type PITPα. However, in these studies only the PITP domain of RdgBα is expressed and used for our investigation. The PITP domain of RdgBα shares only 40 % sequence identity with wild type PITPα [47]. Therefore, the behavior of the PITP domain of RdgBα may not necessarily be similar to that of wild type PITPα. In other words, the Y210 and W211 residues in RdgBα may not be essential for membrane docking as those of W203 and W204 in PITPα. In addition, RdgBα already possesses domains that help with membrane interactions [44].

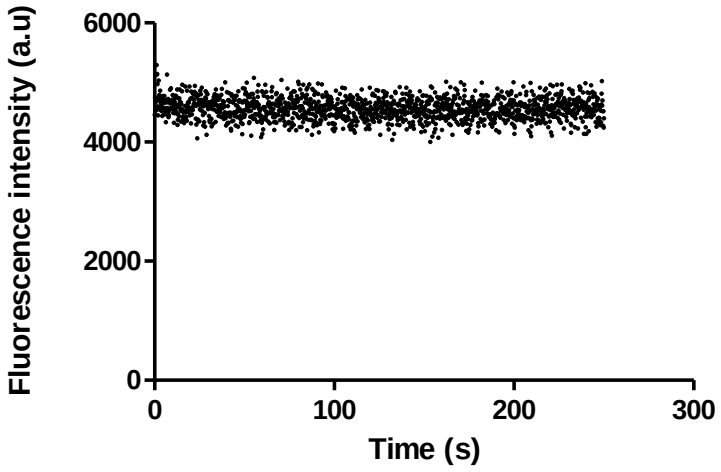

Figure 45: Ligand transfer by RdgBα to PC SUVs
Fluorescence loss during ligand transfer by RdgBα (1 μM) to PC SUVs (100 μM). A single representative data trace is shown.

3.5 FRET Pick-up Studies

3.5.1 FRET Pick-up Studies: Control Experiments

The FRET pick-up assay is the reverse of the FRET transfer assay and it simply measures the ability of PITPs to pick up NBD-PC from lipid vesicles. In this assay, NBD-PC is incorporated into SUVs along with Liss Rhod PE and PC. This means that the fluorescence of NBD-PC in the lipid vesicles is quenched by the presence of Liss Rhod PE. When these lipid vesicles containing NBD-PC is mixed with PITP, the fluorescence of NBD-PC was followed. An increase in NBD-PC fluorescence implies that PITP has successfully picked up NBD-PC from the lipid vesicles. A typical curve depicting this phenomenon is shown in **Figure 46A**. Alternatively, the fluorescence of Liss Rhod PE can also be monitored instead. In this case, a fluorescence decrease is observed as shown in **Figure 46B**. However for the purpose of consistency, the fluorescence of NBD-PC will be reported here.

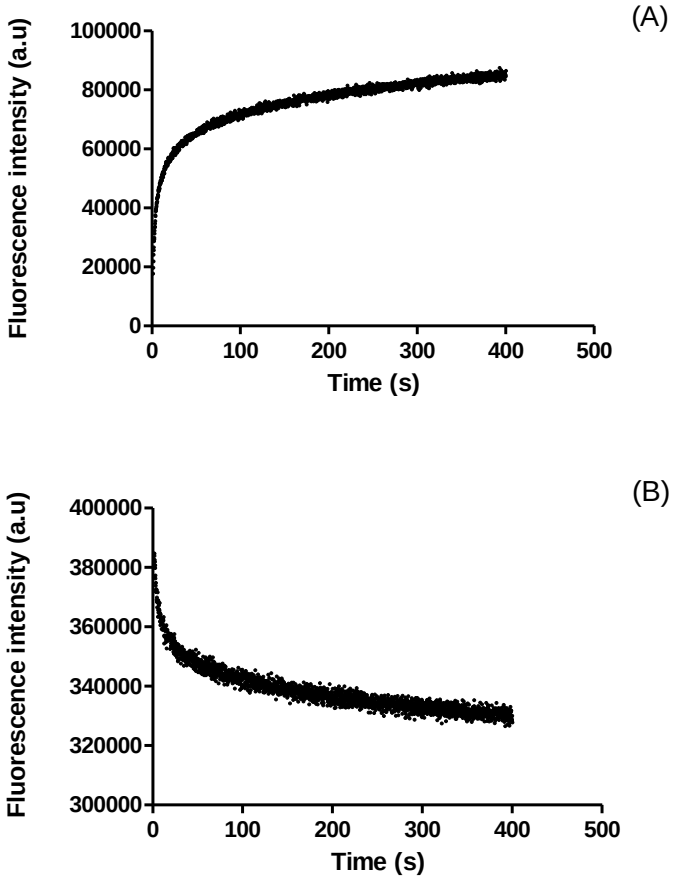

Figure 46: FRET pick-up assay monitored by NBD-PC fluorescence increase (A) and Liss Rhod PE fluorescence quenching (B)
The fluorescence trace of NBD-PC (A) and Liss Rhod PE (B) during ligand extraction by PITPα (2 μM) from PC SUVs (100 μM). A single representative data trace is shown.

When no protein was present, no increase in NBD-PC fluorescence was observed as shown in **Figure 47A**. A control protein, BSA, was also examined in this study. It appears that no increase in NBD-PC fluorescence was observed when BSA was present instead of PITP – **Figure 47B**. This suggested that BSA was not able to pick up NBD-PC from lipid vesicles. In addition this result further verified that the increase in NBD-PC fluorescence observed in the presence of PITP was attributed to the capacity of PITP to pick up NBD-PC from membranes.

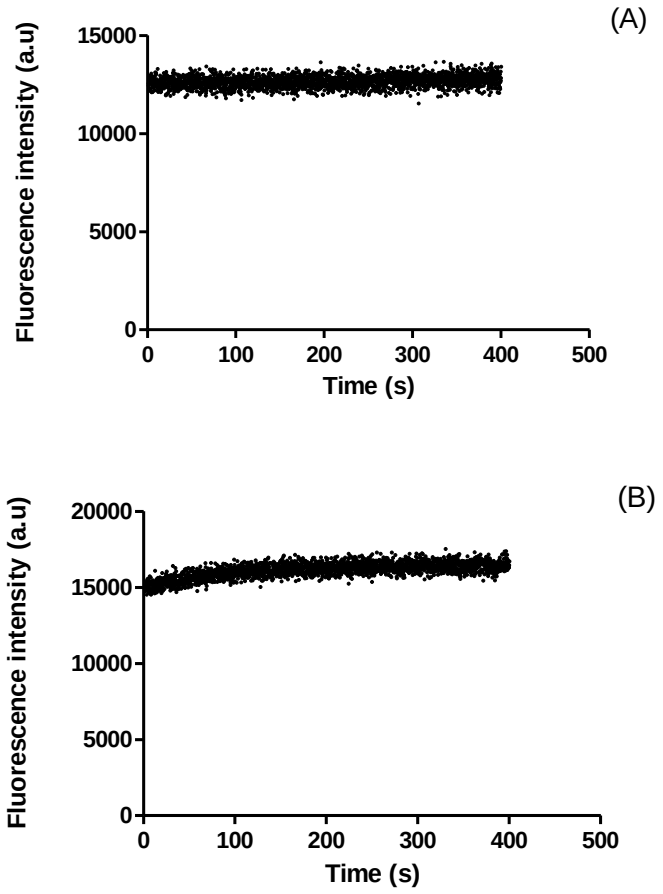

Figure 47: FRET pick-up assay control experiments with no protein (A) and with BSA (B)

The fluorescence trace of NBD-PC in the absence of PITP (A) and in the presence of BSA (B) in the FRET pick-up assay. A single representative data trace is shown.

3.5.2 FRET Pick-up Studies with PITPα and PITPβ

Both PITPα and PITPβ showed the ability to pick up NBD-PC from lipid vesicles as shown in **Figure 48**. From the results shown, it appears that PITPβ can pick up NBD-PC faster than PITPα. This is in line with the observation from the FRET transfer assay where PITPβ had a faster ligand transfer rate compared to PITPα.

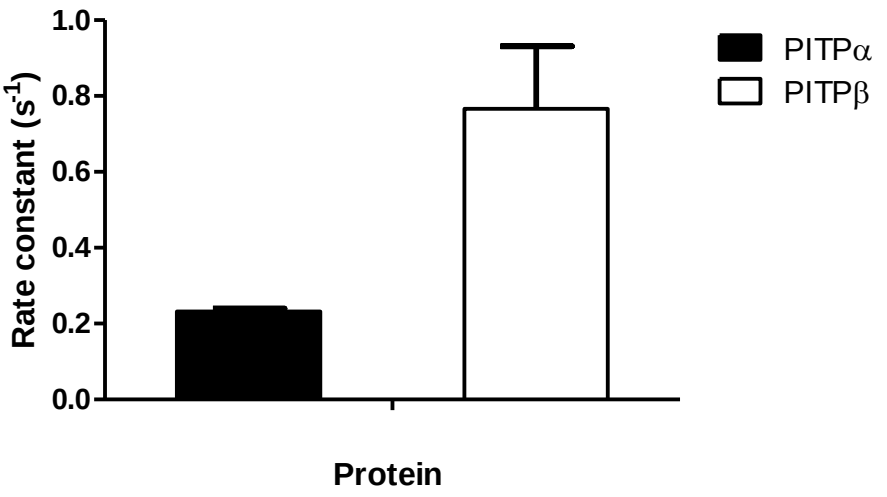

Figure 48: FRET pick-up studies with PITPα and PITPβ
Ligand pick-up rates of PITPα (2 μM) and PITPβ (2 μM) from PC SUVs (100 μM). Data are averages of two measurements with standard error measurement.

3.6 Investigation of Protein-Membrane Interactions by DPI

3.6.1 The Interaction of PITP with DOPC Lipid Layer

The capacity of PITP to bind to membranes was analyzed by means of DPI. In this assay, planar immobilized lipid bilayers are utilized instead of lipid vesicles. The immobilized lipid layer is formed when 100 nm vesicles were adsorbed and ruptured onto the DPI sensor chip surface. Once a stable lipid layer is achieved, protein was introduced over the immobilized lipid layer and the protein mass adsorbed onto the lipid layer was recorded. The same procedure was repeated with different protein concentrations, which allow protein binding affinity to be determined.

Using this methodology, both PITPα and PITPβ showed the capacity to bind DOPC lipid layers with a K_d of 1.85 ± 0.47 μM and 0.81 ± 0.45 μM respectively – **Figures 49** and **50**. The B_{max} values for both PITPα and PITPβ are as follows: 0.53 ± 0.06 ng/mm^2 and 0.42 ± 0.09 ng/mm^2. Interestingly, PITPβ appeared to have a higher

affinity by nearly two-fold for DOPC lipid layers compared to PITPα despite having closely related B_{max} values. However, in comparison to previous proteins analyzed by DPI, the amount of PITP bound to the lipid layer in general appeared to be low. Tocopherol transfer protein (TTP) for example, showed a K_d of 1.64 ± 0.32 μM and a B_{max} value of 2.09 ± 0.23 ng/mm^2 for DOPC:DOPS (90:10) lipid layers [77]. Note that although the K_d was comparable to that of PITPα, the B_{max} for TTP was significantly higher which indicates more protein was bound to the lipid surface.

The binding of W203A/W204A mutant to DOPC lipid layers was also examined by DPI. However, no binding was observed (data not shown). This was anticipated since the W203A/W204A mutant is known to be unable to bind to membranes [30, 36].

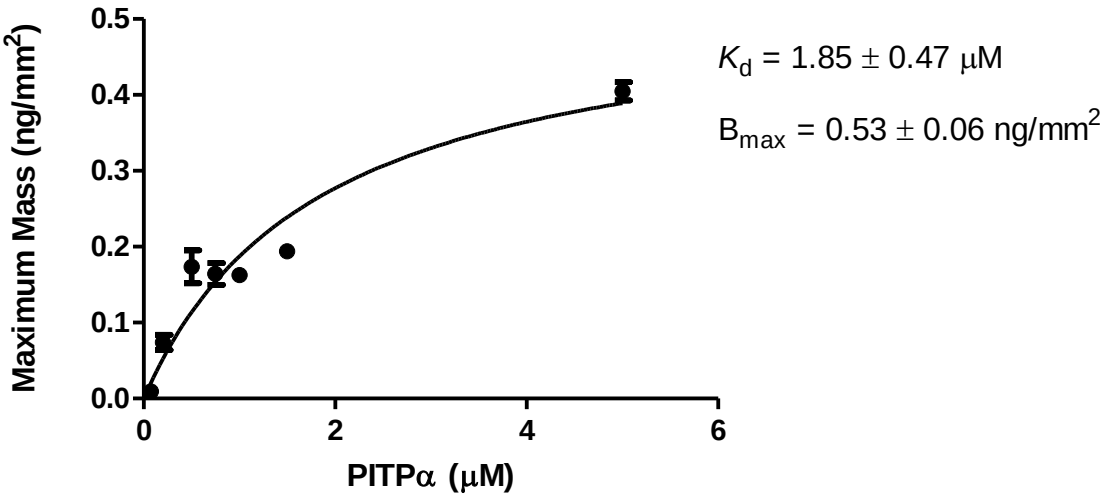

Figure 49: Plot of maximum specific mass of PITPα bound to DOPC lipid layer
Final lipid concentration was 1 mM. Data are averages of two measurements with standard error of measurement.

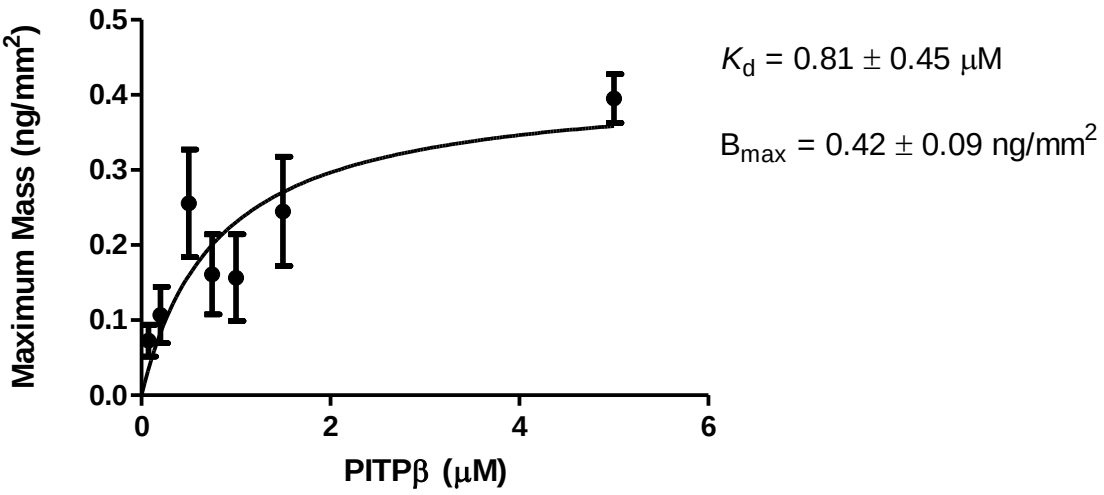

Figure 50: Plot of maximum specific mass of PITPβ bound to DOPC lipid layer
Final lipid concentration was 1 mM. Data are averages of two measurements with standard error of measurement.

3.6.2 The Effect of PI on PITP Binding to Lipid Membranes

To determine whether PI played a role in PITP binding to membranes, PI was incorporated into the immobilized lipid layers. The protein concentration was fixed at 0.5 μM and the amount of mass adsorbed to the lipid layers with increasing PI concentration was monitored. As seen in **Figure 51** the results obtained did not show that PI had a significant effect on PITP binding to membranes. This was true for both PITPα and PITPβ.

3.6.3 The Effect of PS on PITP Binding to Lipid Membranes

The effect of PS on PITP binding to membranes was also determined by DPI. Similar to PI, no significant enhancement or diminishment of PITP binding to membranes was observed in the presence of PS – see **Figure 52**.

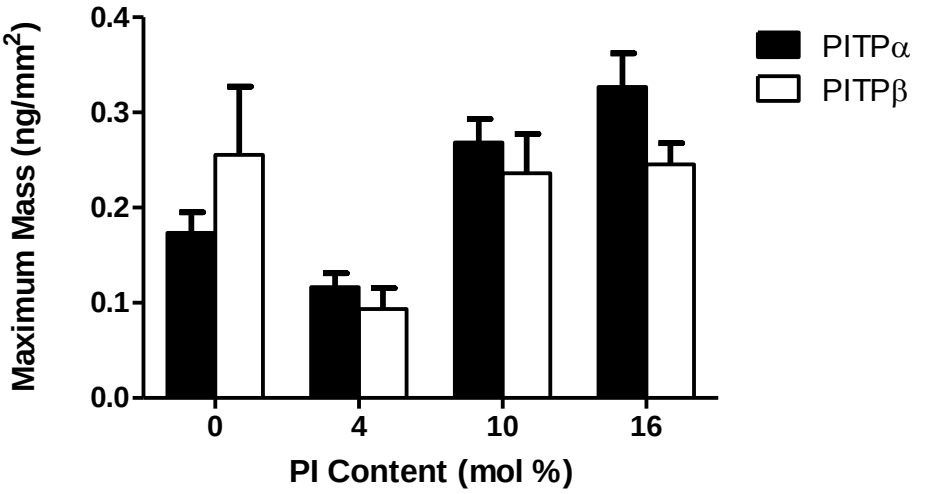

Figure 51: The effect of PI on PITP binding to membranes
The maximum specific mass of PITPα and PITPβ at 0.5 μM to DOPC lipid layers (1 mM) containing PI. Data are averages of two to four measurements with standard error of measurement.

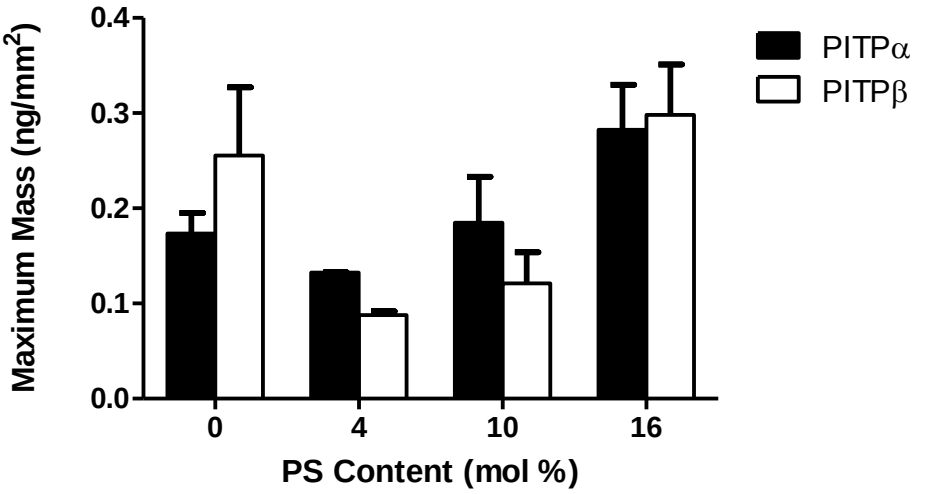

Figure 52: The effect of PS on PITP binding to membranes
The maximum specific mass of PITPα and PITPβ at 0.5 μM bound to DOPC lipid layers (1 mM) containing PS. Data are averages of two measurements with standard error of measurement.

3.6.4 The Effect of PE on PITP Binding to Lipid Membranes

PE is a negative curvature inducing lipid [78] and the effect of PE on PITP binding to membranes was examined. Although in DPI analysis the lipid layers are expected to be planar, incorporation of curvature inducing lipids such as PE is thought to increase the curvature stress within the planar lipid layer. In other words, forcing a lipid that naturally wants to curve into a flat configuration may result in a bilayer that is suffering some physical packing stress. Since in the FRET transfer studies it was observed that PITP had a preference for curved membrane surfaces – it is thought that the same effect on PITP binding to membranes may be seen here. To test this hypothesis a concentration of up to 25 mol% PE was incorporated into the DOPC lipid layer. However, the results showed that the presence of PE did not significantly enhance PITP binding to membranes – **Figure 53**. Comparing the maximum mass of PITPs to just plain DOPC lipid layers versus DOPC lipid layers containing PE – there was no significant difference.

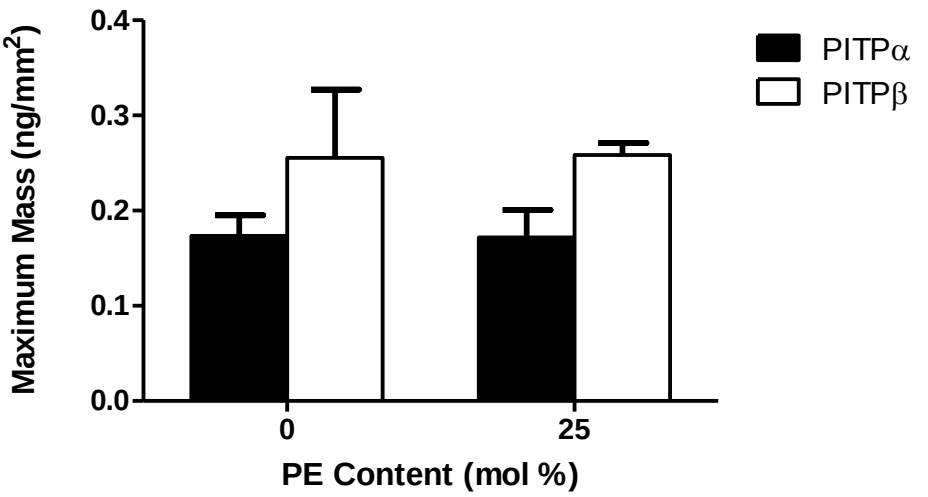

Figure 53: The effect of PE on PITP binding to membranes
The maximum specific mass of PITPα and PITPβ at 0.5 μM bound to DOPC lipid layers (1 mM) containing PE. Data are averages of two measurements with standard error of measurement.

3.6.5 The Effect of Ligand-bound PITP on PITP Binding to Membranes

Both PITPα and PITPβ at 0.5 μM were pre-incubated with either PI or PC for one hour. The pre-incubated PITPs were then introduced over a DOPC lipid layer to determine the amount of PITPs bound to membranes. The purpose of this investigation was to determine the amount of PITPs bound to membranes in its ligand-bound form. In comparison to ligand-free PITPα, the presence of PC did not significantly change the amount of PITPα bound to membranes – **Figure 54**. A similar trend was observed for PITPβ with PC – **Figure 54**. However when PI was pre-incubated with either PITPα or PITPβ nearly ~70 % less PITPα was found to bind to membranes and no binding was observed for PITPβ – **Figure 54**. The data obtained here revealed that PI-bound PITPs showed much reduced membrane affinity.

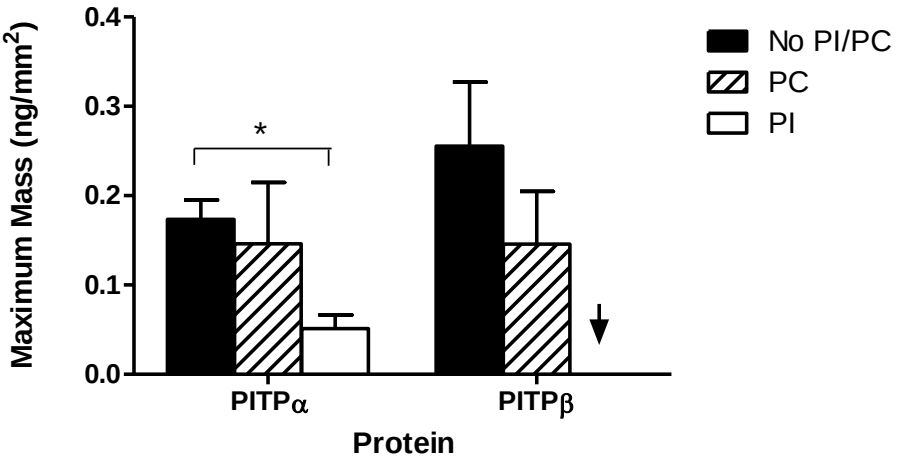

Figure 54: Comparison of maximum specific mass of PITPs bound to DOPC lipid layers with no ligand, bound PC and bound PI
Protein concentration was at 0.5 μM and DOPC concentration was at 1 mM. Data are averages of two to four measurements with standard error of measurement. Arrow indicates no mass data obtained for PITPβ pre-incubated with PI. (* denotes unpaired t-test, p = 0.0099)

3.6.6. The Interaction of RdgBα and Y210A/W211A with Lipid Membranes

The amount of RdgBα at 0.5 μM bound to membranes was also determined by DPI analysis. Three different membrane systems were tested which include DOPC, DOPC containing 10 mol% PI and PS respectively. The results obtained revealed no significant difference between the amounts of RdgBα bound to the different membrane systems – **Figure 55**. Thus, the presence of either PI or PS did not substantially affect RdgBα binding to membranes. Moreover, there was also no significant difference between the amounts of RdgBα bound to DOPC lipid layers in comparison to wild type PITPα. The same amount bound to DOPC lipid layers was observed for the RdgBα mutant, Y210A/W211A (YW/AA) mutant – **Figure 55**.

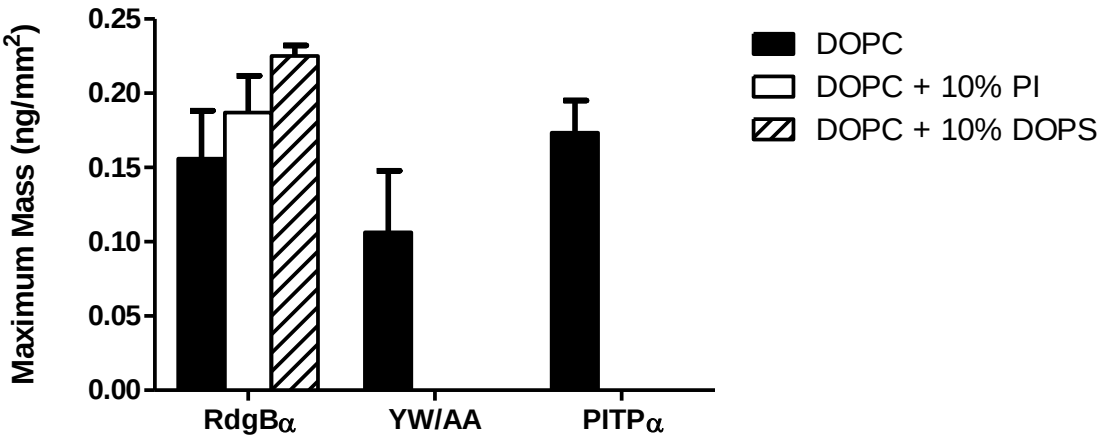

Figure 55: Comparison of maximum specific mass of RdgBα, YW/AA and PITPα bound to lipid membranes

Protein concentration was at 0.5 μM and lipid concentration was at 1 mM. Data are averages of two measurements with standard error of measurement.

3.7 PITP Interaction with Membranes Analyzed through Tryptophan Fluorescence Quenching

The interaction of both PITPα and PITPβ to membranes was analyzed using a tryptophan fluorescence quenching assay. The purpose of this assay was to utilize an alternative but comparative method to measure the membrane binding affinity of PITPs. PITPs possess seven tryptophan residues and two of the seven tryptophan residues are directly involved in membrane interactions. Tryptophan fluorescence quenching assays have been used to examine protein-lipid interactions [79]. Therefore, an attempt was made to measure the protein-lipid interactions of PITPs using this assay. Initially the assay was performed by measuring the fluorescence quenching of tryptophan residues present in PITPs. However, no fluorescence quenching was observed upon addition of PC lipid vesicles. The assay was then modified with the incorporation of pyrene-labeled PE into the lipid vesicles at 3 mol%. Here, the fluorescence of pyrene-PE was measured between 300 – 500 nm. However, no change in fluorescence was observed.

4. DISCUSSION & CONCLUSION

4.1 Ligand Transfer and Pick-up by PITPs

The purpose of performing the FRET transfer and pick-up assay was to show the capacity of PITPs to deliver and extract NBD-PC from membranes, and in each case both assays proved that the proteins can act as lipid transfer catalysts. This is an essential function to know since PITPs are believed to be lipid transfer proteins. Furthermore, the FRET assays employed here have also been used to measure the rate of ligand delivery and pick-up by PITPs. This enables the comparison of rates to different membrane systems, especially using the FRET transfer assay.

One of the most interesting observations was the difference in ligand transfer rate between PITPα and PITPβ to PC SUVs. It appears that PITPβ has a four-fold faster ligand transfer rate compared to PITPα despite their overall similarity in structure. The difference in the ligand transfer rates between PITPα and PITPβ correlates with studies previously conducted by Shadan *et al.* [36]. In Shadan's investigation, it was shown that PITPβ had a higher propensity for membrane binding compared to PITPα. Their results revealed that PITPβ contacted membranes more frequently and within a shorter time frame compared to PITPα [36] – see **Section 1.4.5** for further details. The faster ligand delivery rate of PITPβ could mean that PITPβ is interacting with membranes more quickly and frequently compared to PITPα and consequently gives up its ligand more easily. In support of PITPβ's faster ligand delivery rate, the FRET pick-up studies revealed that PITPβ also had a faster ligand pick-up rate compared to PITPα emphasizing PITPβ's greater efficiency at interacting with membrane bilayers.

Another interesting observation is that both PITPα and PITPβ appeared to have a preference to deliver their ligands to highly curved membranes. The ligand transfer rate for PITPα and PITPβ were significantly higher when SUVs were the accepting membranes versus LUVs. SUVs were prepared by means of probe sonication and were estimated to have an average diameter of 30 nm. LUVs on the other hand were prepared by extrusion using a 100 nm filter membrane and the average diameter of the LUVs used were determined to be about 150 nm. The lipid head-groups of the outer bilayer in SUVs are less densely packed together compared to LUVs [80-81]. The spaces between the lipid head groups allow easier access for PITPs to insert into the head group region of SUVs compared to LUVs. This could possibly explain the faster ligand transfer rate of PITPs to SUVs versus LUVs. PITPs could take a longer time or have less favorable interaction energy to access the densely packed lipid head groups in LUVs, which would explain the slower ligand transfer rate. The propensity for highly curved membranes is a phenomenon that is beginning to be more commonly seen with LTPs [14]. Other examples include TTP [72] and the fatty acid binding protein (FABP) [82] – both proteins showed higher ligand transfer rates to SUVs compared to LUVs.

The relevance of this observation in biological systems can be described as follows. Biological membranes undergo constant remodeling mainly to accommodate cellular events such as cell division and cellular trafficking [60]. These events consequently result in localized areas of membrane curvature. The change in membrane curvature is mainly brought about by proteins and lipids as discussed in **Section 1.6.3**. It is plausible that LTPs have been designed to take advantage of these localized areas of membrane curvature to bind to membranes and deliver or extract its ligands. Therefore,

it is likely that PITPs interact with membranes by sensing the physical changes in membranes which is becoming a more common mechanism for the recruitment of peripheral proteins to membranes [49-51].

Synaptojanin 1 (SYNJ1), although a non-LTP, is an example of a protein where both its recruitment to membranes and activity is sensitive to membrane curvature. SYNJ1 is a phosphoinositide phosphatase which converts PI(4,5)P_2 to PI4P [83]. SYNJ1 is highly expressed in nerve terminals and is found to play a role in clathrin-mediated endocytosis [83]. Using a sedimentation assay, Chang-Ileto *et al.* showed that the binding of SYNJ1 to 50 nm liposomes increased by nearly 50 % compared to 800 nm liposomes. Furthermore, the hydrolysis of PI(4,5)P_2 by SYNJ1 was markedly increase in the presence of 50 nm liposomes in comparison to 800 nm liposomes by approximately 30 % [83].

In the next study I investigated whether the presence of PI in membranes played a role in the ligand transfer rate of PITP. While PI did not affect the ligand transfer rate of PITPβ, only 4 mol% of PI in membranes increased the ligand transfer rate of PITPα (**Figure 38**). However, the ligand transfer rate of PITPα did not show a dramatic increase even with 4 mol% PI. Moreover, when the PI concentration was further increased to 16 mol%, the increase in ligand delivery was diminished. Overall it seems that the occurrence of PI in a bilayer does not have a significant effect on the rate of the ligand transfer mechanism of PITPs. It was hypothesized that due to the higher affinity of PITPs for PI, the presence of PI in membranes may attract PITPs to membranes to deposit the NBD-PC for which it has less affinity, and withdraw PI for transfer to its required destination. However, the results observed here do not support this hypothesis.

Since PI is an anionic lipid, an alternative anionic lipid was also tested to determine if charge played a role in the ligand transfer of PITPs. Here, PS was used instead of PI. The ligand transfer rate for PITPα increased as the concentration of PS in lipid vesicles increased (**Figure 39**). However for PITPβ, the ligand transfer rate only increased at 4 mol% PS. A further increase in PS concentration to 16 mol% did not change the ligand transfer rate of PITPβ. At this point it is inconclusive whether charge plays a role here especially for PITPα. Taking into consideration other LTPs whose ligand transfer and membrane interaction is influenced by anionic lipids, the effect is much more significant than what was observed with PITPα. One such example is FABP which showed up to nearly 20-fold increase in transfer rate when anionic lipids (depending on lipid species) were present in the acceptor membrane [82].

Taking into consideration the data obtained for both PI and PS in regards to PITPβ, it can be deduced that charge likely has no role in membrane recognition by the protein. In contrast, ligand transfer by PITPα in the presence of PS increased to only a minor extent, and no change was observed for PI. However, the rate enhancement effect of PS is not nearly as drastic as seen for FABP. Therefore, it is unlikely that charge affects the ligand transfer rate of PITPα. Moreover, if both PS and PI are negatively charged lipids – it is unclear why PS would have an effect on the ligand transfer rate of PITPα and not PI. Since both PI and PS possess a similar shape whereby both lipids are cylindrical [84-85], it is unlikely that membrane curvature brought about by these lipids is causing the different effects in the ligand transfer rate of PITPα. However, PI and PS may affect other physical parameters of membranes such as lipid packing. The effect of PI in PC model membranes has been previously examined and PI has been found to affect

the lipid packing [86]. This may provide an explanation for the different effects of PI and PS on the transfer rates of PITPα. However, if this is true, it remains unclear why PS did not have the same effect on PITPβ since both PITPα and PITPβ are closely related. There is a possibility that even though both PITPα and PITPβ are structurally similar they may differ in their ligand transfer mechanism. This hypothesis requires further investigation.

PA is also an anionic lipid and we tested the effect of PA on PITP ligand transfer due to the known effect it has in recruiting Nir2 proteins to membranes. The data obtained for both PITPα and PITPβ showed that PA significantly increased the ligand transfer rates by approximately two-fold when 16 mol% PA was present in membranes (**Figure 40**). Both PITPα and PITPβ have been shown not to bind PA directly [41, 87]. In the case of the Nir2 proteins, it has been shown that Nir2 binds PA and it is believed that the capability of Nir2 to bind PA, and at the same time deliver PI, is what associates Nir2 with phosphoinositide signaling [73-74]. However, with the PITP proteins, this is not the case. Besides being an anionic lipid, PA is also a negative-curvature inducing lipid [88-90]. Since PITPs do not bind PA, it is unlikely that the enhanced ligand transfer rate observed for PITPα and PITPβ is due to their capacity to specifically recognize and bind PA in membranes, but rather, to recognize the physical effect that PA has on membranes.

The effect of phosphoinositides in membranes on the ligand transfer rate of PITPs was also examined. It was interesting to note that the presence of 2 mol% of both PI(4,5)P_2 and PI(3,4,5)P_3 decreased the ligand transfer rate of PITPα by nearly half (**Figure 41**). However, increasing the phosphoinositide concentration did not further

diminish the ligand transfer rate. To date there is no evidence showing that PITPs possesses the ability to bind or recognize phosphoinositides. Therefore, this would be an area of interest to pursue further based on the data obtained here. Similarly, PITPβ showed the same trend when PI4P was present in membranes; the ligand transfer rate of PITPβ decreased by half at 2 mol% of PI4P (**Figure 42**). Doubling the PI4P concentration to 4 mol% did not further decrease the ligand transfer rate of PITPβ. This most likely has to do with the phosphoinositides effect on membrane properties such as membrane curvature, which is brought about by the larger head groups of phosphoinositides [91-92].

At this point it is still uncertain whether PITPs can bind phosphoinositides directly. If PITPs binds phosphoinositides as a ligand, then the presence of phosphoinositides in membranes should increase rather than decrease the ligand transfer rate of PITPs. Phosphoinositides are highly negatively charged lipids – they carry more than one negative charge unlike PI, PS and PA, which have only one negative charge [93]. The inner leaflet of the plasma membrane contains a high amount of anionic lipids that act as recruiting agents of peripheral membranes by means of electrostatic interactions [94]. However, with the PITPs, the reverse is seen whereby the ligand transfer rate of PITPs is reduced by phosphoinositides. The possibility of charge repulsion involved here should not be dismissed. To address this hypothesis the electrostatic potential map for PITPα and PITPβ was examined – **Figure 56**. The majority of the negative electrostatic potential (red) of both PITPs is located away from the two tryptophan residues which are essential for membrane docking. Therefore, it is

unlikely that charge repulsion accounts for the diminished ligand transfer rate observed for PITPs when phosphoinositides are present in membranes.

Phosphoinositides have been shown to affect the physical properties of membranes including membrane curvature and elasticity [92]. These physical changes to the lipid bilayer may in turn affect protein function. These physical changes to the lipid bilayer can be brought about by either the depletion or enrichment of phosphoinositides. As mentioned previously, phosphoinositides have larger head groups, which mean they are positive-curvature inducing lipids [91-92]. Our data have demonstrated that PITPs prefer to bind to membranes where the head groups are loosely packed. We have observed higher ligand transfer rates with PC SUVs versus LUVs and also with PC SUVs containing PA, which is a negative-curvature inducing lipid. Therefore, it can be deduced that the decreased ligand transfer rate to SUVs containing phosphoinositides may be due to the lack of head group space for PITPs to insert its tryptophan residues. To test this deduction further, the ligand transfer rate of PITPs to SUVs can be examined with the presence of an alternative lipid with a large head group such as lysophosphatidylcholine [56].

The ability of PITPs to recognize the presence of phosphoinositides in membranes should also not be disregarded. If PITPs truly acts as LTPs and deliver PI for the biosynthesis of membrane phosphoinositides, there is a possibility that phosphoinositides could act as a negative feedback for PITPs to stop or reduce PI delivery. However, this hypothesis needs to be further established by first examining whether PITPs recognizes and binds phosphoinositides as a ligand.

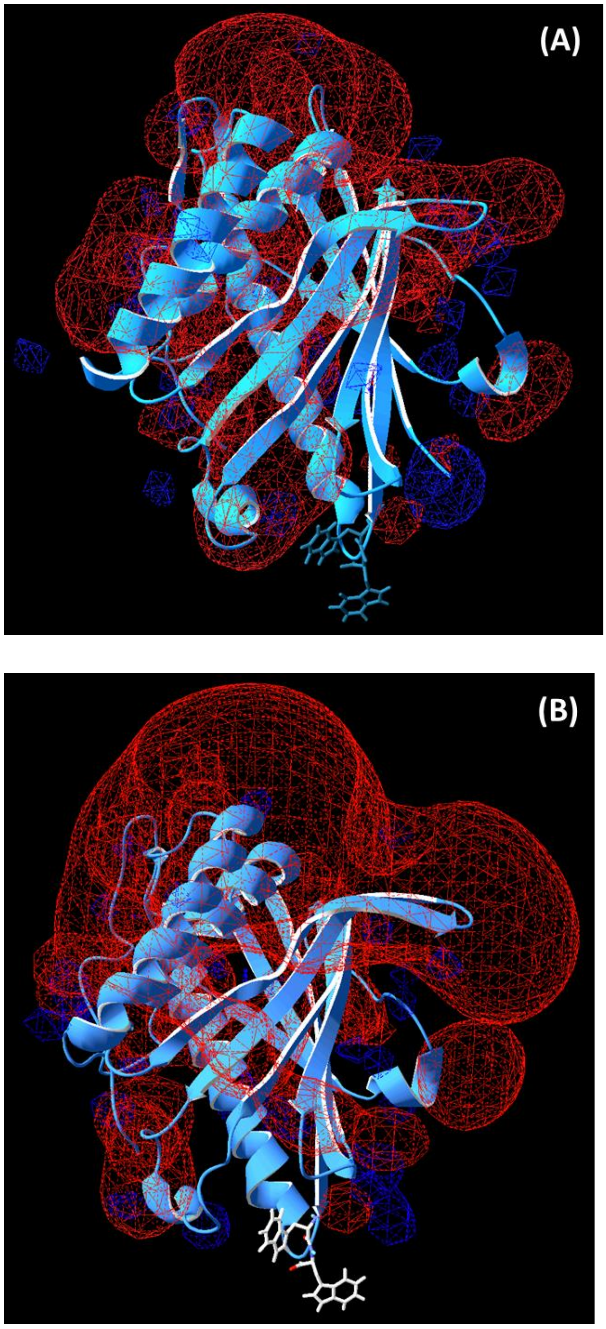

Figure 56: Electrostatic potential map of PITPα (A) and PITPβ (B)
The electrostatic potential map of PITPα (PDB code: 1UW5) and PITPβ (PDB code: 1T27) presented by DeepView. Areas of positive electrostatic potential are represented in blue and negative electrostatic potential is represented in red. Tryptophan residues are highlighted in blue for PITPα and white for PITPβ.

4.2 PITP's Membrane Interactions

DPI analysis revealed that both PITPα and PITPβ are able to bind to DOPC lipid layers (**Figures 49** and **50**). In fact, PITPβ demonstrated a higher affinity for membranes by nearly two-fold compared to PITPα. PITPβ's higher affinity for membranes was also reflected by the faster ligand transfer and pick-up rate in comparison to PITPα, as discussed in the previous section. Though the data showed that PITPs do bind to DOPC lipid layers, the maximum mass of PITPs bound to this membrane system are relatively low compared to other LTPs tested with this method – see **Section 3.6.1**. An approximate calculation of the theoretical adsorbed mass of PITP to a lipid layer was performed assuming 100 % protein coverage – see **Tables 6** and **7**. The approximate cross section dimension of PITPα from the PDB file 1UW5 is 45 Å. Thus the specific mass of bound protein could be determined as shown in **Table 6**. Supposing that PITPα had 100 % coverage on the lipid bilayer, the maximum specific mass would be ~2.6 ng/mm^2. However, this was not observed. Instead, the maximum specific mass was determined to be ~0.5 ng/mm^2. In reference to **Table 7**, this represents ~ 19 % protein coverage.

There are several possible reasons that can explain this lack of protein coverage on the immobilized lipid layer. Either the lipid layer formed is defective or there is incomplete lipid coverage on the surface of the sensor chip. The measured thickness of the lipid bilayer formed during DPI analysis has been shown to be 4 – 5 nm, which is typical of a membrane bilayer. Therefore, it is unlikely that the lipid layer formed on the sensor chip is defective. Moreover, the fact that the thickness of the immobilized lipid

bilayer is between 4-5 nm means full lipid coverage has been obtained. Therefore, this rules out poor lipid coverage on the sensor chip.

Table 6: Estimated theoretical adsorbed mass of PITPα to a planar lipid bilayer assuming 100 % coverage

Estimated dimension (Å)	Area occupied ($Å^2$)	Number of molecules/mm^2	Number of moles/mm^2	Maximum specific mass/mm^2 (g/mm^2)	Maximum specific mass/mm^2 (ng/mm^2)
45	2025	4.94E+10	8.20E-14	2.61E-09	2.61

Table 7: Estimated protein coverage based on the observed specific mass bound to a planar lipid bilayer

Theoretical observed specific mass (ng/mm^2)	Calculated protein coverage (%)
0.1	3.8
0.2	7.7
0.3	11.5
0.4	15.3
0.5	19.2
0.6	23.0
0.7	26.8
0.8	30.7
0.9	34.5
1.0	38.3

Another possible explanation for the poor protein coverage could be due to the way PITPs bind to membranes. Comparing PITPα and TTP, both proteins have closely related K_d values. But the B_{max} value of TTP is nearly four times that of PITPα. Both proteins are about the same molecular weight. However, both proteins interact with membranes differently. TTP binds to membranes via hydrophobic interactions through hydrophobic residues such as phenylalanine, isoleucine, valine, and methionine [95].

PITPα on the other hand interacts with membranes through two tryptophan residues located side by side [30, 36]. The different membrane binding mechanism may account for the difference in protein coverage. Taking this observation into account and the fact that PITPs prefer to bind to curved membrane surfaces as seen with the FRET studies, I feel that the DPI methodology may not be an ideal technique for measuring PITP binding affinity to membranes. An alternative method to investigate the binding of PITPs to membranes was attempted which involves a tryptophan fluorescence quenching assay. This will be discussed in more detail further on.

The incorporation of either PI or PS into DOPC lipid layers did not affect PITP binding to membranes as revealed through DPI analysis (**Figures 51** and **52**). In other words, there was no significant increase or decrease in the maximum specific mass of PITPs bound to membranes. This suggests that both PI and PS may not play a role in PITP binding to membranes. These results are in agreement with the FRET transfer studies. In addition, the effect of PE on PITP binding to membranes was also examined using DPI. However, PE did not appear to enhance or detract PITP binding to membranes (**Figure 53**). The final investigation with DPI involved pre-incubating PITPs with either PC or PI and examining the ligand-bound PITP binding to membranes (**Figure 54**). PC-bound PITPs did not have a higher or lower affinity for DOPC lipid layers. However, PI-bound PITPs showed lower affinity for membranes compared to unloaded PITPs. This is an interesting observation since PITPs has been associated with the production of phosphoinositides [34]. In other words, PITPs are believed to play a role in supplying PI to membranes for the production of phosphoinositides. Based on the data obtained here, it would seem dysfunctional for PITPs bound to PI to have a lower

membrane affinity. As mentioned in **Section 1.4.5**, two models have been proposed to explain the molecular mechanism of PITPs, which include the PI delivery model and the PI presentation model [34]. The lack of membrane affinity with PI-bound PITP clearly does not support the former model. Instead, the data observed here may support the latter model. This could be rationalized as follows: PITP only partially extracts PI, and presents the PI to a lipid kinase possibly through protein-protein interactions. The protein must show some affinity for PI, but when artificially loaded with free PI in an *in vitro* incubation the protein is now incapable of recognizing membranes. However, this notion is still preliminary and requires further investigation.

When comparing the FRET and DPI studies, it appeared that both techniques supported the idea that the ligand-free PITPβ has a higher propensity for binding membranes versus PITPα. The only concern with the DPI results was the low B_{max} values of PITPs, which was addressed previously. However, it should be cautioned that while the FRET and DPI results are in agreement, PITP binding to membranes and PITP ligand delivery are two distinct events. The ligand transfer rate provided by the FRET assays represents a global rate of ligand delivery event as opposed to a specific rate for a single mechanistic step – see **Figure 57**. When interpreting the FRET data, a faster ligand transfer rate may not necessarily mean a higher membrane affinity.

Since it was presumed that DPI may not be an ideal technique for measuring the binding affinity of PITPs to membranes, an alternative method was introduced. A tryptophan fluorescence quenching assay was utilized to measure the affinity of PITPs to membranes. The assay was conducted with and without the presence of a FRET acceptor in the lipid vesicles. Tryptophan has been used as a FRET donor and one common FRET

partner of tryptophan is pyrene. Here, pyrene-PE was used as the FRET acceptor. Upon excitation of tryptophan at 295 nm, if FRET was successful, an increase in the fluorescence signal of pyrene-PE would be observed [65]. In both conditions, no tryptophan fluorescence quenching was observed. Neither was there any fluorescence increase observed for pyrene-PE when incorporated into the lipid vesicles. The position of pyrene in the pyrene-PE utilized here is located on the head group region of PE. Whether the position of pyrene may influence the lack of tryptophan fluorescence quenching remains unclear, alternatively, the assay can be tested using pyrene-PE with the pyrene group located on the hydrocarbon tail [96].

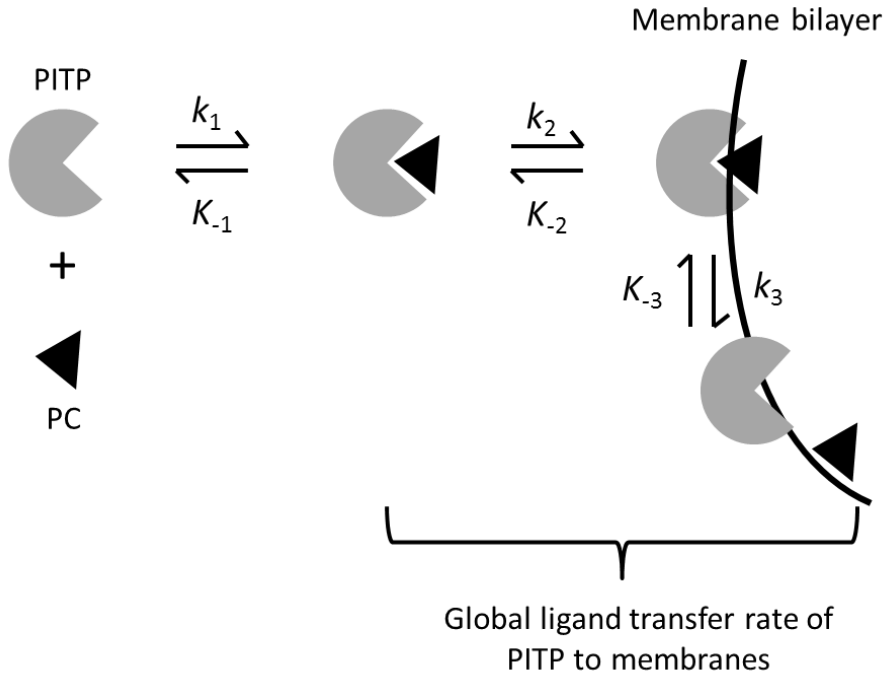

Figure 57: Representation of ligand delivery by PITP
The ligand transfer rate by PITPs represents a global process as opposed to individual kinetic rates; therefore a fast ligand transfer rate may not mean a high membrane affinity as both are separate events as shown here.

4.3 RdgBα: Lipid Transfer and Membrane Interactions

The FRET analysis demonstrated that RdgBα was a poor transporter of NBD-PC to membranes (**Figure 45**). The RdgBα mutant, Y210A/W211A, showed some transfer activity but it was still significantly low compared to wild type PITPα and could be an experimental anomaly. The results obtained here are in agreement with those demonstrated by Yadav *et al.* [76]. As mentioned in **Section 3.4.5**, the PITP domain in RdgBα only shares 40 % sequence similarity with wild type PITPα. Therefore, it is no surprise that its behavior may differ from that of wild type PITPα. Moreover, RdgBα is a multi-domain protein that possesses domains that aids in membrane interactions unlike the single domain PITPα. Therefore, it is possible that the RdgBα's Y210 and W211 residues may not be as crucial as the PITPα's W203 and W204 in membrane docking.

DPI studies revealed that both RdgBα and Y210A/W211A were both able to bind to DOPC lipid layers (**Figure 55**). The maximum specific mass of RdgBα and Y210A/W211A at 0.5 μM protein concentration in comparison to PITPα was similar. The incorporation of either PI or PS into DOPC lipid layers did not significantly change the amount of bound mass of RdgBα. This is indicative that these lipids do not influence RdgBα binding to membranes – a similar trend observed for the PITPs as well.

4.4 Conclusion

In summary, the results obtained from these studies reveal that PITPβ has a higher affinity for membranes compared to PITPα. This was reflected in both DPI measurements of binding affinity and FRET assays that measured ligand transfer rates. Results from the FRET studies showed that PITPβ has nearly four times faster ligand transfer rate than PITPα. DPI analysis on the other hand revealed a higher affinity for

membranes by nearly two-fold compared to PITPα. This is interesting since both proteins are structurally similar. However, their cellular localization and tissue expression differ which implies that both proteins likely serve different functions within the cell.

Both DPI and FRET studies demonstrated that the presence of PI in membranes did not affect the membrane affinity and the ligand transfer rate of PITPs, even though PI is the favored ligand of PITPs. In addition, the role of anionic lipids such as PS also did not affect PITP's membrane interactions and ligand delivery. However, what was interesting was that the presence of PA and phosphoinositides did affect the ligand transfer rate of PITPs. While the presence of PA in membranes enhanced the ligand transfer rate of PITPs, the presence of phosphoinositides had the opposite effect. It is understood that PITPs do not bind PA and therefore the increased in ligand transfer rate is most likely influenced by physical changes to the membranes brought about by PA, which is a negative-inducing curvature lipid [88-90]. While this is true for PA, it is not clear whether phosphoinositides have the same effect on PITPs. Whether PITPs binds phosphoinositides directly or recognizes their effect on membrane structure remains to be established. Future studies should establish whether PITPs bind phosphoinositides directly. In addition, the curvature effect brought on by phosphoinositides can be tested further by replacing phosphoinositides with lipids with larger head groups such as lysophosphatidylcholine.

The FRET analysis also revealed that both PITPα and PITPβ showed a propensity for highly curved membrane surfaces that now seems to be a common trend with LTPs in general. This observation is meaningful since loosely packed lipid head groups allow

easier access for PITPs to bind to membranes and deliver or pick-up its ligand. While DPI was not an ideal technique to examine PITP membrane affinity, a tryptophan fluorescence quenching assay using vesicles rather than flat lipid bilayers was employed as well. Unfortunately, this assay was not successful. The next step would be modifying the assay by using pyrene-PE with the pyrene group located on the hydrocarbon tail to determine if the location of the pyrene group may be significant here [96]. Alternatively, the fluorescence quenching assay can also be conducted using brominated lipids [97]. In addition, the use of immobilized vesicles on the DPI could also be a test that can be utilized to determine PITP's membrane binding affinity without the use of planar lipid layers [98-99]. Once an alternative method for measuring the membrane affinity of PITPs has been established, it would be advantageous to also confirm whether PI-bound PITPs have lower affinity for membranes.

The FRET studies conducted here mainly involved the use of NBD-PC, which at present, is the only commercially available ligand for PITPs. In future, it would be interesting to investigate the ligand transfer rates of PITPs using NBD-PI. This would be particularly useful for the RdgBα protein, which is a poor deliverer of NBD-PC. Since our DPI data showed that PI-bound PITPs have lower membrane affinity; I would expect to see a lower ligand transfer rate for the PITPs. However, a higher ligand transfer rate for the RdgBα proteins would be expected since their PITP domain may behave differently from that of wild type PITPs.

In conclusion, the overall results from this study demonstrate the difference in membrane interaction behavior between PITPα and PITPβ. In addition, the data obtained here suggests that PITPs, like most LTPs, are recruited to membranes through the

recognition of the membranes' physical parameters such as membrane curvature. While still at its preliminary stage, the outcome of this research project may also help favor the PI presentation model over the PI delivery model.

5. BIBLIOGRAPHY

1. Holthuis, J. C. M. & Levine, T. P. (2005). Lipid traffic: floppy drives and a super highway. *Nature Reviews: Molecular Cell Biology*, 6, 209-220.
2. Eeman, M & Deleu, M. (2010). From biological membranes to biomimetic model membranes. *Biotechnology, Agronomy, Society & Environment*, 14 (4), 719-736.
3. Holthuis, J. C. M. & Menon, A. K. (2014). Lipid landscapes and pipelines in membrane homeostasis. *Nature*, 510, 48-57.
4. Van Meer, G. & de Kroon, A. I. P. M. (2011). Lipid map of the mammalian cell. *Journal of Cell Science*, 124, 5-8.
5. Balla, T., Szentpetery, Z. & Kim, Y. J. (2009). Phosphoinositide signaling: new tools and insights. *Physiology*, 24, 231-244.
6. Balla, T. (2013). Phosphoinositides: tiny lipids with giant impact on cell regulation. *Physiological Reviews*, 93, 1019-1137.
7. Shewan, A., Eastburn, D. J. & Mostov, K. (2011). Phosphoinositides in cell architecture. *Cold Spring Harbor Perspectives in Biology*, 3, 1-17.
8. Kutateladze, T. G. (2010). Translation of the phosphoinositide code by PI effectors. *Nature Chemical Biology*, 6 (7), 507-513.
9. Falkenburger, B. H., Jensen, J. B., Dickson, E. J., Suh, B-C & Hille, B. (2010). Phosphoinositides: lipid regulators of membrane proteins. *The Journal of Physiology*, 588 (17), 3179-3185.
10. Sun, Y., Thapa, N., Hedman, A. C. & Anderson, R. A. (2013). Phosphatidylinositol-4,5-bisphosphate: targeted production and signaling. *Bioessays*, 35 (6), 1-18.

11. Manna, P. & Jain, S. K. (2015). Phosphatidylinositol-3,4,5-triphosphate and cellular signaling: implications for obesity and diabetes. *Cellular Physiology & Biochemistry*, 35, 1253-1275.
12. Blom, T., Somerharju, P. & Ikonen, E. (2011). Synthesis and biosynthetic trafficking of membrane lipids. *Cold Spring Harbor Perspectives in Biology*, 3, 1-16.
13. Di Paolo, G. & De Camilli, P. (2006). Phosphoinositides in cell regulation and membrane dynamics. *Nature*, 442, 651-657.
14. Lev, S. (2010). Non-vesicular lipid transport by lipid-transfer proteins and beyond. *Nature Reviews: Molecular Cell Biology*, 11, 739-750.
15. Vanderkooi, J. M. & Callis, J. B. (1974). Pyrene. A probe of lateral diffusion in the hydrophobic region of membranes. *Biochemistry*, 13 (19), 4000-4006.
16. Daleke, D. L. (2007). Phospholipid flippases. *The Journal of Biological Chemistry*, 282 (2), 821-825.
17. Beck, R., Ravet, M., Wieland, F. T. & Cassel, D. (2009). The COPI system: molecular mechanisms and function. *FEBS Letters*, 583 (17), 2701-2709.
18. Vance, J. E., Aasman, E. J. & Szarka, R. (1991). Brefeldin A does not inhibit the movement of phosphatidylethanolamine from its sites of synthesis to the cell surface. *The Journal of Biological Chemistry*, 266 (13), 8241-8247.
19. Prinz, W. A. (2010). Lipid trafficking sans vesicles: where, why, how? *Cell*, 143 (6), 870-874.
20. De Brouwer, A. P. M., Versluis, C., Westerman, J., Roelofsen, B., Heck, A. J. R. & Wirtz, K. W. A. (2002). Determination of the stability of the noncovalent

phospholipid transfer protein-lipid complex by electrospray time-of-flight mass spectrometry. *Biochemistry*, 41, 8013-8018.

21. Helmkamp Jr, G. M., Harvey, M. S., Wirtz, K. W. A. & van Deenen, L. L. M. (1974). Phospholipid exchange between membranes. *The Journal of Biological Chemistry*, 249 (20), 6382-6389.
22. Cockcroft, S. (2001). Phosphatidylinositol transfer proteins couple lipid transport to phosphoinositide synthesis. *Seminars in Cell & Developmental Biology*, 12, 183-191.
23. Carvou, N., Holic, R., Li, M., Futter, C., Skippen, A. & Cockcroft, S. (2010). Phosphatidylinositol- and phosphatidylcholine-transfer activity of PITPβ is essential for COPI-mediated retrograde transport from the Golgi to the endoplasmic reticulum. *Journal of Cell Science*, 123, 1262-1273.
24. Cockcroft, S. & Carvou, N. (2007). Biochemical and biological functions of class I phosphatidylinositol transfer proteins. *Biochimica et Biophysica Acta*, 1771, 677-691.
25. Wirtz, K. W. A., Schouten A. & Gros, P. (2006). Phosphatidylinositol transfer proteins: from closed for transport to open for exchange. *Advances in Enzyme Regulation*, 46, 301-311.
26. Alb, Jr., J. G., Cortese, J. D., Phillips, S. E. Albin, R. L., Nagy, T. R., Hamilton, B. A. & Bankaitis, V. A. (2003). Mice lacking phosphatidylinositol transfer protein-α exhibit spinocerebellar degeneration, intestinal and hepatic steatosis, and hypoglycemia. The *Journal of Biological Chemistry*, 278 (35), 33501-33518.

27. Cockcroft, S. & Garner, K. (2011). Function of the phosphatidylinositol transfer protein gene family: is phosphatidylinositol transfer the mechanism of action? *Critical Reviews in Biochemistry & Molecular Biology*, 46 (2), 89-117.

28. Alb, Jr., J. G., Phillips, S. E., Rostand, K., Cui, X., Pinxteren, J., Cotlin, L., Manning, T., Guo, S., York, J. D., Sontheimer, H., Collawn, J. F. & Bankaitis, V. A. (2002). Genetic ablation of phosphatidylinositol transfer protein function in murine embryonic stem cells. *Molecular Biology of the Cell*, 13, 739-754.

29. Kaiser, S. E., Brickner, J. H., Reilein, A. R., Fenn, T. D., Walter, P. & Brunger, A. T. (2005). Structural basis of FFAT motif-mediated ER targeting. *Structure*, 13, 1035-1045.

30. Tilley, S. J., Skippen, A., Murray-Rust, J., Swigart, P. M., Stewart, A., Morgan, C. P., Cockcroft, S. & McDonald, N. Q. (2004). Structure-function analysis of phosphatidylinositol transfer protein alpha bound to human phosphatidylinositol. *Structure*, 12, 317-326.

31. Yoder, M. D., Thomas, L. M., Tremblay, J. M., Oliver, R. L., Yarbrough, L. R. & Helmkamp Jr., G. M. (2001). Structure of a multifunctional protein. *The Journal of Biological Chemistry*, 276 (12), 9246-9252.

32. Schouten, A., Agianian, B., Westerman, J., Kroon, J. Wirtz, K. W. A. & Gros, P. (2002). Structure of apo-phosphatidylinositol transfer protein α provides insight into membrane association. *The EMBO Journal*, 21 (9), 2117-2121.

33. Vordtriede, P. B., Chuong, N. D., Tremblay, J. M., Helmkamp Jr., G. M. & Yoder, M. D. (2005). Structure of PITPβ in complex with phosphatidylcholine: comparison

of structure and lipid transfer to other PITP isoforms. *Biochemistry*, 44, 14760-14771.

34. Cockcroft, S. (2012). The diverse functions of phosphatidylinositol transfer proteins. In M. Falasca (Ed.), *Phosphoinositides and disease* (pp. 185-208). New York, NY: Springer.
35. Tremblay, J. M., Helmkamp Jr., G. M. & Yarbrough, L. R. (1996). Limited proteolysis of rat phosphatidylinositol transfer protein by trypsin cleaves the C terminus, enhances binding to lipid vesicles, and reduces phospholipid transfer activity. *The Journal of Biological Chemistry*, 271 (35), 21075-21080.
36. Shadan, S., Holic, R., Carvou, N., Ee, P., Li, M., Murray-Rust, J. & Cockcroft, S. (2008). Dynamics of lipid transfer by phosphatidylinositol transfer proteins in cells. *Traffic*, 9, 1743-1756.
37. Segui, B., Allen-Baume, V. & Cockcroft, S. (2002). Phosphatidylinositol transfer protein β displays minimal sphingomyelin transfer activity and is not required for biosynthesis and trafficking of sphingomyelin. *Biochemical Journal*, 366, 23-34.
38. Lomize, M. A., Pogozheva, I. D., Joo, H., Mosberg, H. I. & Lomize, A. L. (2012). OPM database and PPM web server: resources for positioning of proteins in membranes. *Nucleic Acids Research*, 40, D370-D376.
39. http://opm.phar.umich.edu/
40. Yau, W., Wimley, W. C., Gawrisch, K. & White, S. H. (1998). The preference of tryptophan for membrane interfaces. Biochemistry, 37 (42), 14713-14718.
41. Van Paridon, P. A., Gadella Jr., T. W. J., Somerharju, P. J. & Wirtz, K. W. A. (1987). On the relationship between the dual specificity of the bovine brain

phosphatidylinositol transfer protein and membrane phosphatidylinositol levels. *Biochimica et Biophysica Acta*, 903, 68-77.

42. Hsuan, J, & Cockcroft, S. (2001). The PITP family of phosphatidylinositol transfer proteins. *Genome Biology*, 2 (9), 3011.1-3011.8.
43. Bankaitis, V. A., Ile, K. E., Nile, A. H., Ren, J., Ghosh, R., Schaaf, G. (2012). Thoughts on Sec14-like nanoreactors and phosphoinositide signaling. *Advances in Biological Regulation*, 52 (1), 115-121. ,
44. Trivedi, D. & Padinjat, R. (2007). RdgB proteins: functions in lipid homeostasis and signal transduction. *Biochimica et Biophysica Acta*, 1771, 692-699.
45. Vihtelic, T. S., Hyde, D. R. & O'Tousa, J. E. (1991). Isolation and characterization of Drosophila retinal degeneration B (rdgB) gene. *Genetics*, 127, 761-768.
46. Vihtelic, T. S., Goebl, M., Milligan, S., O'Tousa, J. E., & Hyde, D. R. (1993). Localization of Drosophila retinal degeneration B, a membrane-associated phosphatidylinositol transfer protein. *The Journal of Cell Biology*, 122 (5), 1013-1022.
47. Milligan, S. C., Alb, J. G., Elagina, R. B., Bankaitis, V. A., & Hyde, D. R. (1997). The phosphatidylinositol transfer protein domain of Drosophila retinal degeneration B protein is essential for photoreceptor cell survival and recovery from light stimulation. *The Journal of Cell Biology*, 139 (2), 351-363.
48. Cho, W. & Stahelin, R. V. (2005). Membrane-protein interactions in cell signaling and membrane trafficking. *Annual Review of Biophysics & Biomolecular Structure*, 34, 119-151.

49. Bigay, J. & Antonny, B. (2012). Curvature, lipid packing, and electrostatics of membrane organelles: defining cellular territories in determining specificity. *Developmental Cell*, 23, 886-895.

50. Kurafeva, I., Lenoir, M., Dancea, F., Sridhar, P., Raush, E., Bissig, C., Gruenberg, J., Abagyan, R. & Overduin, M. (2014). Discovery of novel membrane binding structures and functions. *Biochemistry & Cell Biology*, 92 (6), 555-563.

51. Suetsugu, S., Kurisu, S. & Takenawa, T. (2014). Dynamic shaping of cellular membranes by phospholipids and membrane-deforming proteins. *Physiological Reviews*, 94, 1219-1248.

52. Lemmon, M. A. (2008). Membrane recognition by phospholipid-binding domains. *Nature Reviews Molecular Cell Biology*, 9, 99-111.

53. Mattjus, P. (2009). Glycolipid transfer proteins and membrane interaction. *Biochimica et Biophysica Acta*, 1788, 267-272.

54. Mattjus, P., Pike, H. M., Molotkovsky, J. G. & Brown, R. E. (2000). Charged membrane surfaces impede the protein-mediated transfer of glycosphingolipids between phospholipid bilayers. *Biochemistry*, 39 (5), 1067-1075.

55. Neumann, S., Opacic, M., Wechselberger, R. W., Sprong, H. & Egmond, M. R. (2008). Glycolipid transfer protein: clear structure and activity, but enigmatic function. *Advances in Enzyme Regulation*, 48, 137-151.

56. Sprong, H., Van der Sluijs, P. & Van Meer, G. (2001). How proteins move lipids and lipids move proteins. *Nature Reviews Molecular Cell Biology*, 2, 504-513.

57. Ohvo-Rekila, H. & Mattjus, P. (2011). Monitoring glycolipid transfer protein activity and membrane interaction with the surface plasmon resonance technique. *Biochimica et Biophysica Acta*, 1808, 47-54.

58. Tuuf, J., Kjellberg, M. A., Molotkovsky, J. G., Hanada, K. & Mattjus, P. (2011). The intermembrane ceramide transport catalyzed by CERT is sensitive to the lipid environment. *Biochimica et Biophysica Acta*, 1808, 229-235.

59. Piomelli, D., Astarita, G. & Rapaka, R. (2007). A neuroscientist's guide to lipidomics. *Nature Reviews Neuroscience*, 8, 743-754.

60. McMahon, H. T & Gallop, J. L. (2005). Membrane curvature and mechanisms of dynamic cell membrane remodeling. *Nature*, 438, 590-596.

61. Contreras, F-X., Ernst, A. M., Wieland, F. & Brugger, B. (2011). Specificity of intramembrane protein-lipid interactions. *Cold Spring Harbor Perspectives in Biology*, 3 (6), a004705.

62. Escorihuela, J., Gonzalez-Martinez, M. A., Lopez-Paz, J. L., Puchades, R., Maquieira, A. & Gimenez-Romero, D. (2014). Dual-polarization interferometry: a novel technique to light up the nanomolecular world. *Chemical Reviews*, 115, 265-294.

63. Cross, G. H., Reeves, A. A., Brand, S., Popplewell, J. F., Peel, L. L., Swann, M. J. & Freeman, N. J. (2003). A new quantitative optical biosensor for protein characterization. *Biosensors & Bioelectronics*, 19, 383-390.

64. Terry, C. J., Popplewell, J. F., Swann, M. J., Freeman, N. J. & Fernig, D. G. (2006). Characterization of membrane mimetics on a dual polarization interferometer. *Biosensors & Bioelectronics*, 22, 627-632.

65. Loura, L. M. S. & Prieto, M. (2011). FRET in membrane biophysics: an overview. *Frontiers in Physiology*, 2 (82), 1-11.

66. Panja, S., Aich, P., Jana, B. & Basu, T. (2008). How does plasmid DNA penetrate cell membranes in artificial transformation process in *Escherichia coli*? *Molecular Membrane Biology*, 25 (5), 411-422.

67. http://www.emdmillipore.com/CA/en/product/NovaBlue-Singles%E2%84%A2-Competent-Cells---Novagen,EMD_BIO-70181

68. Chattopadhyay, A. (1990). Chemistry and biology of N-(7-nitrobenz-2-oxa-1,3-diazol-4-yl)-labeled lipids: fluorescent probes of biological and model membranes. *Chemistry and Physics of Lipids*, 53, 1-15.

69. Huang, B. X. & Kim, H-Y. (2004). Probing three-dimensional structure of bovine serum albumin by chemical cross-linking and mass spectrometry. *Journal of the American Society for Mass Spectrometry*, 15, 1237-1247.

70. Choi, J-K., Ho, J., Curry, S., Qin, D., Bittman, R & Hamilton, J. A. (2002). Interactions of very long-chain saturated fatty acids with serum albumin. *Journal of Lipid Research*, 43, 1000-1010.

71. McIntyre, J. C, & Sleight, R. G. (1991). Fluorescence assay for phospholipid membrane asymmetry. *Biochemistry*, 30 (51), 11819-11827.

72. Zhang, W. X., Frahm, G., Morley, S., Manor, D. & Atkinson, J. (2009). Effect of bilayer phospholipid composition and curvature on ligand transfer by the α-tocopherol transfer protein. *Lipids*, 44 (7), 631-641.

73. Kim, S., Kedan, A., Marom, M., Gavert, N., Keinan, O., Selitrennik, M., Laufman, O. & Lev. S. (2013). The phosphatidylinositol-transfer protein Nir2 binds phosphatidic

acid and positively regulates phosphoinositide signaling. *European Molecular Biology Organization*, 14 (10), 891-899.

74. Kim, Y. J., Guzman-Hernandez, M-L., Wisniewski, E. & Balla, T. (2015). Phosphatidylinositol-phosphatidic acid exchange by Nir2 at ER-PM contact sites maintains phosphoinositide signaling competence. *Developmental Cell*, 33, 549-561.
75. De Matteis, M. A., Godi, A. & Corda, D. (2002). Phosphoinositides and the Golgi complex. *Current Opinion in Cell Biology*, 14, 434-447.
76. Yadav, S., Garner, K., Georgiev, P., Li, M., Gomez-Espinosa, E., Panda, A., Mathre, S., Okkenhaug, H., Cockcroft, S. & Raghu, P. (2015). RDGBα, a PtdIns-PtdOH transfer protein, regulates G-protein-coupled PtdIns(4,5)P_2 signaling during *Drosophila* phototransduction. *Journal of Cell Science*, 128, 3330-3344.
77. Baptist, M., Panagabko, C., Nickels, J. D., Katsaras, J. & Atkinson, J. (2015). 2,2′-Bis(monoacylglycero)PO4 (BMP), but not 3,1′-BMP, increases membrane curvature stress to enhance α-tocopherol transfer protein binding to membranes. *Lipids*, 50 (3), 323-328.
78. Jouhet, J. (2013). Importance of the hexagonal lipid phase in biological membrane organization. *Frontiers in Plant Science*, 4, 1-5.
79. Bustad, H. J., Underhaug, J., Halskau Jr., O. & Martinez, A. (2011). The binding of 14-3-3γ to membranes studied by intrinsic fluorescence spectroscopy. *FEBS Letters*, 585, 1163-1168.
80. Brouillette, C. G., Segrest, J. P., Ng, T. C., & Jones, J. L. (1982). Minimal size phosphatidylcholine vesicles: effects of radius of curvature on head group packing and conformation. *Biochemistry*, 21(19), 4569–4575.

81. Yang, Q., Guo, Y., Li, L., & Hui, S. W. (1997). Effects of lipid headgroup and packing stress on poly(ethylene glycol)-induced phospholipid vesicle aggregation and fusion. *Biophysical Journal*, 73(1), 277–282.

82. Wootan, M. G. & Storch, J. (1994). Regulation of fluorescent fatty acid transfer from adipocyte and heart fatty acid binding proteins by acceptor membrane lipid composition and structure. *The Journal of Biological Chemistry*, 269 (14), 10517-10523.

83. Chang-Ileto, B., Frere, S. G., Chan, R. B., Voronov, S. V., Roux, A. & Di Paolo, G. (2011). Synaptojanin 1-mediated PI(4,5)P_2 hydrolysis is modulated by membrane curvature and facilitates membrane fission. *Developmental Cell*, 20 (2), 206-218.

84. McMahon, H. T. & Boucrot, E. (2015). Membrane curvature at a glance. *Journal of Cell Science*, 128, 1065-1070.

85. Flis, V. V. & Daum, G. (2013). Lipid transport between the endoplasmic reticulum and mitochondria. *Cold Spring Harbor Perspectives in Biology*, 5 (6), pii: a013235.

86. Peng, A., Pisal, D. S., Doty, A. & Balu-lyer, S. V. (2012). Phosphatidylinositol induces fluid phase formation and packing defects in phosphatidylcholine model membranes. *Chemistry & Physics of Lipids*, 165 (1), 15-22.

87. Garner, K., Hunt, A. N., Koster, G., Somerharju, P., Groves, E., Li, M., Raghu, P., Holica, R. & Cockcroft, S. (2012). Phosphatidylinositol transfer protein, cytoplasmic 1 (PITPNC1) binds and transfers phosphatidic acid. *The Journal of Biological Chemistry*, 287 (38), 32263-32276.

88. Kooijman, E. E., Chupin, V., de Kruijff, B., & Burger, K. N. J. (2003). Modulation of membrane curvature by phosphatidic acid and lysophosphatidic acid. *Traffic*, 4 (3), 162–174.

89. Kooijman, E. E., Chupin, V., Fuller, N. L., Kozlov, M. M., De Kruijff, B., Burger, K. N. J., & Rand, P. R. (2005). Spontaneous curvature of phosphatidic acid and lysophosphatidic acid. *Biochemistry*, 44, 2097–2102

90. Kooijman, E. E., Kooijman, E. E., Burger, K. N. J., & Burger, K. N. J. (2009). Biophysics and function of phosphatidic acid: a molecular perspective. *Biochimica Et Biophysica Acta*, *1791*(9), 881–888.

91. van den Bogaart, G. & Beest ter, M. (2015). Domains of phosphoinositides in the plasma membrane. In Cambi, A. & Lidke, D. S. (Eds), *Cell Membrane Nanodomains* (pp. 173–198). Boca Raton, Fl: CRC Press.

92. Rusinova, R., Hobart, E. A., Koeppe II, R. E. & Andersen, O. S. (2013). Phosphoinositides alter lipid bilayer properties. *The Journal of General Physiology*, 141 (6), 673-690.

93. Tucker, S. J. & Baukrowitz, T. (2008). How highly charged anionic lipids bind and regulate ion channels. *The Journal of General Physiology*, 131 (5), 431-438.

94. Stahelin, R. V., Scott, J. L. & Frick, C. T. (2014). Cellular and molecular interactions of phosphoinositides and peripheral proteins. *Chemistry & Physics of Lipids*, 182, 3-18.

95. Zhang, W. X., Thakur, V., Lomize, A., Pogozheva, I., Panagabko, C., Cecchini, M., Baptist, M., Morley, S., Manor, D. & Atkinson, J. (2011). The contribution of

surface residues to membrane binding and ligand transfer by the α-tocopherol transfer protein (α-TTP). *Journal of Molecular Biology*, 405 (4), 972-988.

96. Pap, E. H., Bastiaens, P. I., Borst, J. W., van den Berg, P. A., van Hoek, A., Snoek, G. T., Wirtz, K. W. & Visser, A. J. (1993). Quantitation of the interaction of protein kinase C with diacylglycerol and phosphoinositides by time-resolved detection of resonance energy transfer. *Biochemistry*, 32 (48), 13310-13317.
97. Heymann, J. B., Zakharov, S. D., Zhang, Y. L. & Cramer, W. A. (1996). Characterization of electrostatic and nonelectrostatic components of protein-membrane binding interactions. *Biochemistry*, 35 (8), 2717-2725.
98. Masson L, Mazza A, Brousseau R. (1994). Stable immobilization of lipid vesicles for kinetic studies using surface plasmon resonance. *Analytical Biochemistry*, 218, 405–412.
99. Ishizuka-Katsura, Y., Wazawa, T., Ban, T., Morigaki, K. & Aoyama, S. (2008). Biotin-containing phospholipid vesicle layer formed on self-assembled monolayer of a saccharide-terminated alkyl disulfide for surface plasmon resonance biosensing. *Journal of Bioscience and Bioengineering*, 105 (5), 527-535.

6. APPENDIX I
Nucleotide Sequence of PITPα Mutants Showing Mutated Nucleotides

Query represents mutant; Sbjct represents wild type PITPα

W203A/W204A

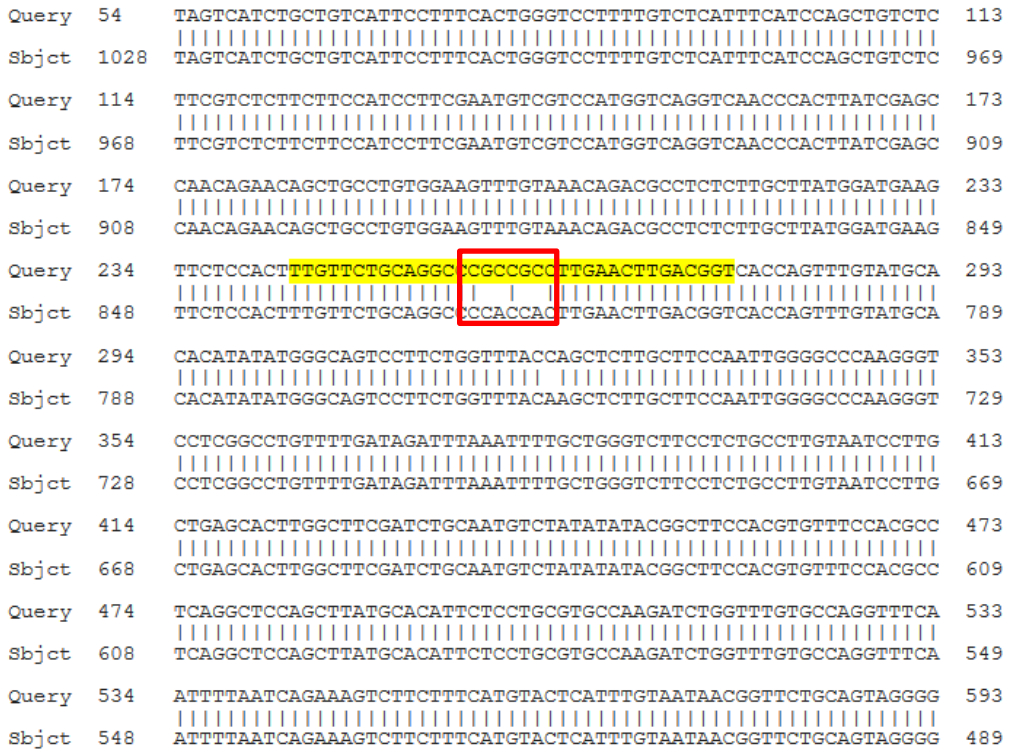

K61A

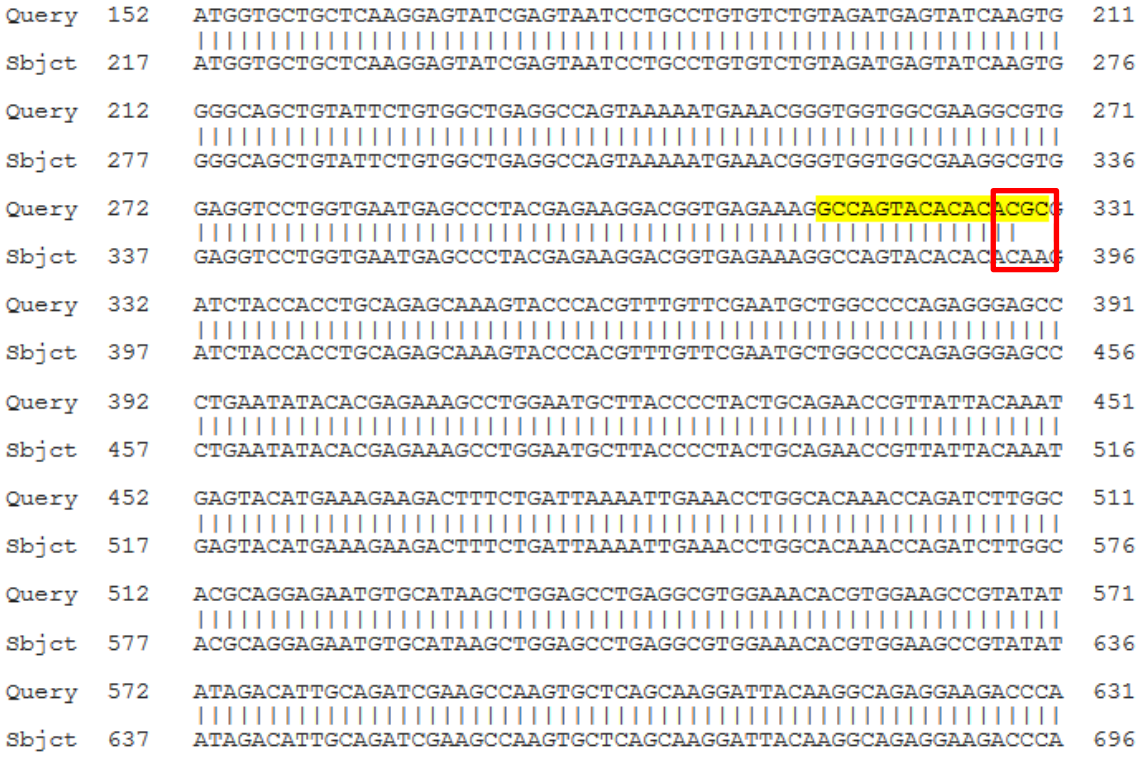
Query 152 ATGGTGCTGCTCAAGGAGTATCGAGTAATCCTGCCTGTGTCTGTAGATGAGTATCAAGTG 211
Sbjct 217 ATGGTGCTGCTCAAGGAGTATCGAGTAATCCTGCCTGTGTCTGTAGATGAGTATCAAGTG 276
Query 212 GGGCAGCTGTATTCTGTGGCTGAGGCCAGTAAAAATGAAACGGGTGGTGGCGAAGGCGTG 271
Sbjct 277 GGGCAGCTGTATTCTGTGGCTGAGGCCAGTAAAAATGAAACGGGTGGTGGCGAAGGCGTG 336
Query 272 GAGGTCCTGGTGAATGAGCCCTACGAGAAGGACGGTGAGAAAGGCCAGTACACACACGCG 331
Sbjct 337 GAGGTCCTGGTGAATGAGCCCTACGAGAAGGACGGTGAGAAAGGCCAGTACACACACAAG 396
Query 332 ATCTACCACCTGCAGAGCAAAGTACCCACGTTTGTTCGAATGCTGGCCCCAGAGGGAGCC 391
Sbjct 397 ATCTACCACCTGCAGAGCAAAGTACCCACGTTTGTTCGAATGCTGGCCCCAGAGGGAGCC 456
Query 392 CTGAATATACACGAGAAAGCCTGGAATGCTTACCCCTACTGCAGAACCGTTATTACAAAT 451
Sbjct 457 CTGAATATACACGAGAAAGCCTGGAATGCTTACCCCTACTGCAGAACCGTTATTACAAAT 516
Query 452 GAGTACATGAAAGAAGACTTTCTGATTAAAATTGAAACCTGGCACAAACCAGATCTTGGC 511
Sbjct 517 GAGTACATGAAAGAAGACTTTCTGATTAAAATTGAAACCTGGCACAAACCAGATCTTGGC 576
Query 512 ACGCAGGAGAATGTGCATAAGCTGGAGCCTGAGGCGTGGAAACACGTGGAAGCCGTATAT 571
Sbjct 577 ACGCAGGAGAATGTGCATAAGCTGGAGCCTGAGGCGTGGAAACACGTGGAAGCCGTATAT 636
Query 572 ATAGACATTGCAGATCGAAGCCAAGTGCTCAGCAAGGATTACAAGGCAGAGGAAGACCCA 631
Sbjct 637 ATAGACATTGCAGATCGAAGCCAAGTGCTCAGCAAGGATTACAAGGCAGAGGAAGACCCA 696

C95A

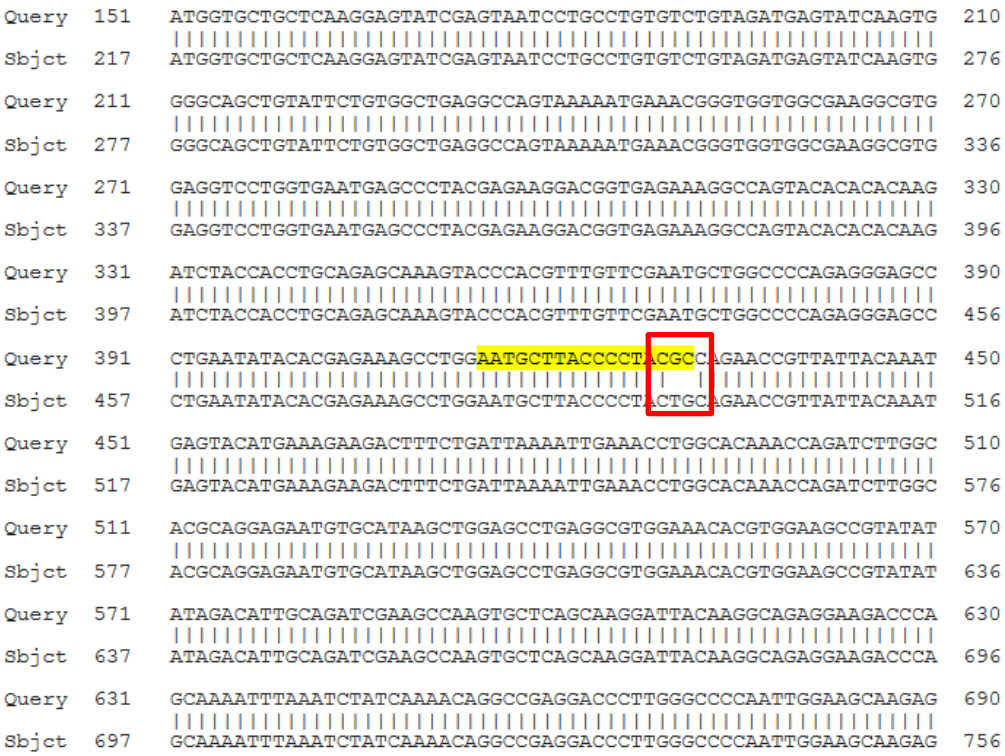
Query 151 ATGGTGCTGCTCAAGGAGTATCGAGTAATCCTGCCTGTGTCTGTAGATGAGTATCAAGTG 210
Sbjct 217 ATGGTGCTGCTCAAGGAGTATCGAGTAATCCTGCCTGTGTCTGTAGATGAGTATCAAGTG 276
Query 211 GGGCAGCTGTATTCTGTGGCTGAGGCCAGTAAAAATGAAACGGGTGGTGGCGAAGGCGTG 270
Sbjct 277 GGGCAGCTGTATTCTGTGGCTGAGGCCAGTAAAAATGAAACGGGTGGTGGCGAAGGCGTG 336
Query 271 GAGGTCCTGGTGAATGAGCCCTACGAGAAGGACGGTGAGAAAGGCCAGTACACACACAAG 330
Sbjct 337 GAGGTCCTGGTGAATGAGCCCTACGAGAAGGACGGTGAGAAAGGCCAGTACACACACAAG 396
Query 331 ATCTACCACCTGCAGAGCAAAGTACCCACGTTTGTTCGAATGCTGGCCCCAGAGGGAGCC 390
Sbjct 397 ATCTACCACCTGCAGAGCAAAGTACCCACGTTTGTTCGAATGCTGGCCCCAGAGGGAGCC 456
Query 391 CTGAATATACACGAGAAAGCCTGGAATGCTTACCCCTACGCCAGAACCGTTATTACAAAT 450
Sbjct 457 CTGAATATACACGAGAAAGCCTGGAATGCTTACCCCTACTGCAGAACCGTTATTACAAAT 516
Query 451 GAGTACATGAAAGAAGACTTTCTGATTAAAATTGAAACCTGGCACAAACCAGATCTTGGC 510
Sbjct 517 GAGTACATGAAAGAAGACTTTCTGATTAAAATTGAAACCTGGCACAAACCAGATCTTGGC 576
Query 511 ACGCAGGAGAATGTGCATAAGCTGGAGCCTGAGGCGTGGAAACACGTGGAAGCCGTATAT 570
Sbjct 577 ACGCAGGAGAATGTGCATAAGCTGGAGCCTGAGGCGTGGAAACACGTGGAAGCCGTATAT 636
Query 571 ATAGACATTGCAGATCGAAGCCAAGTGCTCAGCAAGGATTACAAGGCAGAGGAAGACCCA 630
Sbjct 637 ATAGACATTGCAGATCGAAGCCAAGTGCTCAGCAAGGATTACAAGGCAGAGGAAGACCCA 696
Query 631 GCAAAATTTAAATCTATCAAAACAGGCCGAGGACCCTTGGGCCCCAATTGGAAGCAAGAG 690
Sbjct 697 GCAAAATTTAAATCTATCAAAACAGGCCGAGGACCCTTGGGCCCCAATTGGAAGCAAGAG 756